Marquette University

e-Publications@Marquette

Surface Acoustic Wave (SAW)-Based Gas Flow Sensor

Nisar Ahmad
Marquette University

Recommended Citation

SURFACE ACOUSTIC WAVE (SAW)-BASED
GAS FLOW SENSOR

by

Nisar Ahmad, M.S. (Physics), M.S. (EECS)

A Dissertation submitted to the Faculty of the Graduate School,
Marquette University,
in Partial Fulfillment of the Requirements for
the Degree of Doctor of Philosophy in Electrical and Computer Engineering

Milwaukee, Wisconsin
May, 2015

ABSTRACT
SURFACE ACOUSTIC WAVE (SAW)-BASED

GAS FLOW SENSOR

Nisar Ahmad, M.S. (Physics), M.S. (EECS)

Marquette University, 1982

There has been a growing interest in using SAW devices for sensing various physical parameters such as pressure, acceleration, temperature, and gas. The current research has been undertaken to derive a model of a SAW-based gas flow rate sensor, using the principle of heat transfer with the flow of gas. It consists of a SAW delay line fabricated on a suitable substrate and a thin film heater to heat the SAW device to a suitable temperature above the ambient. The delay line is connected in the feedback loop of an rf-amplifier resulting in a delay line stabilized SAW oscillator. When gas flows over the SAW device, it carries away heat thus lowering the temperature of the substrate. The change in the frequency of the SAW oscillator, which can be accurately measured, is proportional to flow rate of gas. The device is similar in principle to a hot wire or hot-film anemometer.

This dissertation is concerned with the quantitative analysis of SAW flow sensor. Theoretical analysis to determine the characteristics of SAW flow sensor for various substrate material and geometries will be presented. From the analyses, a design of an optimal SAW flow sensor will be proposed.

Mathematical model(s) will be derived to determine and predict SAW gas flow sensor behavior and characteristics for a wide range of variables and boundary conditions. These characteristics include:
- Steady state temperature characteristics
- Transient time response characteristics
- Frequency versus temperature characteristics
- Frequency characteristics versus input power to the integrated thin film heater element
- Frequency change versus flow rate at constant current to the thin film heater element
- Determine temperature distribution to derive average temperature

The model developed in this work enables us to characterize SAW-based sensor by including substrate material properties, dimensional and wide range of operating conditions. It can predict frequency changes, temperature changes, for given values of heater power, under steady state free and forced convection conditions of fluid. It allows time response analyses and thus enables us determine parameters that can be used to obtain an optimal SAW-based sensor designs. Experimental results carried out on preliminary design of SAW flow sensor are presented and result compared with theoretical analyses.

ACKNOWLEDGMENTS

Nisar Ahmad, M.S. (Physics), M.S. (EECS)

TABLE OF CONTENTS

TABLE OF FIGURES

LIST OF TABLES

CHAPTER 1: INTRODUCTION

Devices based on the propagation of elastic waves on the free surface of a solid have been extensively studied in the last four decades. These devices provide very high frequency (VHF) / ultra high frequency (UHF) signal processing functions that are not readily available by other means. Such devices have rapidly advanced from laboratorial to actual system use and have made a major impact in the electronics industry in an exceptionally short amount of time.

Surface Acoustic Wave (SAW) devices are now being used extensively in the storage and processing of a wide variety of analog, and sometimes even digital, signals. Their applications range from sophisticated radar, sonar, and communication systems to mass-produced components for radio and television receivers (Mathews, 1977; Oliner, 1978; Owens, 1986; Pedi & McManus, 1983; Edmonds, 1981). SAW devices have also seen major application in the area of radio frequency (RF) signal processing. However, more than these, the usability of SAW devices has also been extended for the purpose of sensing various physical and chemical parameters.

This chapter includes the statement of the problem and the purpose of the study. An overview of the study's structure is also presented along with the rationale behind the research and its significance and implications to future practice. The terminology used in this dissertation is also defined in this chapter.

Statement of the Problem

A Surface Acoustic Wave (SAW) gas flow rate sensor can be realized using the principle of heat transfer with the flow of gas (Ahmad, 1985). The SAW gas flow sensor (Cheng, Dong, and Feng, 2000; Ahmad, 1985) consists of a SAW delay line and an

integrated thin-film heater on a suitable SAW substrate. The delay line is connected to the feedback loop of a radio frequency (RF) amplifier, resulting in a delay line stabilized SAW oscillator. The SAW substrate is heated causing the SAW device to operate at an elevated temperature. Gas flowing over the SAW device carries away heat, thus lowering the temperature of the substrate. The change in the frequency of the SAW oscillator, which can be accurately measured, is proportional to the flow rate of the gas.

To date, only experimental and empirical findings have been reported. This study, on the other hand, deals with a quantitative and theoretical analysis of a SAW-based gas flow sensor model to support previously established experimental and empirical results. In addition, the study will enable the characterization of a SAW-based gas flow sensor for varied substrate material, different flow geometries, and sensor structure. The findings will then guide the assessment of an optimal SAW-based gas flow sensor design.

Purpose of the Study

There has been extensive research efforts geared towards the discussion of SAW-based sensing. SAW sensors for the measurement of force, pressure, acceleration, temperature, and humidity, among others physical parameters, have been reported in literature (Ahmad, 1985; Ahmad, 1986). SAW techniques have also been applied in the field of chemical sensing with sensors for gas detection, and specific antibody detection having been demonstrated in literature (Inaba and Wasa, 1982; Joshi & Brace, 1976; Hauden, Jaillet, & Coquerel, 1985; Vellekoop & Visser; 1988; Leblois & Tellier, 2000; Reeder, Cullen & Gilden, 1975). SAW sensors have shown performance levels that are superior to previously used bulk acoustic wave approaches and other types of sensors.
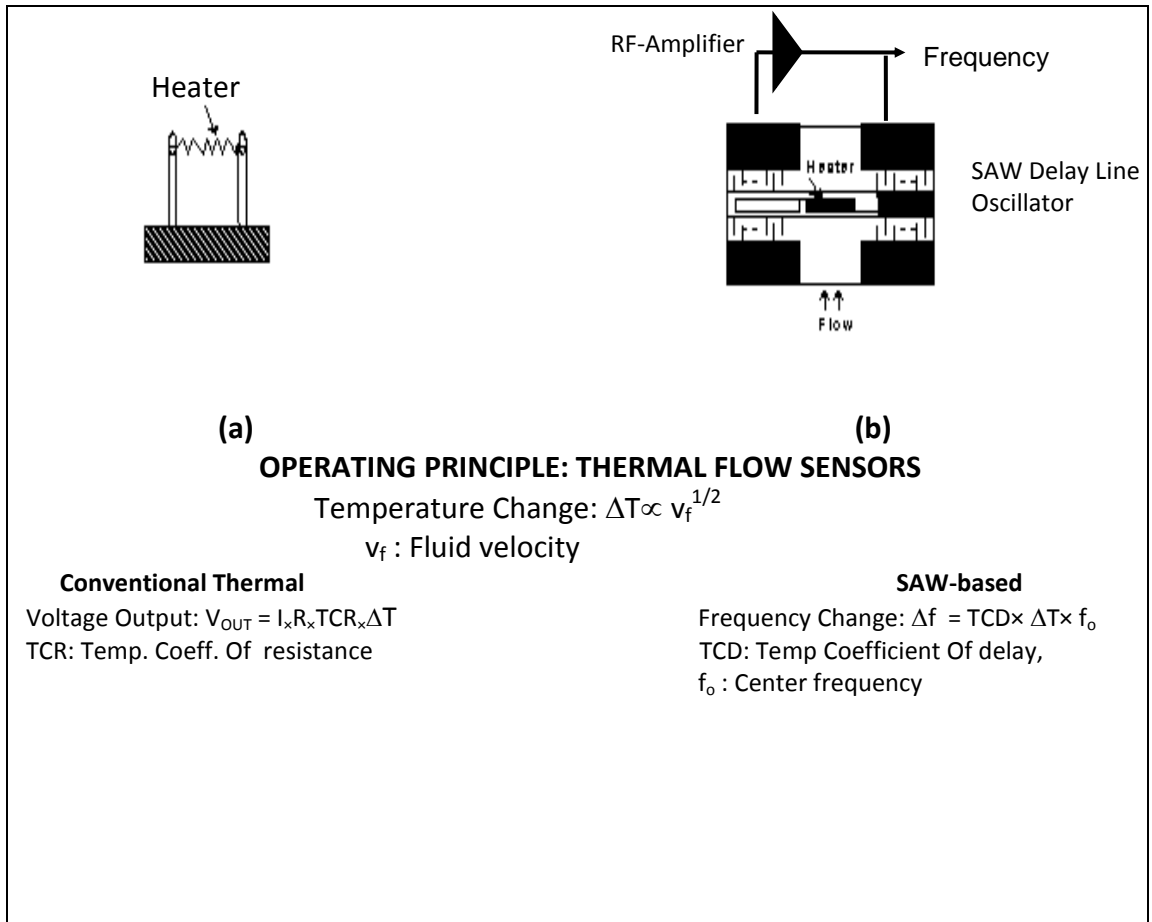
Figure 1. Sketch of thermal flow sensors: (a) a hot-wire anemometer, (b) a silicon-based thermal sensor, and (c) a SAW gas flow sensor.

The thermal gas flow sensor operates on the principle of heat transfer by mass flow. Figure 1 (a) is a conventional thermal gas flow sensor; the heater element is operated at a higher temperature. Gas flow over it carries heat away by convection; the output is generally measured as a change in analog voltage across the heater element. Similarly, a SAW-based gas flow rate sensor can be realized using the principle of heat transfer with the mass flow. Figure 1(c) shows a diagram of a SAW gas flow sensor (Ahmad, 1985). It consists of a SAW delay line (or resonator) fabricated on a suitable substrate. The output of the delay line is fed back to its input through a suitable amplifier, resulting to a delay-line-stabilized SAW oscillator. Since SAW propagation is very

sensitive to external variables such as pressure, temperature, etc., the frequency of the

oscillator could vary in the event that any of these parameters changes. A second

identical oscillator is usually fabricated on the substrate to serve as a reference oscillator,

and the difference between the two oscillator frequencies is used as the sensor output.

This "dual oscillator technique" has the advantage of canceling out the effect of

unwanted variables. For example, in a pressure sensor or a gas detector, the effect of

ambient temperature variations can be eliminated by using the "dual SAW oscillator

technique" (Reeder, Cullen, & Gilden, 1975; Risch, 1984).

Importance of the Study

Gas flow sensing is important in process and analytical chemistry as well as in the

semiconductor industry where device and material processing depends critically upon the

accurate measurement of the flow rates of various gases. The SAW gas flow sensor

operates similarly to a thermal gas flow sensor (see Figure 1); the output, however, is a

frequency signal as opposed to an analog *Voltage signal* of a conventional thermal gas

flow sensor.

Summarizing this brief discussion, the attractive features of using surface acoustic

waves for sensor applications can be stated as follows:

1. The output of a SAW sensor is directly available as a frequency that can be
   conveniently read out in digital form thus no separate analog-to-digital conversion
   is required;

2. The SAW sensor can be interrogated wirelessly based on the radar system
   principle. An interrogation electromagnetic signal is launched by the antenna of

the interrogation unit and is received by the antenna connected with the IDT of

the SAW device (Cheng, Dong, & Feng, 2000);

3. Since frequency can be measured very precisely, the sensor has a high degree of

accuracy;

4. The "dual-oscillator-technique" cancels out the effects of unwanted variables like

ambient temperature variations;

5. Since SAW propagation is very sensitive to changes in the ambient and boundary

conditions, the sensor has high sensitivity;

6. The response of SAW sensors is generally found to be linear over a wide dynamic

range; and

7. These sensors are compatible with the well-established silicon microelectronics

technology.

Scope and Contributions of the Study

The author of this dissertation (Ahmad, 1985) reported the first experimental

SAW gas flow sensor based on the principle of forced convection. A dual SAW resonator

scheme was also developed as an anemometer (Ahmad, 1986). Since then, there has been

consistent progress on this area of study. Numerous citations (Wohltjen, Snow, &

Ballantine, 1985; Anisimkin & Verona, 1998; Wang, Li, Qin, Chyu, & Wang, 2011;

Wang, Li, Qin, Chyu, & Wang, 2012) and patents (Liu, James, Carlson, Magee, 2008;

Brace,and Sanfelippo, 1990; Joshi, 1991; Liu, Rahman, Honeywell International, 2006)

based on gas flow have been reported. A thermometric mass flow rate sensor which

measures the temperature change of the device from the heat drawn from the surface with

constant temperature due to the fluid has also been developed based on the similar

principle of thermal change (Nomura, Saitoh, & Koyama, 2007. However, no analytical/mathematical models for SAW-based gas flow measurements has been reported in the literature.

This dissertation bridges the literature gap regarding SAW-based gas flow measurements proposes the following contributions to advance the discipline:

1. A mathematical model that will enable the characterization of a SAW-based gas flow sensor model for any substrate material, flow geometry, and sensor structure; the findings of which will govern the production of an optimal SAW-based gas flow sensor design.

2. A theoretical model of a SAW-based gas flow sensor derived with the following considerations:

    a. Model must make use of a flat thermal sensor with adjustable dimensions

    b. Model must be applicable to any gaseous fluid

    c. Model must be a thermal gas flow sensor independent of a given substrate and evaluates characteristics under the following conditions:

        i. Steady state *no flow* condition

        ii. Steady state *laminar forced flow* conditions

3. Determine/model the time response for the sensor given

4. Develop an optimal model for various SAW-based gas flow sensor

5. To validate the model, a SAW-based gas flow sensor experimental setup was designed and experiments were carried out. The structure, geometry with dimensions of the SAW devices and flow cell used in this research are described. The experimental measurements consisted of the following variables:

a. Changes in the frequency of the SAW oscillator as a function of input power to thin-film heater element.

b. Temperature rise of the SAW oscillator versus input power to thin-film heater element.

c. Changes in the frequency of SAW oscillator as a function of flow rate for various values of power to heater.

d. Power changes of the thin-film heater as a function of flow rate.

This study exemplified the fusion of technologies as it demonstrates how SAW can be used in conjunction with conventional heat transfer theories as a means of producing new sensing techniques. Being the author of first reported SAW-based gas flow sensor (Ahmad, 1985), the author was keen to develop a theoretical model for the SAW-based flow sensor and thus design an optimal SAW-based gas flow sensor that can provide features that are equal to or better than conventional thermal sensors. The rationale of the study was supported and carried out by modeling the behavior of SAW-based gas flow sensing as follows:

- **SAW Characteristics –** Review, description and application of the principles of SAW devices, SAW oscillator, and sensing techniques followed by the evaluation of SAW characteristics' suitability for different substrate materials.

- **Heat Transfer Analysis** – Thermal analysis dealing with flat plate geometry with an internal heat source is carried out. An electro-thermal analog circuit will be derived.

- **Analytical Heat Flow Model** – The models allow SAW gas flow sensor characterization. The power-temperature results from the electro-thermal analog

circuit analysis are used. The analytical heat flow model will predict temperature distribution under steady-state condition as a function of input power to the heater element. It considers all sources of energy dissipation, e.g., conduction, free/natural convection and radiation. The model predicts the steady state temperature distribution and allows us to derive average temperature under a wide-range of operating conditions.

- **Time Response –** Theoretical model that predicts time response of SAW gas flow sensor is also developed.

Definition of Terms

Definitions and terms used in this dissertation are provided in Table 1.

Table 1 – Definition of Terms (Mathews, 1977)

Parameters	Descriptions
Coupling factor, K^2 (Mathews, 1977)	The coupling parameter expresses the fractional change in the phase velocity of a surface wave produced by a change in the electrical boundary condition from free to short circuit. Similarly, an effective electromechanical coupling factor for surface waves is defined as: $K^2 = -2\Delta v/v$ where v is the phase velocity of the SAW.
IDT	Used to refer to an interdigital transducer which converts one energy form into another form in a digit-like periodic pattern of parallel electrodes to build up the capacitance associated with electric fields which penetrate material samples or coating.
Q factor	Q is defined as the ratio of energy stored to that of energy lost.
Synchronous or Center Frequency, f_o	The center frequency, f_o, is the synchronous frequency of the SAW device determined by the spacing of the IDTs.
SAW	Surface Acoustic Wave; an acoustic or Rayleigh wave which propagates along the surface of an elastic substrate whose amplitude decays along with increased substrate depth.
SAWR	Surface Acoustic Wave Resonator
Center Wave Length, λ_o	Defined as ratio v/f_o where v is SAW velocity.

Overview of the Study

Chapter 1 presents the introduction to the study; moreover, it states the problem clearly as well as its significance and implications to future practice. The scope of the study is also defined along with the definition of the terms that govern the study.

Chapter 2 reviews the fundamentals of SAW technology. SAW oscillators have significantly improved RF signal processing and have been successfully applied in frequency synthesis applications. Saw oscillators are now a key component to the development of SAW-based sensors. Studies covering the necessary design considerations for highly stable SAW oscillators are also reviewed. An overview of SAW-based sensors using SAW oscillators is provided in Chapter 2. In addition, the literature thermal sensors based on the principle of hot wire/hot film anemometer is also reviewed.

Chapter 3 presents theory of heat transfer applicable to enclosed flat plate with an embedded internal heat source. It will be applied to develop a theoretical model to characterize SAW-based gas flow sensors. The presented model will be applicable to accommodate a wide range of possible geometrical dimensions for the sensor and varied flow set-up. In addition, it allows sensor characterization based on the properties of SAW substrate materials.

Models developed in Chapter 3 are applied, and an analysis of the resulting data is provided in Chapter 4. Based on the knowledge obtained, a design of an optimal SAW-based gas flow sensor is presented.

Chapter 5 provides experimental results on a preliminary SAW-based gas flow sensor. Theoretical calculations based on the model are applied for verification.

Chapter 6 provides a final summary of the analysis, recommendations, and conclusions. A comparative analysis of SAW-based and conventional thermal flow sensors are also provided in the chapter followed by recommendations that may provide useful data in the design of a commercial SAW-based gas flow sensor.

Finally, the bibliography presents a list of the references contained within this study.

CHAPTER 2: BACKGROUND RESEARCH

To model the behavior of and to design an optimal SAW-based gas flow sensor, a review was conducted in different disciplines of technologies. Of importance are the following areas:

- Fundamentals of SAW technology

- Latest developments in SAW sensors and SAW-based gas flow measurement

- Principle of thermal flow sensors

SAW Technology

Surface acoustic waves (SAWs) are generated and detected by using metallic interdigital transducers (IDTs) deposited in a vacuum on a piezoelectric substrate. A typical structure of an interdigital transducer is shown in Figure 2. The fingers of the IDT are $\lambda/2$ distance apart, where $\lambda=v/f$. Here, f is the excitation frequency, v is the surface wave velocity, and λ is the wavelength.
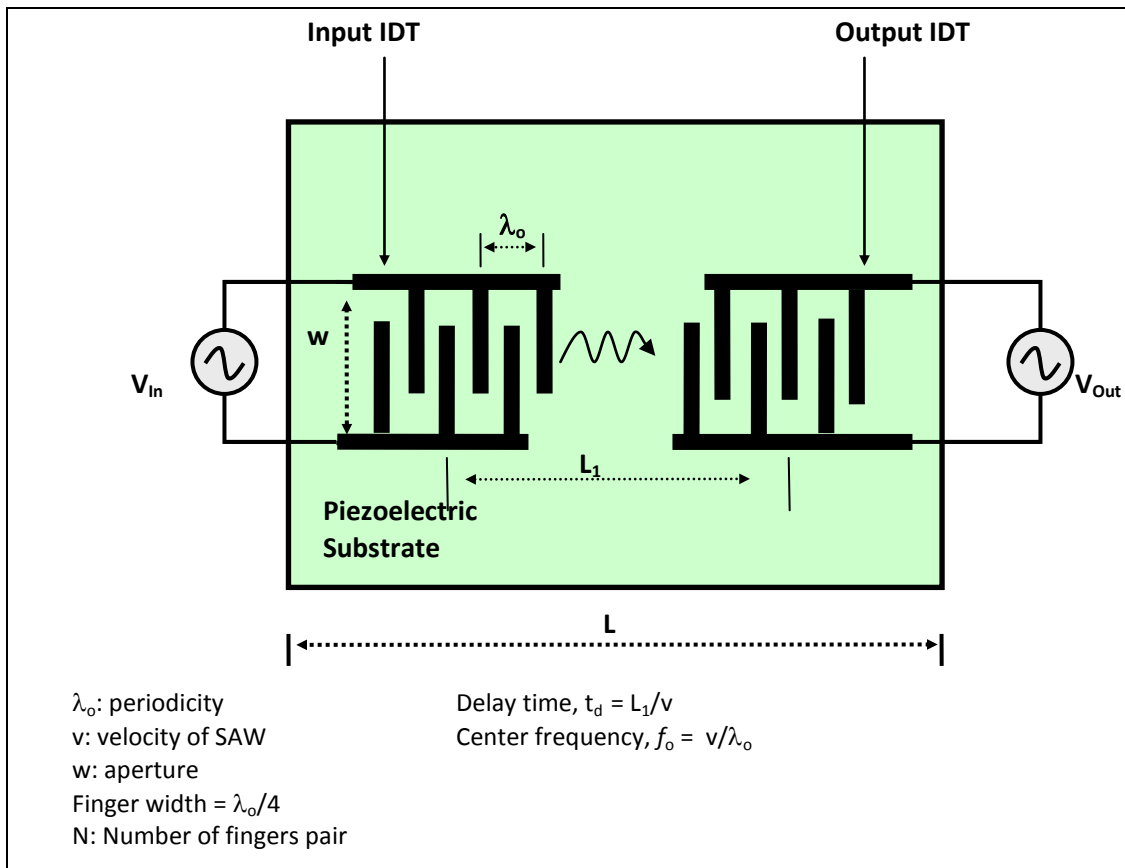
Figure 2. Schematic diagram of a SAW device (delay line).

The figure contains the following labels and annotations:

Input IDT
Output IDT
λ_o
w
V_{In}
V_{Out}
L_1
Piezoelectric Substrate
L

λ_o: periodicity
v: velocity of SAW
w: aperture
Finger width = $\lambda_o/4$
N: Number of fingers pair

Delay time, $t_d = L_1/v$
Center frequency, $f_o = v/\lambda_o$

When an alternating voltage of frequency f is applied to the IDT, an electric field is created between adjacent fingers. A strain field is also generated due to the electromechanical interaction in the piezoelectric substrate; this strain field is an imprint of the IDT and propagates away from the IDT in both directions as a surface wave. The surface wave can be detected by a second remote IDT as the SAW passes through it because the surface wave carries an electric field with it via the piezoelectric effect which generates a voltage between adjacent IDT fingers. The IDT is a planar structure that can be made through a single metallization step. The SAW devices are fabricated by means of planar integrated circuit technology. The growing research in this field has led to new piezoelectric materials and material cuts that have been optimized for particular requirements such as temperature stability or large fractional bandwidth.

SAW devices have been identified as potentially useful for sensing elements (Ebata & Kinoshita, 1982; Inaba & Wasa, 1982; Hauden, Jaillet, & Coquerel, 1985; Vellekoop & Visser; 1988; Leblois & Tellier, 2000; Reeder, Cullen, & Gilden, 1975). The SAW resonator in particular, with its high Q factor, can be used to design a stable and sensitive sensor. This sensor can be fabricated by creating a feedback path for a SAW oscillator. The phase and time delay of the frequency of the oscillator varies almost linearly with applied pressure; this suggests that the oscillator frequency also varies linearly with temperature, pressure, and/or other physical changes; and since the information from a frequency output sensor can be easily converted to digital form by a frequency counter, the SAW sensor serves as a high precision application.

SAW Oscillators

An oscillator circuit consists of an amplifier with a gain $A(\omega)$ and a frequency dependent open loop gain $H(\omega)=\beta A$. The general expression is as follows (Parker, 1982):

$$V_0/V_i = \frac{A}{1-\beta A} \qquad (1.)$$

The expression states that the system will oscillate, provided $\beta A = 1$. At the frequency of oscillation, the total phase shift around the loop must be 360°.

A SAW resonator (SAWR) has the potential of being used as a frequency control device such as an oscillator. The advantages of using a SAWR over LC circuits, coaxial delay lines, and metal cavity resonators are its high Q, low series resistance, small size, and good frequency stability. The high stability and spectral purity in the 50MHZ to 1GHZ range of SAWR oscillators have also been reported (Oliner, 1978; Cheng, Dong, & Feng, 2000)

A schematic diagram of an oscillator using a SAW as a feedback component is shown in Figure 3. The conditions for sustaining the oscillations are:

- The total phase shift around the loop is 0 or equal to $2\pi n$ where n is integer.

- The total insertion loss of the loop is less than the amplifier gain.
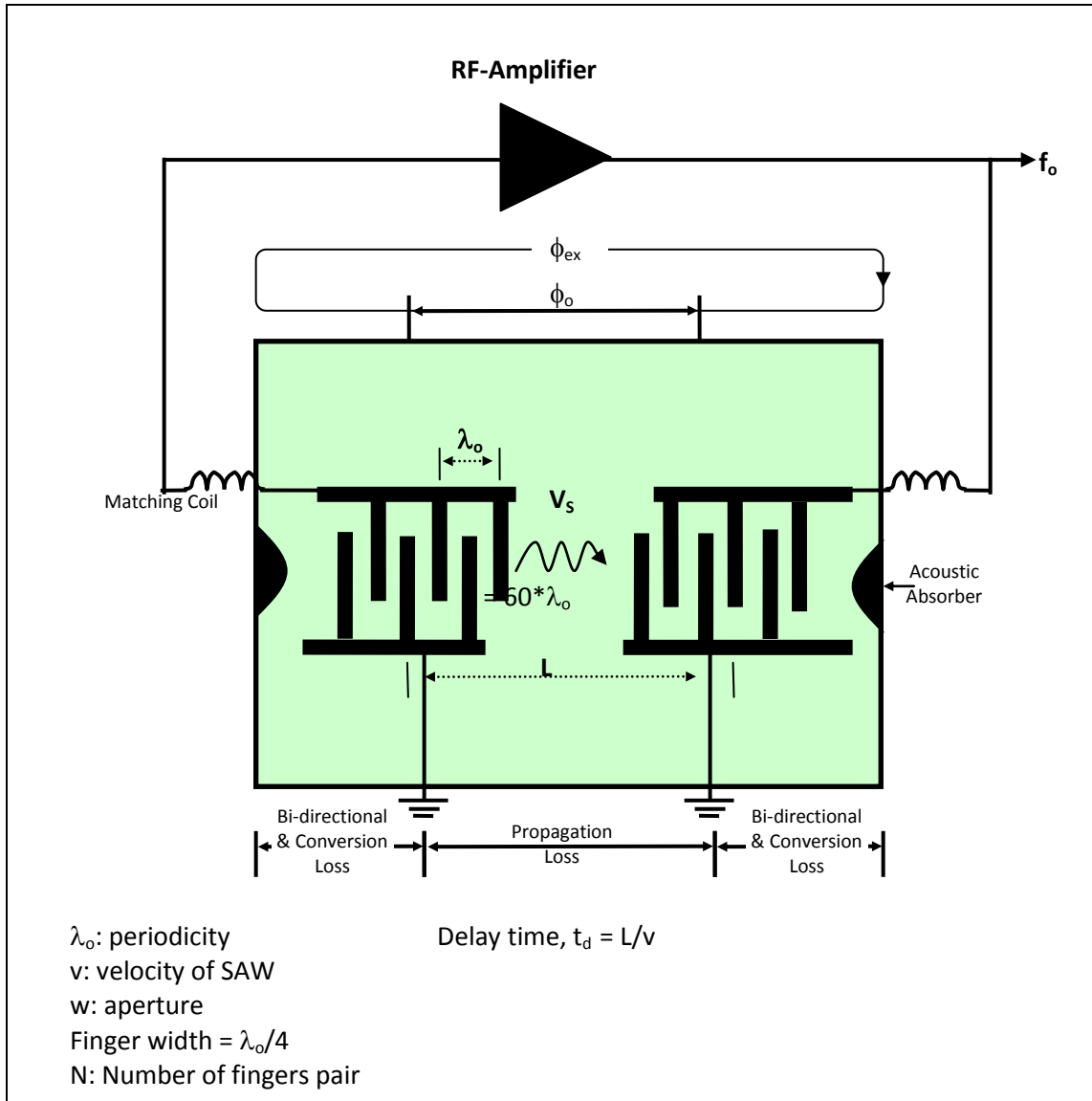
Figure 3. Schematic diagram of a SAW delay line oscillator.

The total phase shift around the loop is:

$$\sum \Phi = \ \Phi_0 + \Phi_{EX} \tag{2.}$$

For oscillation to be sustained:

$$\sum \Phi = 2n\pi = 2\pi f_n(t_d + t_{ex}) \tag{3.}$$

where

$$f_n = \frac{n}{t_d + t_e} \tag{4.}$$

t_d = time delay of the SAW device
t_{ex} = delay time due to the external electric circuit
n = mode integer selected by the frequency passband of the SAW IDT.

Now $t_d \gg t_e$, thus:

$$f_n \approx \frac{n}{t_d} \tag{5.}$$

The fractional change in frequency is described as:

$$\frac{\Delta f_n}{f_n} = -\frac{\Delta t_d}{t_d} = \left|\frac{\Delta t_d}{t_d}\right| \tag{6.}$$

$\Phi_0 = \omega t = 2\pi f L/v_s$ is the phase shift experienced by a wave traveling from an input IDT to a similar IDT situated a distance L from it. Φ_{EX} is the electrical phase shift associated with the amplifier and transducers. The acoustic phase shift $2\pi f L/v_s$ is typically 200-2000π which greatly exceeds 2π. Therefore, the oscillator generates a comb of frequencies $w = 2n\pi c/L$ with different integer values n.

To obtain a precise frequency control, an oscillator must contain an element having a phase characteristic which varies very steeply with frequency. In the SAW oscillator, this element is the delay line which has a transfer phase slope $d\Phi/df$ proportional to length. The spacing of the resonant frequencies is f_0/N, where f_0 is the center frequency of the transducers, and N is the number of wavelengths contained in L. Generally, the mode spacing is much narrower than the width of the gain characteristic of the amplifier so that oscillations can be obtained at a number of different frequencies separately or even simultaneously. Normally, a single frequency output is required;

having said that, there are applications in which the simultaneous presence of a set of frequencies is required. A mode control operation, however, is required regardless of the frequency.

Single mode operation is ensured when the loop gain is made less than unity for all but the desired oscillation frequencies. To alternate the unwanted frequencies, an additional selectivity is built into the device. This is accomplished by making one of the transducers sufficiently narrow band. Specifically, by making the transducer's length $N_T\lambda$ and by spacing its center from the center of the other short transducer by the same distance, it can be ensured that all of the solutions of *Equation (2)* will fall on the zeros of the transducer response. This method of mode control is effective; however, as shown in Figure 4, half of the average acoustic path lies under the long transducer. For the usual mark to space ratio of 1:1, a metallic thin film covers one quarter of the path. This causes a significant increase in the alteration and subsequently decreases the Q factor.

Furthermore acoustic reflections and regeneration may cause serious problems in such a long transducer and lead to unwanted responses. These undesirable characteristics are avoided and the location of zeros and length of the long transducer are retained by a configuration as shown in Figure 4(b). This structure for the SAW oscillator was very popular, but there have been succeeding studies regarding the SAWR oscillator which proved to be more advantageous and will be discussed in the following section.
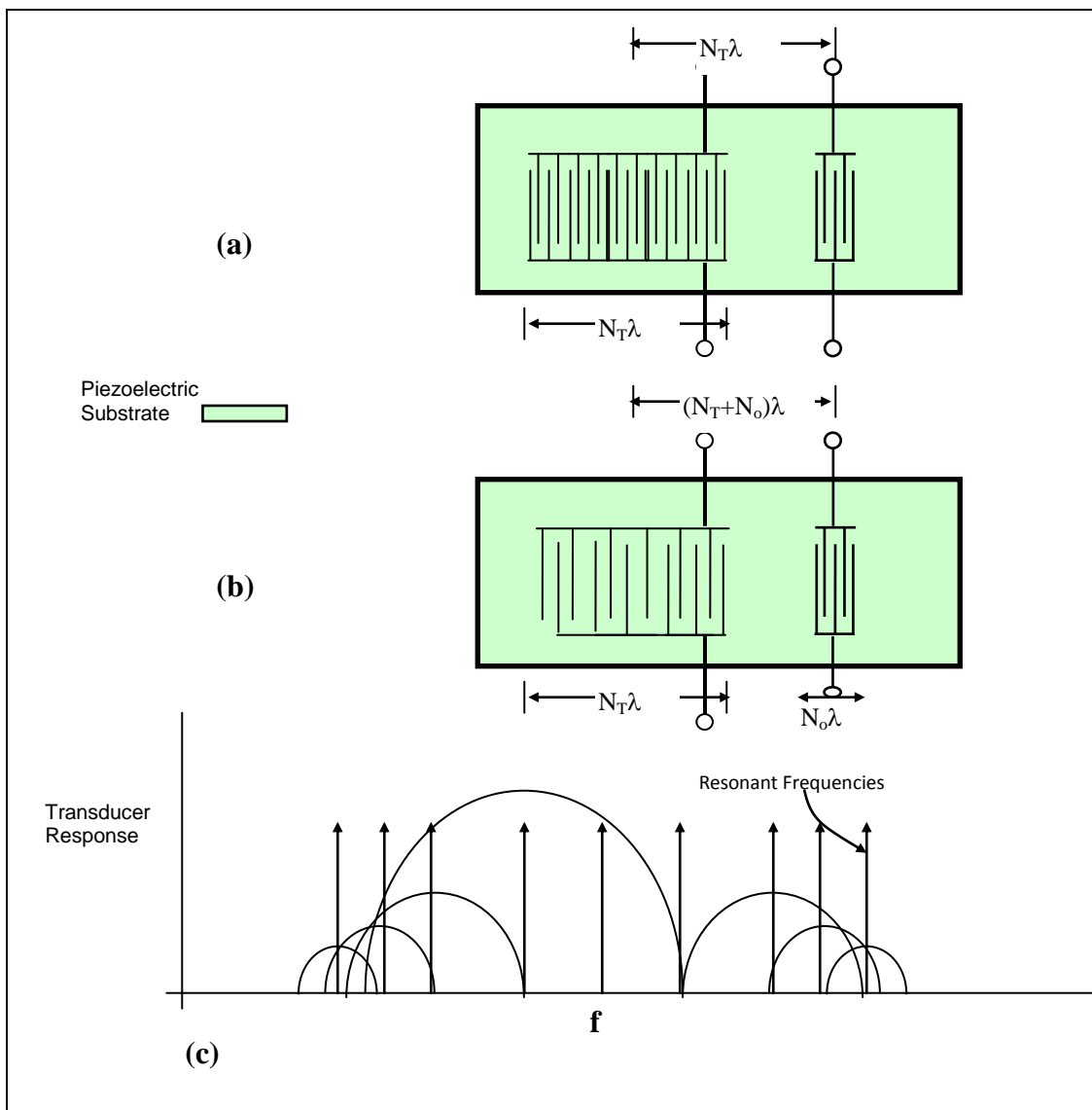
Figure 4. Strategies for choosing mode propagation; (a) use of a long transducer; (b) use of a long thinned transducer; and (c) response of transducer in (b) (Lewis, 1974).

Oscillator Stability

There have been many reports dealing with the study of the frequency stability of

SAW oscillators (Matsumoto, Sudo, Sinha, & Niwa, 2000; Cross & Scott, 1981; Bray &

Chu, 1981; Wall & Wainwright, 1975; Joseph, 1976; Miyasaka et al., 1985; Parker, 1982;

Lewis, 1974; Lee, 1979; Penavaire et al., 1980; Shereve et al., 1981; Ebata et al., 1982;

Stokes & Delaney, 1983; Stokes, 1982; Campbell, 1987; Parker & Callerame, 1981;

Parker, ; Parker, 1979; Allan, Shoaf, & Halford, 1974). SAW oscillator stability is divided into three regions:

a. **Short term** (~ one second)

   The dominant cause of short term stability is the phase noise or 1/f. The phase noise of SAW oscillators can be predicted by calculating the Allan-variance of frequency.

b. **Medium term** (~ one hour)

c. **Long term** (~ one year)

   Long-term frequency stability has been studied in terms of aging behavior. Two processes may contribute to long term aging of SAW oscillators: a) random fluctuations and b) systematic drift. The random fluctuations are due to a random walk noise, which may be referred to as aging noise, and is less predictable. Systematic physical processes such as stress relaxation, aluminum oxidation, or driving current levels, among others cause the more predictable systematic component. The contributions due to systematic drift can be of the order of a few ppm/year. It has been found that long-term aging is generally lower on resonators than on delay lines.

   The short-term stability measured within intervals of a second or less is determined largely by noise. Thus, the performance and the stability of the oscillator can be seen through its output power spectrum, $S_{RF}(\omega)$. To obtain quantitative insight of $S_{RF}(\omega)$ and hence, other measures of short term stability, the following assumptions are made:

1. The oscillator frequency of the oscillator is equal to the center frequency of the transducer, i.e. $\omega_0 T = 2\pi n$, where T is the SAW delay time.

2. Amplifier acts as an isolator to suppress unwanted waves traveling round the loop in the "wrong" sense.

If the oscillator is below threshold and an input signal $Ve^{j\omega t}$ is injected at the input of the amplifier, then the output will be given by (Shereve, 1981):

$$V_{0UT}(\omega) = GVe^{je\omega} + A(\omega)e^{j\omega(t-T)} + A^2(\omega)e^{j\omega(t-2T)} \tag{7.}$$

Here, $A(\omega)$ is the amplitude transmission factor round the loop, and T is the delay line. Also,

$$A(\omega) = GL(\omega) \tag{8.}$$

where G is the amplifier gain and $L(\omega)$ is the delay line loss. The output power $P(\omega)$ varies with ω as (Shereve, 1981):

$$P(\omega) = \frac{G^2V^2}{R_{0UT}} \left[\frac{1}{1+A^2(\omega)-2A(\omega)\cos(\omega-\omega_o)\tau} \right] \tag{9.}$$

The output impedance R_{OUT} of the amplifier is assumed equal to the input impedance. When $A(\omega) < 1$, this expression is analogous to the response of a Fabry-Perot interferometer with a series of equally intense peaks at frequencies $w \approx 2\pi n/T$. In the case of SAW oscillator, $A(\omega)$ is determined by the transducers, when a mode selecting arrangement is employed, only one transmission peak at ω_o remains.

For the SAW oscillator above threshold, the input to the amplifier is the noise from its first stage, while $A(\omega)$ is determined by the condition:

$$\int_{\omega_0-\pi/\tau}^{\omega_0+\pi/\tau} P(\omega)d\omega = P_o \tag{10.}$$

which yields:

$$1 - A^2(\omega_o) \cong 2[1 - A(\omega_o)] = 4kT(NF)G^2/P_o\tau \tag{11.}$$

Substituting this derived value for $1\text{-}A^2(\omega_o)$ in *Equation (9)*, the output power

spectrum of the oscillator, $S_{RF}(\omega)$ can be obtained. Short-term stability can then be

calculated from a plot of $S_{RF}(\omega)$ versus offset frequency for a SAW oscillator. Noise

measurements from the plot yield short-term stability and SAWR oscillators exhibit low

values of short-term stability (10^{-11} from 0.001 to sec). The output power spectrum

$S_{RF}(\omega)$ valid for frequencies well within the main lobe of the transducer response can be

expressed as (Shereve, 1981):

$$S_{RF}(\omega) \cong \frac{(2/\pi)kT(NF)G^2}{\left[\frac{2kT\omega_o}{P_oQ}\right]^2 + \left[\frac{Q(\omega-\omega_o)}{\omega_o}\right]^2} \tag{12.}$$

Therefore, the optimum short term stability can be achieved using the following:

1. A low-noise high-power amplifier

2. A low-loss delay line (since the amplifier gain G^2 has to offset this loss)

3. A long acoustic path

One way to express the results is to compute the degradation in Q from $w_o\tau$ to an

effective value

$$Q_{eff} = \omega_o\tau(D)^{-1/2} \tag{13.}$$

The variation of Q_{eff} with path length results in the limiting values attainable at different

frequencies. The full potential of the lower frequency SAW oscillators cannot be met

with quartz samples less than 100 cm long, and a SAW resonator is necessary in this

respect.

L. Penavaire, et al. (1980) studied the short term stability of SAW resonator oscillators. To achieve the good short-term stability of a SAW resonator oscillator, it is necessary to optimize the resonator in terms of insertion loss and loaded Q as well as the associated electronics in terms of noise-figure and flicker noise. The analysis of the phase noise spectrum is made with the assumption that the only noise source is in the loop amplifier. The noise power in 1HZ bandwidth to available input power ratio, is given by (Penavaire et al., 1980):

$$\frac{P_N(f)}{P_0} = \frac{K_f}{f^\alpha} + \frac{(NF)kT}{P_0} \tag{14.}$$

where kT is the thermal noise power in 1HZ bandwidth, NF the noise-figure of the amplifier of the frequency and a number close to 1. K_f is the parameter characterizing flicker noise. For a SAWR oscillator oscillating at f_0, the transfer function of the loop is (Penavaire et al., 1980):

$$|H(f)|^2 = 1 + \left(\frac{f_0}{2Q}\right)^2 \frac{1}{f_m^2} \tag{15.}$$

where f_m is the offset frequency. The phase noise spectral density of the oscillator is then given by (Penavaire et al., 1980):

$$\left[\frac{P_{SSB}}{P_c}\right]_{\frac{dBc}{Hz}} = 10\log\left[\frac{k}{f_m} + \frac{F_0kT}{P_c}\right]\left[1 + \left(\frac{f_0}{2Q}\right)^2 \frac{1}{f_m^2}\right] \tag{16.}$$

where P_{SSB} and P_C are respectively the single side band phase noise power in a 1Hz bandwidth and the carrier power. F_0 is the noise-figure of the oscillator given by $F_0 =$ (NF) × A. A is the insertion loss of the resonator and k is the factor giving the amount of flicker phase noise of the oscillator.

In order to make an oscillator with a noise floor lower than -175dBc/HZ and a low noise spectrum close to the carrier (~ 150 dBc/HZ at 1KHz offset), *Equation (16)*

shows that it requires a low loss (< 6dB) and high loaded Q (> 20000) and (iii), a loop

amplifier delivering l3 dBm with a noise-figure less than 4dB and a K factor near 10^{-13}.

Q_{UL} is unloaded Q and T the transmission gain through the resonator at resonance:

$$Q_{UL} = \frac{1}{1-T} Q_L \qquad \text{(17.)}$$

This implies that Q_{UL} must be even higher than 40,000. The resonator must be designed

so as to minimize all losses such as diffraction, bulk wave radiation, ohmic losses, and

radiation through the arrays. The quoted characteristics of an example of a 120-MHz

resonator are:

- reflector type: grooved array

- two part structure

- transducers type: split electrodes with cosine weighting

- number of grooves per array 750

- nominal groove depth: 0.0l λ_0

- distance between transducers (axis to axis): 50 λ_0

- aperture: 2500 µm (about 95 λ_0)

- substrate: 36 ^{o} rotated y-cut quartz

     Encapsulating the resonator in a vacuum eliminates the air loading losses and

therefore Q_{UL} is limited only by propagation losses in the material. The resonator thus

fabricated had an insertion loss between 5dB and 6dB, loaded Q's between 20,000 and

22,000, and unloaded Q's between 45000 and 50,000.

Increasing resonators unloaded Q would further improve the short term stability to even

figures like −160 dBc/Hz at 1 kHz and a noise floor below −175 dBc/HZ.

In addition, the **short-term stability** can be improved by reducing amplifier gain and increasing amplifier input power.

      Medium term stability arises by temperature drifts. The variation of a quartz SAW oscillator frequency f with temperature T ^{o}C is expressed as (Hauden, Jaillet, & Coquerel, 1981)

$$f(T) \cong f(T_o)[1 + a_o(T - T_o) + b_o(T - T_0)^2] \tag{18.}$$

where a and b are temperature coefficients (TC s) of the first and second order of the frequency at reference temperature T (25^oC) (static thermal behavior), $f(T_o)$ is the maximum frequency occurring at temperature T_0. This effect can be reduced in two ways: to use a superior orientation of quartz with a better temperature of delay (TCD) or to thermostat the oscillator.

      Long-term stability is associated with aging rate. The SAW oscillator is an order of magnitude worse than conventional quartz crystal oscillators. The possible aging mechanisms are:

- The relaxation of strains in the quartz crystal

- Atomic diffusion of electrode material into quartz crystal

- Miscellaneous dirt effects like the pressure of water or organic layers on the quartz surface, oxidation of the aluminum film, etc.

      W. R. Shreve et al. (1981) observed that the aging rate in SAWR oscillators vary as the power is varied. They reported their results at power levels from −10 dBm to +20 dBm. The power level was determined by probing the circuit with a vector voltmeter and checking this value by assuming current limiting in the transistor amplifier. The drive level of the oscillator was determined by finding the power dissipation in the SAWR. The

power dissipation could be determined from the SAWR equivalent circuit and the current through or voltage drop across the resonator independent of the source and load. The relation between power dissipated in the resonator, P_d and the peak stress is given by (Shereve et al., 1981):

$$|T_{11}|_P = J_m \left[\frac{Q_u P_d}{LW}\right]^{1/2}$$

(19.)

where J_m is a constant of the material, Q_u is the unloaded resonator Q, L and W are the effective cavity, length, and width respectively. This stress, the peak compressional stress in the propagation direction, can be used to characterize the stress field at the piezoelectric surface; however, it is accompanied by a stress perpendicular to the propagation direction T_{22} and shear stresses T_{12} and T_{21}. The ratio of these stresses is determined by the crystal constants and crystal cut. At -7dBm drive level the peak stress was $(2.1\pm0.2)\times10^7$ N/m^2.

The aging results on two part SAWR oscillators indicated that the maximum stress corresponding to the onset of aluminum migration appears to be 5 to 10 x 10^7 N/m^2 and also appears to vary somewhat presumably due to processing differences between devices. The aluminum in the center of the cavity migrates and forms dendrites protruding from the film. The frequencies at high stress level (9 to 11 x 10^7 N/m^2) shifts dramatically and the oscillators stop oscillating. In those cases, it was found that the series resistance had increased, the Q had decreased, and the frequency response was distorted by transverse modes. The increased series resistance caused the oscillators to quit.

The phenomenon of acousto-migration is similar to that of electromigration induced by high currents in their aluminum films, and therefore the copper-doped

aluminum film should improve the film lifetime. The SAW resonators fabricated with pure aluminum and with copper-doped aluminum were compared in an accelerated aging system at high stress levels. It was found that doping increases the power handling capability by at least l2 dBm.

Great deals of efforts have been devoted to studying the frequency stability of SAW oscillators. The dominant cause of short-term stability is the 1/f or phase noise[1]. The phase noise of SAW oscillators can be predicted by calculating the Allan-variance of frequency. Long-term frequency stability has been studied in terms of aging behavior. Two processes may contribute to long term aging of SAW oscillators: a) random fluctuations and b) systematic drift. The random fluctuations are due to a random walk noise which may be referred to as aging noise and is less predictable. The more predictable systematic component is caused by systematic physical processes such as stress relaxation, aluminum oxidation, or driving current levels, etc. The contributions due to systematic drift can be of the order of a few ppm/year. It has been found that long-term aging is generally lower on resonators than on delay lines.

SAW Sensing Applications

Surface Acoustic Wave (SAW) devices have their most profound impact has been in the area of signal processing. A simple example is a SAW delay line. An electrical input signal applied to an IDT produces an ultrasonic signal, which ultimately propagates to an output IDT. Other signal processing devices include filters (bandpass, notch matched, inverse, programmable, pulse compression comb), oscillators, resonators, coders, convolvers, and correlators.

---

[1] The term phase noise is phase fluctuations due to random frequency fluctuations of a signal. Frequency stability is a measure of the degree to which an oscillator maintains the same value of frequency over a given time.

Unique features of SAWs include the concentration of energy near the surface, the ability to tap or sample waves as they propagate, and the existence of a traveling electric field accompanying the wave in piezoelectric media. Applications of SAWs consist of sensing applications, thin-film properties, measuring fields, determining semiconductor properties, and measuring elastic properties at surfaces. The remote interrogation of the SAW signal for sensor applications could potentially be another attractive feature that will propel SAW-based sensors to the commercial success it deserves.

A block diagram using a SAW delay line (or resonator) stabilized oscillator as a sensor was shown in Figure 1(b). Since SAW propagation is very sensitive to external variables (pressure, temperature, etc.), the frequency of the oscillator varies when any of these parameters is changed. The change in frequency of the oscillator is interpreted in terms of the external variable to be sensed.

SAW Temperature Sensor

Temperature variations affect SAW properties. In particular, the propagation velocity to temperature relationship follows a polynomial equation given as:

$$f(T) = f(T_o)[1 + a_o(T - T_o) + b_o(T - T_o)^2 + \cdots]$$
(20.)

where a_0 and b_0 are temperature coefficients (TCs) of the first- and second-order of frequency at reference temperature T_o (25 ^{o}C). Large temperature sensitivity and a good linearity are possible if a_o is large and b_o is negligible in *Equation (20)*. For anisotropic mediums such as *quartz* or *lithium-niobate*, the thermal behavior of SAW depends on three angular parameters (cut angles ϕ, θ, ξ) and propagation direction (Mathews,

1977). Table 2 lists first- and second-order temperature coefficients of *quartz* and *lithium-niobate* substrates.

Temperature sensors have demonstrated high sensitivity and broad range. If one considers stability of a SAW oscillator between 3×10^{-10} and 10^{-9}/a few seconds, resolutions in temperature measurement of the order of $10 \ \mu \ ^{o}C$ to $30 \ \mu \ ^{o}C$ are possible.

Table 2 – Temperature coefficients of delay (TCD) for several SAW substrate materials.

Temperature coefficients of various substrates (Mathews, 1977)			
Substrate	Cut	First order (ppm/^{o}K)	Second order $(10^{-9}/K^{2})$
LiNbO$_3$	Y-Z	-88.4	5.6
LiNbO$_3$	128°, X	-72	-
Quartz	JCL	18	-1.5
Quartz	LST	28	-2

SAW Gas Flow Sensor

A SAW-based gas flow sensor based on the principle of forced convection has already been reported in literature (Ahmad, 1985). A SAW gas flow rate sensor can be realized using the principle of heat transfer with the flow of a gas over the substrate. It consists of a SAW delay line fabricated on a suitable substrate and a thin-film heater to heat the SAW device to a suitable temperature above the ambient. The delay line is connected in the feed-back loop of an RF amplifier creating a delay-line-stabilized SAW oscillator. When gas flows over the SAW device, it carries away heat thus lowering the temperature of the substrate. The change in the frequency of the SAW oscillator, which can be accurately measured, is proportional to flow rate of gas. The device is similar in principle to a hot-wire or hot-film anemometer.

The phase velocity v(x,t) of a SAW delay line oscillator in one dimension can be expressed as a power series:

$$v(x, t) = v_o(1 + a_o \Delta T(x, t) + \cdots) \tag{21.}$$

where a_o is the temperature coefficient of velocity and $\Delta T(x,t)$ is the variation in temperature along the x-axis with respect to time. When gas flows over the heated substrate, it carries away some thermal energy and reduces the substrate temperature. The change in the phase velocity Δv is expressed as:

$$\Delta v = v_o a_o \Delta T(x, t) \tag{22.}$$

and the resulting phase difference, $\Delta\phi$, between the input and output transducer is given as:

$$\Delta\phi = -f/2l \int_{-l}^{+l} a_o \Delta T(x, t) dx \tag{23.}$$

where 2l is the distance between center of the transducers. If there exists a thermal gradient between two regions, heat is transferred from a high-temperature region to low temperature-region by conduction, convection, and radiation processes. A SAW flow model must account for the heat losses due to all mechanisms of heat transfer. However, an optimal SAW flow sensor thus must have minimal heat loss due to conduction and radiation processes.

The author first reported a SAW-based gas flow sensor (Ahmad, 1985). Since then, many researchers have reported SAW-based flow sensors. These studies have mostly focused on refining geometries and packaging schemes (Shen, Qin, Huang, 2006; Nomura, Saitoh, Koyama, 2007; Wang et al., 2011; Wang et al., 2012; Liu, Carlson, & Magee, 2008; Joshi & Sanfelippo, 1990; Joshi, 1991; Liu & Rahman, 2006). Recent

papers (Nomura, Saitoh, & Koyama, 2007; Wang et al., 2012) that report SAW-based gas flow measurements are reviewed and analyses are provided below.

The paper by Tooru Nomur et al. (2007) validated the author's original paper (Ahmad, 1985) that a SAW flow sensor based on the principle of forced convection can be realized. A comparative analysis of this paper with this dissertation is provided is provided in Table 3. The experimental set up and the summary of results are also described below.
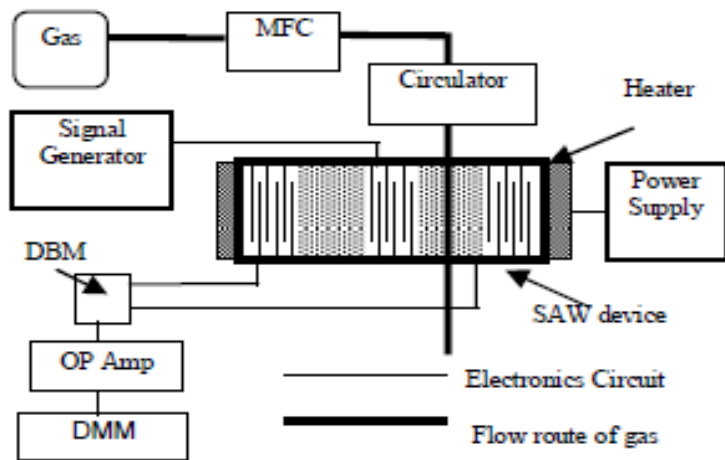
Figure 5. Experimental setup for mass flow rate sensor (Nomura, Saitoh, & Koyama, 2007).
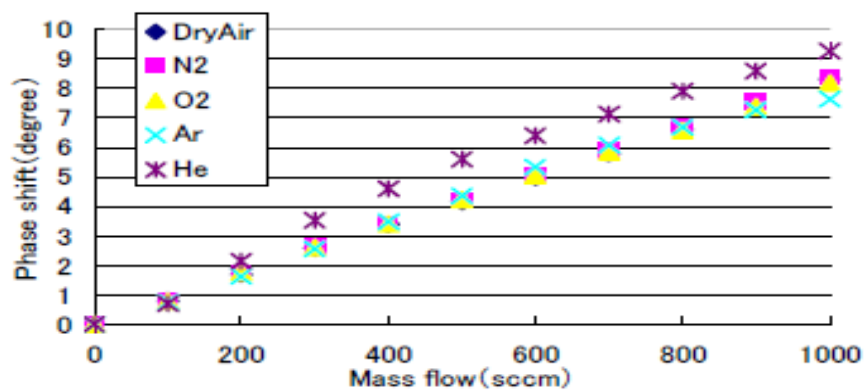
Figure 6. Phase shift versus mass flow rate (Nomura, Saitoh, & Koyama, 2007).

Table 3 – Comparative analysis of latest research with dissertation.

	Reported studies (Nomura et al. , 2007)	**Dissertation**
1.	Tooru Nomura et al. reported an application of SAW -based flow rate sensor that utilizes the temperature characteristics of SAWs. The experiment used a substrate of 128° Y cut X prop. LiNbO3 (128° YX - LiNbO3) has a relatively large temperature coefficient of -74 ppm that provides high sensitivity to small changes in temperature	The paper validates the author, Nisar Ahmad's original paper (Ahmad, 1985) that a SAW flow sensor based on the principle of forced convection can be realized. The paper is empirical in nature and lacks exhaustive analytical and mathematical analyses. This dissertation's mathematical modeling is applicable provided that all dimensions of the set-up are available.
2.	The sensor described in the paper consists of two channels of delay lines on a piezoelectric substrate; one being the sensing channel and the other is the reference channel. While these two delay lines are maintained at a constant temperature, the fluid to be measured is applied to the sensing channel. Heat is then transferred to the fluid, changing the corresponding delay line's temperature, and this change is detected as a change in the SAW's velocity (phase	The sensor set up provides design improvements by including a reference SAW device for compensating any fluctuation in ambient temperature and stabilizing response time.
3.	The studies and results are empirical; it lacks exhaustive analytical and mathematical modeling and/or analyses.	The paper does not provide the analytical and detailed theoretical analyses that the author is proposing in the dissertation. The theoretical analyses derived by the author for the dissertation can equally be applied to verify the sensor behavior. However, the geometry of the proposed design is not well defined and/or documented in the paper.

Wang et al. (2011; 2012) reported a novel SAW-based gas flow sensor that
operates on stress sensitivities of the SAW device. The study, however, approaches the
problem differently from this dissertation work. They propose a SAW flow sensor based
on pressure measurement. The relationship between the flow rate and the pressure
difference along the flow path is utilized to devise a SAW-based flow meter. The
proposed flow meter essentially functions as a pressure sensor. A comparative analysis of
this pressure-based flow sensor and the work proposed in the dissertation is captured in
Table 4.

Table 4 – Comparative analysis of latest research with dissertation.

No.	Reported studies by Wang et al. (2011, 2012)	Dissertation
1.	Wang et al. (2011; 2012) reported a SAW-based flow sensor that operates on stress sensitivities of the SAW device.	This dissertation is on a SAW flow sensor based temperature dependence of SAW. The sensor is operated at elevated temperature and utilizes principle of forced convection to carry heat and thus result in change in temperature.
2.	The resonant frequency shows hardly any change with flow rate since there is no temperature dependence.	Several SAW substrates such as $LiNbO_3$ has high temperature sensitivities so the sensor has high sensitivities and wide operating range.

Wang et al. (2011; 2012) also derived a detailed theoretical analysis is and
compared the findings with experimental results. ST-X cut quartz SAW delay line device
was chosen for its ultra-high temperature stability. For pressure driven laminar flow, as
shown in Figure 7, the pipe wall is subject to pressure along the flow direction. The
pressure on the wall decreases linearly towards the exit. When a sensor is mounted on the
pipe wall, the sensor will also be subjected to linearly decreased pressure. For sensors

with small surface area compared to pipe dimension, the pressure can be assumed to be uniform as shown in Fig. 7 (c). Since flow rate depends linearly on pressure, the flow meter essentially functions as a pressure sensor.
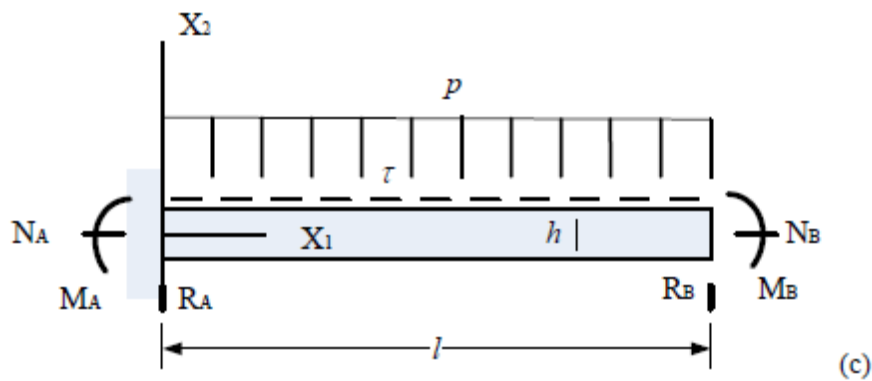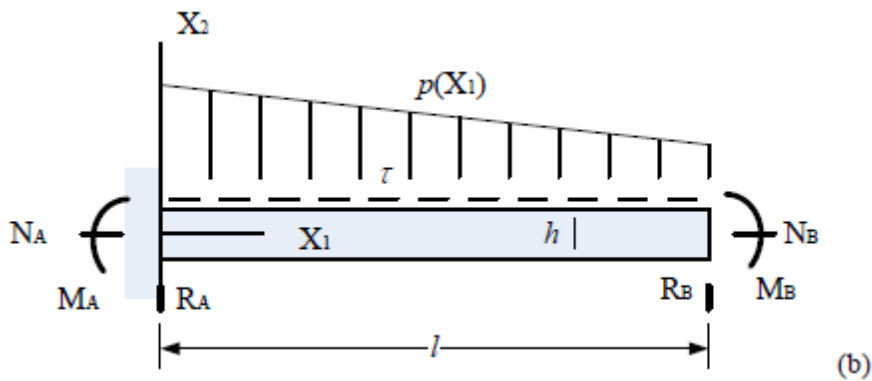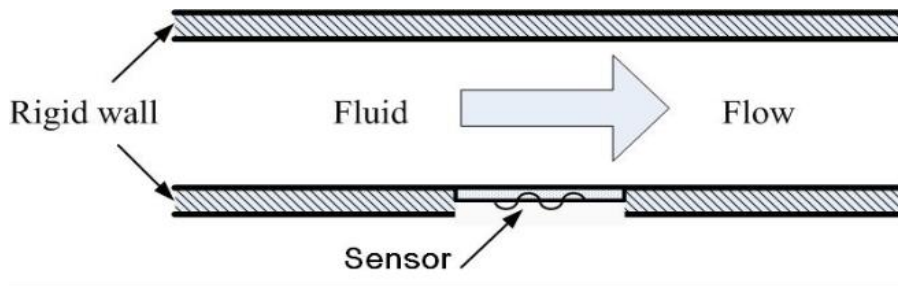
Figure 7. Schematic view and physics model of flow sensor; (a) schematic view of the pipe and sensor, (b) sensor is subject to linearly decreased pressure, (c) normal pressure can be simplified as uniform for small sensor surface area, Wang et al. (2011; 2012).
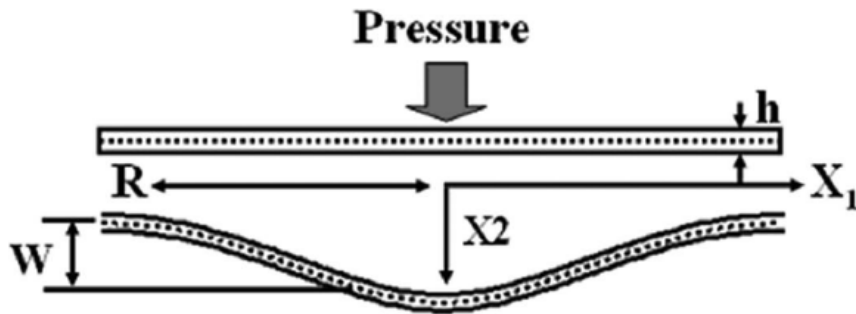
Figure 8. Simulation of the substrate deformation under pressure, Wang et al. (2011; 2012).

As shown in Figure 7(a), along the symmetrical line of the substrate, the area close to the clamped end will be subjected to compression and the area on the center will be subjected to tension. The IDTs are selected to have a minimal deformation under pressure and the SAW propagation path is entirely located on tension area.
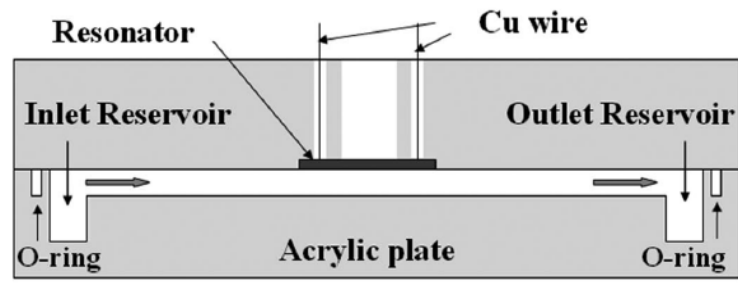
Figure 9. Designed and completed test setup, Wang et al. (2011; 2012).

The experimental result (Figure 10) shows irregular frequency change with the increase of the flow rate which is different from the expected frequency decrease. The output of the sensor is measured in terms of phase change ($1^{\circ}/11.8$ mL/min) because of change in delay time.
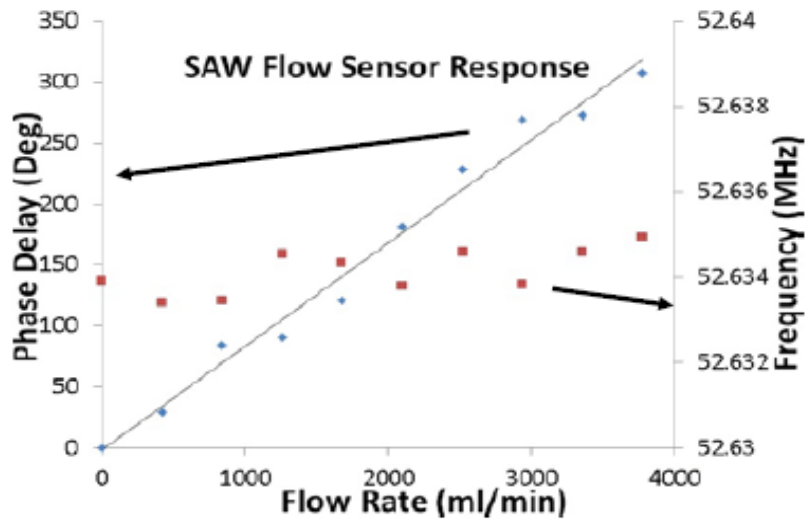
Figure 10. Experimental results (Wang et al., 2011).

The auther (Wang et al. 2011) did not explain why the phase changes appear to be linear with flow rate, yet, the corresponding frequency change is not.

SAW Pressure Sensor

SAW resonator pressure sensors based on stress sensitivity of quartz have been reported (Reeder, Cullen, & Gilden, 1975, Risch, 1984; Weirauch, Scwartz, & Bennet, 1979; Dias, 1981). Using a dual oscillator scheme, a non-linearity of 0.18 percent in full pressure range of 0 to 50 psia was obtained. The scheme also demonstrated a high temperature stability of -1.7 Hz/$^{\circ}$C from 50 to 100 $^{\circ}$C temperature range.

Dias (1981) described a force sensor using a double oscillator scheme. Temperature compensation and double force sensitivity was obtained by fabricating SAW delay lines on both faces of the substrate. A force sensor was created by using a cantilevered structure of a SAW device. When the substrate was deflected, one surface

was under tension and the other was in compression. The shifts in oscillator frequencies were thus in opposites directions, thereby doubling the sensitivity. Changes in frequency caused by temperature variations were in the same direction, however. The force-frequency experiments on Y and ST cuts are compared to the theoretical calculations in Table 5.

Table 5 – Force-frequency sensitivity of SAW oscillator for two Quartz cuts.

Force-frequency sensitivity of SAW oscillator (Reeder, M. Cullen, D. E., & Gilden, G.,1975)		
Orientation	Measured	Calculated
ST, X	1140	1200
Y, X	740	930

The sensitivity of SAW delay lines to hydrostatic pressure is generally small. Indeed, strains and stress fields are homogeneous in the overall volume of crystal plate. The strain in terms of pressure P is given as: $S_i = -\sigma_i P$ where

$$\sigma_i = \sum_{i=1 \text{ to } 3} S_{i,j} \qquad j = 1 \text{ to } 6 \tag{24.}$$

and $S_{i,j}$ are the stiffness constants. The sensitivity of ST-cut quartz SAW oscillators subjected to hydrostatic pressure from 0 to 35 PSI was reported to be 25 Hz/PSI.

Thin Films Properties

Characterizations of thin films are possible from the measured phase velocity of attenuation of surface waves propagating a thin-film on a substrate. On a pulse-to-pulse basis it may be determined that the delay time on amplitude of an RF signal that is less than the transit time through the delay line. Another approach in determining the phase

velocity is to use SAW oscillator scheme. The frequency shift of SAW oscillator provides information about a change of phase velocity with high precision.

The phase velocity of surface waves, in layered media, may be related to material properties. The deposition of electrically conducting materials along the propagation path will cause surface wave attenuation on a piezoelectric substrate.

One observes a maximum attenuation when the electrical conductivity of the layer is such that the product of the dielectric relaxation time times the angular frequency of the surface wave is roughly unity. This occurs because, for those conditions, piezoelectric fields are most effective at bunching and dragging electrons through the resistive medium thereby transferring maximum energy from wave. For gold and aluminum, the attenuation maxima for 20-MHz waves occur for film thickness of between about 30 and 100 ^{o}A.

Thermal Flow Sensors

Hot wire & hot-film anemometers are widely used to measure velocities in the field of fluid mechanics. A hot-film anemometer is constructed by depositing a thin-film of metal (such as gold) on insulators (such as quartz or mica) (Polla et al., 1983; Qin-Yi & Jin-Biao, 1987; Al-Salaymeh & Ashhab, 2006). The principle of operation is based on convective heat transfer from the heated sensor to the surrounding fluid to measure the velocity. The amount of heat transferred per unit time is calculated from an electric signal that is related to the temperature of the sensor. This signal results from the unique relationship between the temperature and the resistance of the sensor.

The resistance of the sensing element R is related to its temperature T by:

$$R = R_o[1 + \alpha(T - T_o)] \tag{25.}$$

where R_o and T_o are the average resistance and temperature at a reference condition, and α is the temperature coefficient of resistivity. An important parameter governing the operation of hot-film anemometers is the overheat ratio defined as:

$$a_T = \frac{(T - T_0)}{T_0} \tag{26.}$$

where T is the temperature of the heated element and T_o is a reference temperature in Kelvins. In operation, it is more practical to use a resistive overheat ratio defined by:

$$a_R = \frac{(R - R_0)}{R_0} \tag{27.}$$

where R is the resistance of the heated sensor and R_o is the resistance in the reference state often called the cold resistance. Note that $a_R = \alpha T_o a_T$. A basic circuit for constant operation, shown in Figure 11, consists of a voltage supply, variable resistor R_1, limiting resistor R_2, and sensor R.
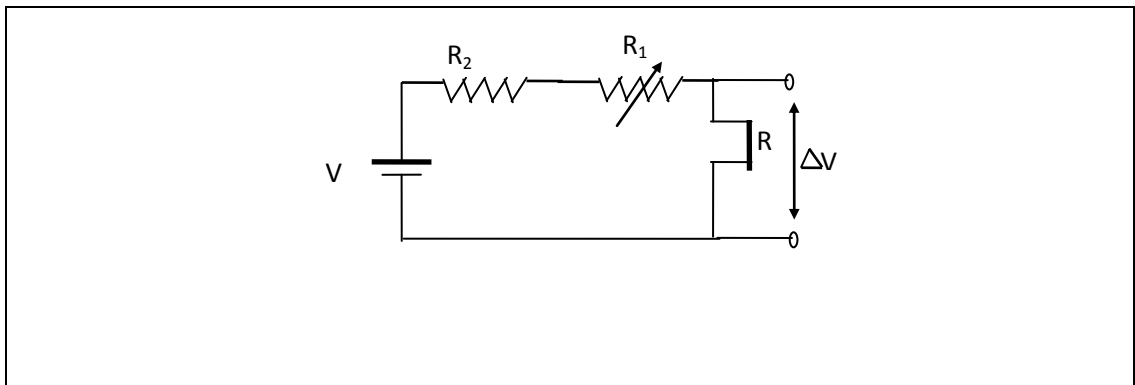
Figure 11. A basic circuit for constant current operation (R. M. Rich: Editor, 1981**).**

The output of the circuit is the voltage drop ΔV across the sensing element. If the supply voltage is constant, a change in the resistance R will change the current by:

$$\Delta I = \frac{I\Delta R}{(R_1+R_2+R)} \qquad (28.)$$

To reduce the current fluctuations to a relatively small value requires:

$$\frac{\Delta R}{(R_1+R_2+R)} \ll 1 \qquad (29.)$$

so that $R_1 + R_2$ must be large. The fixed resistor R_2 should be sufficiently large to eliminate the possibility of accidentally burning out the wire when either the variable resistor R_2 or the velocity decreases. If the value of R_2 is accurately known, the current through the sensor can be determined by measuring the voltage drop across R_2 using Ohm's law. With the current determined and the output voltage known, one can compute the resistance of the sensor and thus the overheat ratio in situ.

The hot-film operates by passing a current through the sensor from an external power supply. To obtain an electric signal, which is representative of the fluctuating flow quantities, the hot-film is usually operated so that either the current or the resistance is held constant. The power input for a constant current operation can be represented as $P(i,R)$. The time rate of the change of energy within the sensing element must equal the difference between the power input and the heat leaving the device. The power input to the sensor, i.e., the Joule heating, is:

$$P = IV = I^2R \qquad (30.)$$

where V is the voltage drop across the sensor; I, the current through it; and R, its resistance. Likewise, the energy loss can be represented by the sum of the various types

of heat flows; this is expressed as F(U,T); where U is the velocity. The heat flow F may

be sum of convection, substrate conduction and radiation terms. Therefore, the energy

equation can be written as (Rich, 1981):

$$\frac{dQ}{dT} = P - F \qquad (31.)$$

where Q is the total heat stored in the element. Letting c, m, and T represent the average

values of the specific heat, mass, and temperature of the sensor, Q can be expressed as Q

= cmT for a hot-film. The value of the specific heat and mass may be some average/the

sensing element and the substrate. It may be pointed out that the mass of the sensing

element in our case is much smaller than the mass of the substrate; therefore, contribution

from the heating element may be ignored. For small temperature fluctuations, the

specific heat is a constant and *Equation (31)* can be written as:

$$cm\frac{dT}{dt} = P(i, T) - F(U, T)' \qquad (32.)$$

This relation provides the basic differential equation for the operation of hot-wire and/or

hot-film anemometers. The output signal from the hot-wire or hot-film is an electrical

signal proportional to the velocity U. Two major obstacles thwart this: first, the

relationship in *Equation (32)* is a nonlinear function of the velocity; second, some

additional constraints must be used to eliminate one of the three variables I, T, and U.

The dynamic response of the hot-wire or hot-film is expressed as (Rich, 1981):

$$M = \frac{cm}{\left[\frac{\partial F}{\partial T}|_U - \frac{\partial P}{\partial T}|_i\right]\Delta T} \qquad (33.)$$

The time constant *M* is a measure of this lag, and hence the reason for its name and

importance. The time constant determines how well temperature fluctuations in the hot-

film correspond to the fluctuations in the forcing function. To have the temperature fluctuations correspond to the velocity fluctuations uniformly for all frequencies, the time constant must be zero. This could only occur if the sensing element had zero heat capacity, as shown by *Equation (34)*.

Prediction of the time constant for the hot-film is a complicated problem. To calculate the time constant, the heat flux from the sensor must include conduction losses to the substrate. Thus there are two mechanisms by which the hot-film can lose heat: 1) by convective loss directly to the ambient fluid, and 2) by conduction through the substrate and indirectly to the fluid. Two time constants are associated with these different mechanisms of heat loss. For slow temperature variations, adequate time is available for the heat to be conducted to an exposed surface and escape, thus both mechanisms are operative. For rapid variations, the heat has insufficient time to penetrate the substrate, and only convection losses are important.

Over the past few years, microelectronics-processing technologies have placed stringent demands on conventional thermal flow transducers (Johnson, G., & Higashi, R. E., 1987; Polla, L., 1983; Qin-Yi, T., & Jin-Biao, H., 1987; Tabata, O. 1986; Tai, Y.C, R. S. Muller, R. S., Howe, R.T., 1985; Petersen, K., & Brown, J., 1985). Mass flow measurement by thermal techniques involves flow of the gas through a reasonably well-defined heated flow channel. Flow sensing using polysilicon bridges has been reported by Tai, Muller, & Howe (1985). Doubly supported polycrystalline silicon beams were used as thermistor elements to measure the flow rate of air. The thermistor-detector anemometers consisted of free-standing polycrystalline silicon beams, thermally isolated

from silicon surface with mechanically supported ends. The use of polysilicon has many advantages: polysilicon is a part of MOS technologies and can be easily integrated with on-chip circuitry; it is easily protected by oxide and/or nitride encapsulation to avoid interaction with corrosive ambient; and it has a temperature coefficient of resistance (TCR) that can be very large (up to 7% per ^{o}C) if doped heavily. Figure 1(b), in Chapter 1, shows the cross-section of a polycrystalline silicon microbridge. The polysilicon beams constructed for flow sensing were 10 μm wide, 50 μm long and 1.35 μm thick, with a spacing of 2 μm between the beams and silicon substrate.

The average temperature of operation is between $350^{o}K$ and $500^{o}K$. The convection coefficient H was found to vary as a $v_f^{1/2}$ where v_f is the gas velocity. This scheme has two drawbacks: the structure of the microbridge is fragile and can make packaging a problem, and the operating temperatures are high. Johnson and Higashi (1983) have reported a micro-miniature gas flow sensor on a silicon chip. The transducer consists of a central thin-film heater and two identical temperature-sensitive resistors located adjacent to the heater. All of the elements are supported by a thin dielectric film and are suspended over a silicon etch pit in a 0.067 inch chip, as shown in Figure 12. A gas flow cools the upstream resistor while heating the other located downstream. The common mode operation is achieved by the symmetrical nature of the arrangement (see Figure 13).

Any offsets due to interfering factors such as minor variations of temperature, gas composition, supply voltage, and ambient pressure are minimized using this configuration. The sensitivity of the sensor is very high. Small air flow velocities produce

large temperature changes in the sensor resistor. The characteristics of the sensor are illustrated in Figure 14. The response of the device can be optimized over a wide range of flow rates and differential pressures by varying the cross-section and length of the channel. The output voltage can be calibrated either in terms of average velocity through the channel, mass flow, or differential pressure between input and output ports. As a mass flow sensor, the response is quite independent of ambient pressure and temperature variations, and only slightly sensitive to molecular species variations. Some disadvantages are:

1. The package design must incorporate a well-designed housing and flow channel to provide an accurately reproducible flow over the chip, and to protect the microstructure elements in the application environment.

2. The sensor must be protected from dust in the gas stream. The sensor microstructure is in the plane of the silicon chip surface, and is not immersed centrally in the gas stream, it is highly tolerant of micrometer-sized particles that can flow over the chip surface.
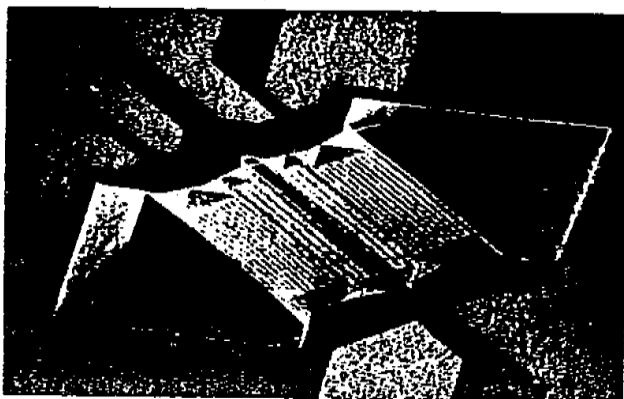
Figure 12. Scanning electron microscope view of the flow sensor microstructure suspended over an etch pit in Silicon, Johnson & Higashi (1983).
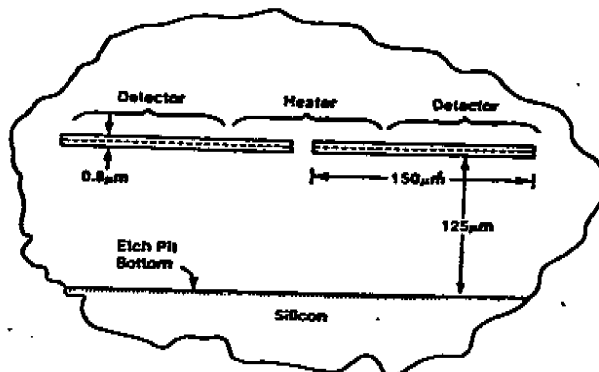
Figure 13. Cross-section of the flow sensor microstructure , Johnson & Higashi (1983).
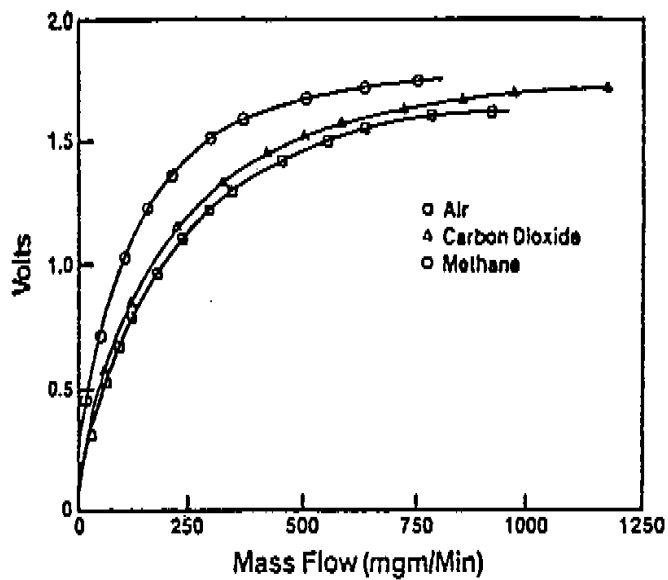
Figure 14. Response characteristics for mass flow for air, carbon dioxide and methane (Arpaci & Larsen, 1984).

PLATINUM THIN-FILM (500Å)

FLUID TEMPERATURE
SENSING ELEMENT   HEATING ELEMENT

4

0.36

(mm)

SILICON FRAME   SILICON NITRIDE (2000Å)
+
OXIDIZED POROUS SILICON (20μm)
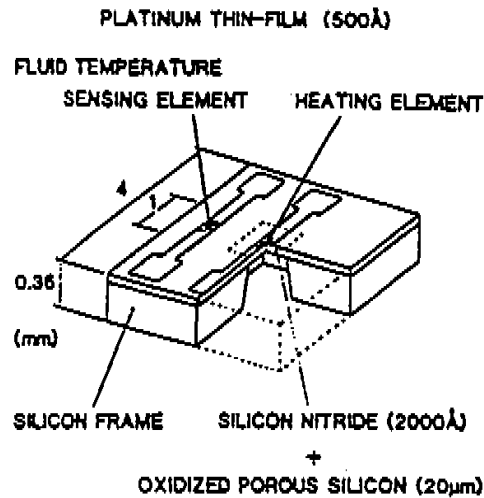
Figure 15. Structure of a silicon flow sensor chip (Tabata, 1986).

A mass-flow sensor using micromechanical bridges in silicon has been reported

by Petersen & Brown (1985). The bridges are suspended over channels etched in silicon.

The purpose of the investigations was to optimize strength, minimize thermal losses to

the supporting substrate, maintain structural stability under high gaseous velocities,

provide very high corrosion resistance, and simplify fabrication procedures. The thermal

resistance from the bridge to the substrate is 10,000^{o}C/W. This feature makes it possible

to operate thin-film resistive element at greatly reduced temperature (25°C above

ambient) while having a fast response time. This sensor has invoked much interest and

was featured on the cover of Sensors magazine (August 1987 issue). The sensor is

realized by micro-machining the silicon. A brief description of the fabrication is

summarized:

- Start with heavily Boron doped, p type, [100] oriented, silicon wafers. The p+

  silicon layer also functions as an etch-stop.

- The height of the flow channel was defined by growing a 70 μm thick epitaxial layer. A dielectric film was deposited, and the channel region was defined by etching through the dielectric film into the epitaxial layer.

- A corrosion-resistant silicon nitride was grown on the channel region.

- The wafer was metalized to a thickness of about 0.2 mm. The metal film was etched into meandering resistor patterns with line-widths of about 7 μm and with a resistance of about 1000 ohms per bridge element.

- The etched metal pattern was fully encapsulated by depositing a dielectric film to protect thin-film resistors from the environment.

- Gold film was deposited and patterned for bonding.

- The bridges were formed after the bridge pattern was etched completely through the two insulating layers and the exposed silicon was anisotropically etched down to the p+ etch-stop layer.

- To coat and protect the bare silicon itself, a final insulating layer was deposited over the wafers, and then etched away from the bonding pad areas.

- Finally, two wafers were aligned, clamped, and bonded with an intermediate adhesive layer. Since the bridge elements were protected by the bonded 'cap' wafer, ordinary   sawing procedures can be employed to dice the wafer assembly and to expose the electrical contacts pads.

Osamu[56] has reported a fast-response silicon flow sensor with a robust thermal isolation structure. The isolation structure is made of a 20 μm thick silicon nitride (Si_3N_4). The structure of such a sensor is shown in Figure 12. The membrane is supported on

a frame of silicon. The chip has two platinum (Pt) thin-film resistors, a heating element, and a fluid temperature sensing element on its top surface. The heating element is placed on the membrane, and the sensing element is placed on the rim of the chip. The fabrication consists of a 5-steps procedure:

1. The substrate is a p-type, [100] oriented silicon wafer having a thickness of 360 μm and of 40 W-cm resistivity. The porous silicon is formed by anodic reaction in 50 % hydrofluoric acid (HF).

2. Oxidation of the porous silicon is performed at 1000 ^{o} C for 15 min in wet O_2 ambient,

3. The $Si_3 N_4$ film with 2000 ^{o}A thickness is formed by low pressure chemical vapor deposition (LPCVD). Arrays of windows are formed in $Si_3 N_4$ on the backside of the wafer using reactive ion etching (RIE),

4. 500°A thin-film of Pt is deposited by dc sputtering and is patterned using a liftoff.

5. Finally, the membrane is formed by etching the exposed silicon on the back side of the wafer in anisotropic etching solution containing potassium hydroxide (KOH) and water.

Response time for a step change of air flow velocity from 0 to 10 m/s is about 10 msec. Qin-Yi and Jin-Biao, (1987) reported a CMOS flow sensor with constant chip temperature (CCT) operation. Under flow conditions power dissipation of the heated CMOS transistor will change. The power needed to keep the chip temperature constant is used to measure the flow rate. Silicon integrated flow sensors based on differential temperature measurements depend on chip size. The sensitivity for smaller chip size is

low, and optimum size for flow measurement is about 6 x 8 μm^2. These result to low-yields, high costs, and a mismatch between the temperature-sensitive devices located at the two ends of the chip.

The constant chip temperature (CCT) employs MOSFETs as the temperature-sensitive element as well as heat source of the chip. When the fluid flows over the heated sensor chip, the power consumption of the heating transistor must be increased in order to keep the chip temperature constant. The change of power consumption of the heating transistor is interpreted in terms of fluid velocity. Input impedance of a MOSFET is very high; the MOSFET's high output power can be controlled by an extremely small input power. The power consumption of the chip is expressed in terms of fluid velocity $v_f^{1/2}$ and temperature difference (T_G - T_f) as (Qin-Yi & Jin-Biao, 1987):

$$IV_{DD} = \frac{0.664\left(\frac{v_f}{\eta}\right)^{\frac{1}{2}}Pr^{-\frac{1}{3}}(T_G-T_f)(A\lambda)}{L} + (T_G - T_f)/R_T \qquad (34.)$$

where I is the thermal conductivity of the fluid, Pr is the Prandtl number, η is the kinematic viscosity of the fluid, L is the chip length along the flow direction, A is the chip area and R_T is the thermal resistance of the chip.

The power supply voltage V_{DD} is constant; therefore the total current I, in the chip represents the power consumption of the chip. If the temperature difference (T_C - T_f) is unchanged, then the current difference δI for keeping the chip temperature constant is proportional to the square root of the flow rate v_f. The typical response time to a step change in flow rate of 24 cm/s at TC = 43°C and T_f = 30°C is 40s.

Thin Film Heater

An important application of thin film resistors is their use as stable heating sources. The characteristic of thin films may differ from the characteristics of the same bulk material. Properties such as resistivity, conductivity, dielectric constant, and temperature coefficient vary with method of deposition, film thickness, substrate material, and substrate surface properties. Generally, above 400^oA, the film properties usually approach those of the bulk material. The most popular thin film resistor materials are nickel-chromium (Nichrome), tantalum nitride, and chromium-silicide. Radio-frequency (RF) sputtering of films is preferred over vacuum deposition, because the RF sputtered film retains the composition of the source material. For many applications, ratio tracking of resistance with temperature in a circuit may be more important than the absolute changes with temperature. The absolute temperature coefficient of resistance and ratio temperature coefficient of resistance in ppm are defined below (Ashcroft, 1976).

$$\text{Absolute TCR} = \frac{R_{T1} - R_{T1}}{R_{T1}} \times \frac{10^6}{T_2 - T_1} \tag{35.}$$

where R_{T2} = resistance at temperature T_2; and R_{T2} = resistance at temperature T_2

$$Ratio\ TCR = \frac{\left(\frac{R_{AT2}}{R_{BT2}}\right) - \left(\frac{R_{AT1}}{R_{BT2}}\right)}{\left(\frac{R_{AT1}}{R_{BT1}}\right)} \times \frac{10^6}{T_2 - T_1} \tag{36.}$$

Where $\left(\frac{R_{AT1}}{R_{BT1}}\right)$ = ratio of resistance R_A and R_B at temperature T_1

and $\left(\frac{R_{AT2}}{R_{BT2}}\right)$ = rthatio of resistance R_A and R_B at temperature T_2

Well-designed film resistors, both nichrome and tantalum nitride, have ratio TCR's less than 2 to 5 ppm/^{o}C. Power dissipation and voltage stress may impose

restrictions on resistor size. Rule of thumb design guidelines are 50 watt/inch^2 and 1V/mil although, under certain circumstances, these figures may be exceeded.

The resistance value is generally kept below the design value and later trimmed to the required value. In cases where sheet resistance is constant over the entire substrate, all the resistors on it can be trimmed in one step (substrate trimming) either by a) a heat treatment which changes the resistivity through annealing or through grain boundary oxidation or b) thickness reduction by RF sputter etching or anodic oxidation (wherever possible). The latter has an additional advantage of providing a protective layer on top of the resistor. In cases where substrate trimming is not feasible, as when local sheet resistance varies from one resistor to other, individual resistor trimming is employed. In addition to heat treatment and anodic oxidation, an individual resistor may also be trimmed by changing its geometry by removing a portion of the film completely, for example, by burning using a laser beam (laser trimming) or by abrasion; whereas trimming by heat treatment also changes the TCR, trimming by other means does not.

Refractory metals like tungsten and niobium alloys make exceptionally stable resistors by sputtering them in controlled atmospheres (Hamilton & Howard, 1975). Their refractory nature provides thermal stability to films, implying that the imperfections frozen in during deposition do not anneal out during their operational life. Stability against oxidation is provided due to their ability to form tough, self-protective oxides on the surface either by thermal oxidation or by anodization.

Amorphous-like/disordered thin films of tungsten (W), Moledenum (MO), and Rhenium (Re), deposited by ion-beam sputtering, having a resistivity $\approx$ 100 μm cm and a

very small (<50 ppm/ $^{\circ}$C) TCR, are attractive for resistors. With thin film capacitors and insulated crossovers using tantalum oxide making it possible to base RC technology completely on Ta. It has also been found that the film composition corresponding to Ta_2N exhibits maximum stability during load-life tests. Rhenium is another refractory material that has been used for fabrication of resistors. These differ from Ta resistors in that the films used are ultra-thin and the high resistivity arises due to discontinuities in the island-like structure of the films. Good stability is achieved with a protective overlayer of 2000 $^{\circ}$A thick silicon monoxide (SiO).

Cermets are another important class of materials for resistor fabrication. A large number of such metal-dielectric systems have been investigated, the most promising being Cr-SiO. Thin films of these materials can be prepared by flash evaporation, RF sputtering, and diode sputtering. The resistivity of these films is strongly dependent on the composition of the cermets and the amount of disproportion and lies anywhere between 10^3 to 10^5 μOhm-cm. An important property of cermets is that high resistances are obtained without large negative TCR values.

The most commonly material used for metallization purpose is aluminum. The resistance of evaporated aluminum thin film is determined by the resistivity of aluminum and the thickness, length, and width of the interconnection according to familiar resistance relation:

$$R = \rho l/tw \qquad\qquad (37.)$$

where

ρ = metal resistivity

l = connection length

w = connection width

t = film thickness

Thickness and resistivity are combined and may be expressed in terms of sheet resistance:

$$R_s = \rho/t \qquad (38.)$$

For example, sheet resistivity of $1500°A$ thin film of aluminum is $0.187\ \Omega$ per square. The values of sheet resistance for various metals are listed in Table 6. While relatively this may seem to be relatively small, this can be used to realize thin aluminum heating elements.

Table 6 – Sheet Resistance of metal films (Seidman, 1983; Ashcroft, 1976; Hamilton & Howard, (1975).

No.	Metal	Bulk Resistivity (µOhm-cm)	Sheet Resistance for 1000 °A
1.	Copper	1.7	0.20
2.	Gold	2.4	0.27
3.	Aluminum	2.8	0.33
4.	Palladium	11	1.30
5.	Titanium	55	10
6.	Palladium-Gold (50-50 Alloy)	21	3
7.	Nichrome	100	15

The above resistance relation holds as long as the film is thick enough for conduction to take place directly along the aluminum film. For very thin films (hundreds

of angstroms), the conduction mechanism changes because of greater distance between nucleation sites of aluminum composing the film; consequently for thin films the effective resistivity is greater than $2.8 \times 10^{-6} \, \Omega$ cm.

Thin films of aluminum with high electrical conductivity are ideally suited for contacts and interconnections. The films can also be used for the fabrication of resistors. Extensive use of aluminum films for integrated-circuit connections has led the discovery of new high current density effects in thin metal films (Chopra & Kaur, 1983). One such phenomenon, electromigration, is a progressive failure of interconnection during continuous operation. Consider a typical integrated-circuit interconnection, $1500^{o}A$ thick and 1 mil wide. For a 5-ma current flow in the connection, the current density in the aluminum film is 1.3×10^{5} A/cm^2. At current densities of this order and larger, two effects may contribute to the failure of aluminum interconnections. The first is the transport of aluminum by momentum exchange with electrons. It has been proposed that the thermally activated aluminum ion gain energy from collisions with electrons and is transported away   from the contact area. Since there are no aluminum ions available to fill the vacancies created by the departing ions, these vacancies cluster and form a void, which eventually extends across the aluminum stripe, causing a failure.

Thin aluminum film on silicon also suffers failure due to transport of silicon in aluminum. At the contact regions, silicon dissolves in aluminum until the solid solubility limit is reached. Because the activation is about 70 percent that at aluminum in aluminum, it is proposed that the silicon is readily activated and is swept away at the positive end of the stripe from the contact area by the force resulting from the rate of

momentum exchange between activated ions and electrons. More silicon can dissolve at the contact. It is thought that as silicon is transported down the film, some regions or the film may become supersaturated with silicon, causing the growth of silicon crystallites, which weaken the film and lead failure.

The failure rate of aluminum films can be reduced by the deposition of several thousand angstroms of glass over the aluminum. The presence of glass reduces the diffusion of aluminum at the aluminum surface. Theoretical analysis predicts that the teen time to failure for aluminum films is related to the current density (Chopra & Kaur, 1983):

$$\frac{1}{MTF} = AJ^2 e^{-\emptyset/kT} \tag{39.}$$

where

$$
\begin{aligned}
MTF \quad &= \quad \text{mean time to failure in hours} \\
J \quad &= \quad \text{current density} \\
A \quad &= \quad \text{constant relating to the properties of metal} \\
\Phi \quad &= \quad \text{activation energy for aluminum in aluminum}
\end{aligned}
$$

Experiments performed on glassed aluminum films indicate that the mean time to failure is given by (Chopra & Kaur, 1983):

:

$$\frac{1}{MTF} = 1.88 \times 10^3 J^2 e^{-1.2/kT} \tag{40.}$$

The properties that make aluminum very desirable include:

- It is a good conductor (only silver, copper, and gold are better)
- It has a relatively high eutectic temperature with silicon (577 ^{0}C)

- It adheres well to both silicon and silicon dioxide

- It is easy to evaporate and etch.

One major problem, however, is the reaction of aluminum with gold and silicon to form binary and ternary compounds of the three materials. Since gold wires are often used to make connection between aluminum connections on the chip and the header connections, and since the gold-aluminum reaction causes the connection to fail, this can be a troublesome problem. Failure also occurs as a result gold-aluminum-silicon compounds, which can form a wire bond on the chip, since silicon is present in the SiO_2. It is therefore desirable to use aluminum bonding wires.

The optimum power density for any resistor material is a function of the resistor material, the substrate, and any conductive films on the substrate and external heat sinks. The resistor material itself affects the power density in that it imposes an upper limit on the temperature of the film because of stability considerations. The temperature of the resistive film is given by:

$$T = T_A + Q/k \qquad\qquad (41.)$$

where T_A is the ambient temperature, Q is the power dissipation and k_S is the thermal conductivity of the substrate to an infinite heat sink.

CHAPTER 3: HEAT TRANSFER THEORY FOR FLAT ENCLOSED PLATE

In this chapter, heat theory applicable to enclosed flat plate with an embedded internal heat source will be described. Following this, a theoretical model of heat transfer applicable to this research will be developed.

If there exists a thermal gradient between two regions, heat is transferred from a high-temperature region to a low temperature-region by means of conduction, convection, and radiation processes. If an infinitesimal volume element has an internal source of heat generation, the temperature may change with time. The equilibrium equation for the infinitesimal element is expressed in terms of the rate of internal heat generation, energy conducted out of the system, and change in internal energy; the energy balance equation can be expressed as (Bar-Cohen, 1983):

Energy Storage = Energy Generation + Net Heat Transfer   (42.)

Assuming that the substrate/crystal thickness t_S is small compared to its length, L; the variation of temperature/thickness can be neglected; hence, the sensor temperature T_S may be assumed to be a function of only ξ and time t. $\xi = \frac{x}{L}$, where L lies between $\xi=0$ and $\xi=1$.

The transient (momentary) heat balance in the sensor can be written as (Jian-Bio, July 2007):

$$\rho c_S t_S \; \frac{\partial T_S}{\partial t} = \; k_S \frac{t_S}{L^2}\frac{\partial^2 T_S}{\partial \xi^2} - \; q_f + \; q_h \qquad (43.)$$

$\xi = \frac{x}{L}$, where L lies between $\xi=0$ and $\xi=1$; q_h refers to the heat generation and q_f refers to the convective heat loss. $\rho_S,$ c_S, t_S and k_S refer to the density, the specific heat,

thickness, and the thermal conductivity of the substrate material, respectively. Finally, x represents the distance from which the flow has travelled over the surface.

The first term on the right-hand side of the equation represents the redistribution of heat due to the thermal conduction of the substrate material. The heat transfer due to flow q_f and the heat generation q_h are both expressed as heat flux per unit surface area. *Equation (43)* contains the time-transient effect, caused by the redistribution of heat in the sensor due to conductive heat flows.

The energy balance equation that includes heat transfer by conduction, convection, and radiation is given by Bar-Cohen et al. (Bar-Cohen, 1983):

$$P = Q_{COND} + Q_{CONV} + Q_{RAD} \tag{44.}$$

The rate of energy supplied is equal to the rate of energy carried away from a substrate by conduction, convection, and radiation. The heat transfer theory for enclosed flat plate geometry with an embedded heat source is applied to develop a model for calculating the steady state contributions of each component of heat transfer present in *Equation (44)*. The model has the following components:

- Conduction losses

- Free Convection Losses

- Forced Convection Losses

- Temperature Distribution Model

- Response Time

Assumptions

1. The flat plate, functioning as the SAW substrate, has an internal heat source. The
    heat source is a thin-film heater fabricated at the middle of a rectangular substrate.

2. The thermal properties like thermal conductivity stay uniform within operating
    range.

3. To avoid thermal conduction losses, the flat plate must have high thermal
    isolation with surrounding.

4. There are steady state laminar flow convection conditions.

5. Thermal derivation are rendered to:

    *   Quantify input (power) sources

    *   Quantify output (heating dissipation) sources with and without flow
        conditions

    *   Determine temperature distribution for thermal characterizations

    *   Derive time response

6. The model can be applied to a wide range of substrate and flow set-up
    geometrical dimensions.

A model based on the energy balance equation as applied on flat plate geometries
with an embedded heating source is utilized (Figure 16). In addition, heat transfer
mechanisms for the flat plates in enclosed spaces for several boundary conditions were
investigated. Heat transfer mechanisms under laminar flow which includes mixed
convection, thermal properties of gas, and entrance effect were investigated and included
in the model (Bohn, 1986). This section describes a theoretical treatment to predict the

temperature rise of the flat plate crystal for a given input power to the heater element at steady state.

The steady-state temperature of the SAW substrate can be determined by quantitatively solving *Equations (43) and (44)*. The conduction process is characterized as occurring within a solid body or between two solid bodies in contact. The rate of heat transfer, Q_{COND}, is proportional to the temperature gradient:

$$Q_{COND} = -k\,\frac{\partial T}{\partial x} \tag{45.}$$

where k is the thermal conductivity and $\partial T/\partial x$ is the temperature gradient in the direction of heat flow.

In the convection process, the heat transfer occurs due to the motion of a fluid over the surface of a body. The rate of heat transfer, Q_{CONV} is dependent upon the rate at which the heat is carried away. If h is convection coefficient of heat transfer, A is surface area, and ΔT is change in transfer due to convection, the Q_{CONV} is given by:

$$Q_{CONV} = h \times A \times \Delta T \tag{46.}$$

and Q_{RAD}, exchanged between two bodies at temperatures T_1 & T_2 is computed as follows (Kreith & Bohn, 1986):

$$Q_{RAD} = \frac{A_1 \times A_2 \times \sigma \times \varepsilon\left[(T_1)^4 - (T_2)^4\right]}{\pi d^2} \tag{47.}$$

where σ is the Stefen-Boltzmann constant, ε is the emissivity, d is the separation between the bodies, and A_1, A_2 refer to the respective surface areas.

To derive the temperature distribution and thus the average temperature, published heat flow model were applied (Tai, 1985). Similar arguments hold for temperature response analyses (Giarratano, 1984). Assume that a substrate/crystal with flat geometry is suspended in the air with high isolation due to contact area and that the sensor thickness t_S is small compared to its length. This renders the variation of temperature/thickness as insignificant; thus, the sensor temperature T_S may be assumed to be a function of only ξ and time t.

Equation (43) presents the time-transient effect caused by the redistribution of heat in the sensor due to conductive heat flows. Using the method of variable separation, the time-dependent function is expressed as a Fourier series which results to a solution for the response time. Fourier number at time t is defined as ratio of the rate of heat conducted to rate of heat stored at that time.

Where, fourier number $= \frac{\alpha t}{L^2}$, where α is the thermal diffusivity (m^2/sec), a material-specific quantity depending on the thermal conductivity k, the mass density ρ, and the specific heat capacity c_S (Kreith & Bohn, 1986). The response time τ (Giarratano, 1984)÷

$$\tau = \frac{c_S \rho_S\, L^2}{k_S \pi^2}$$

(48.)
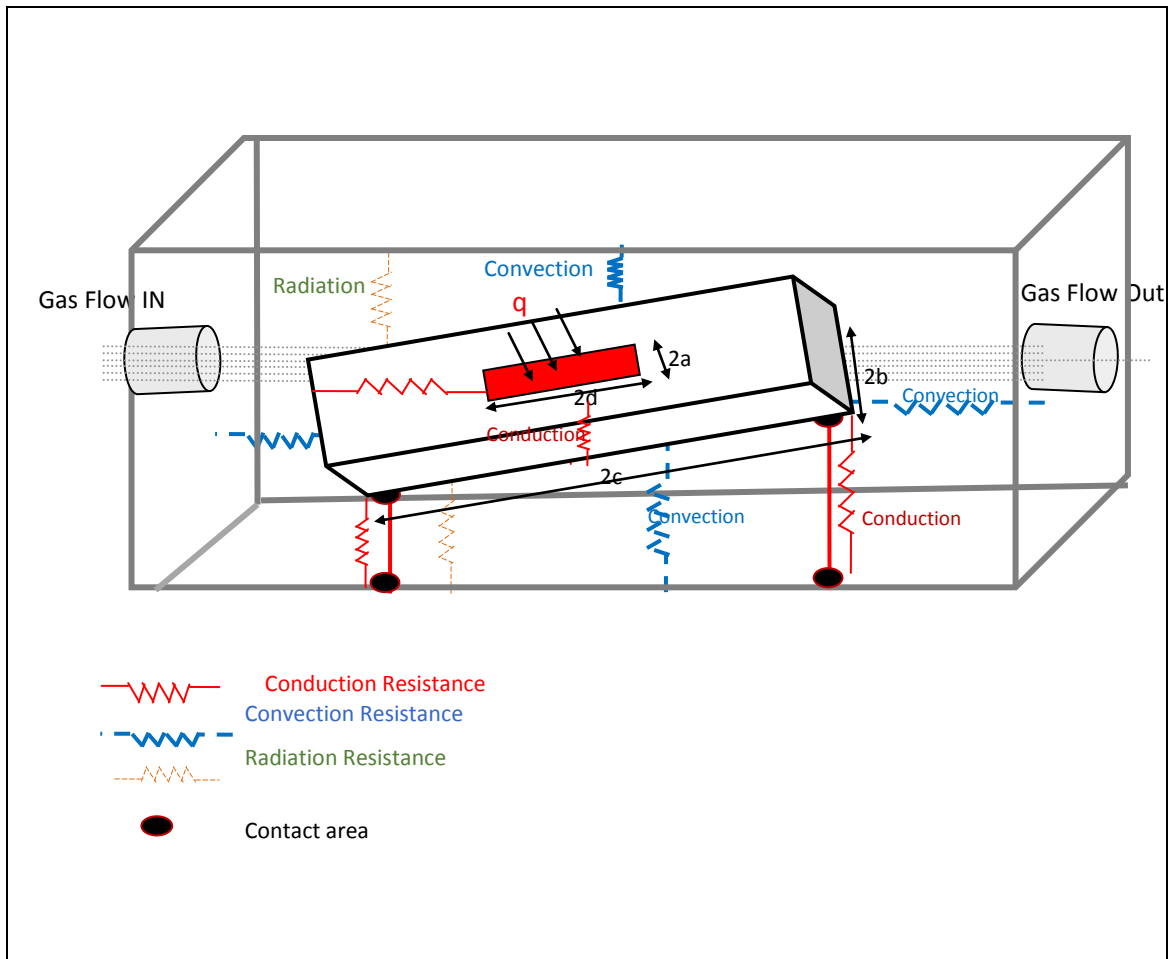
Figure 16 Enclosed flat plate with embedded heat source.

The steady-state temperature of a substrate can be determined by quantitatively solving *Equation (42).*

Table 7 – Listing of variables and constants (Guang-Ping Shen, 2006)**.**

Thermal Parameter	Unit	Electrical Parameter	Units
Temperature (T)	^{o}K	Voltage (V)	Volt (V)
Heat Flow (q or Q_{HTR})	Watt (W)	Current (I)	Ampere (A)
Heat (Q)	Joule = W*sec	Charge (Q)	Coulomb = A*sec
Thermal Resistance (R)	^{o}K/W	Resistance (R)	Ohm (Ω) = V/A
Heat Capacity (C)	J/^{o}K	Capacitance (C)	Q/V = A*sec/V

An electro-thermal analog circuit of the set-up is drawn in Figure 17. Heat transfer by conduction, free convection, and radiation take place in parallel with respect to one another. Thermal resistance of each of the dissipating source will be computed.
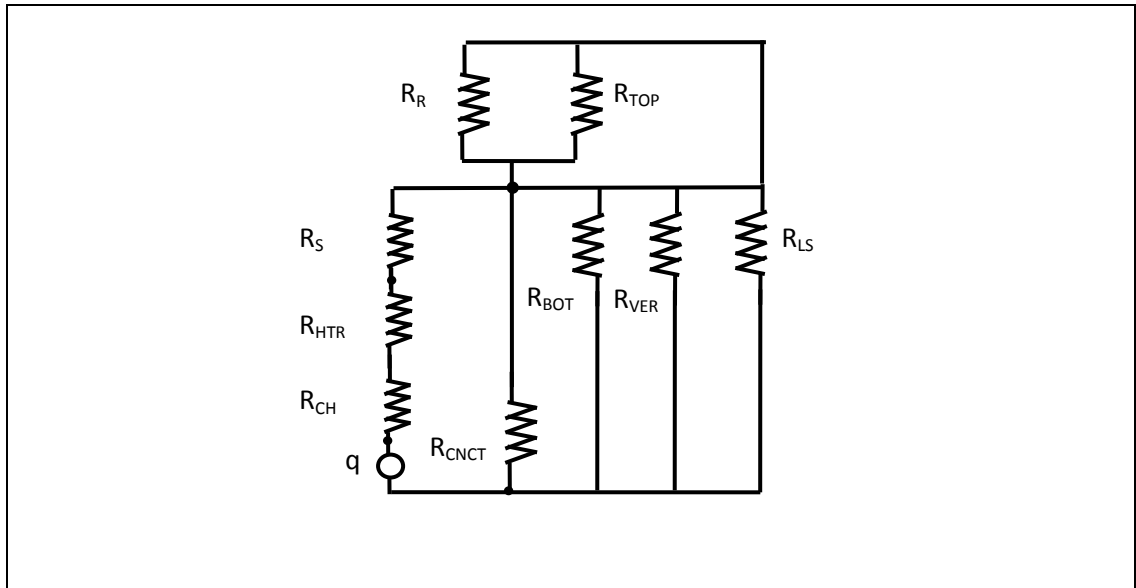
Figure 17 — An electrothermal analog equivalent circuit for the setup in Figure 16.

Theoretical temperature rise at various nodes in the circuit of Figure 17 can be predicted once the values of the thermal resistance's are known. In Figure 17, q is heat flow (watts), R_{CH} is constriction resistance proposed by Mickic (Bar-Cohen, 1983), R_{HTR} is the thermal resistance of heater element, R_S is thermal resistance of the substrate; R_{CNTC} is the contact resistance between the substrate and flow cell; R_{BOT} is convection thermal resistance from the bottom of the substrate; R_{VER} is convection thermal resistance from the side walls of the substrate; R_{TOP} is convection thermal resistance from the top surface of the substrate; R_R is the radiation thermal resistance of the substrate and R_{LS} is the is thermal resistance from the lid to substrate holder/flow cell.

Theoretical Derivation

Variables and Constraints

A list of the variables, constants and constraints used to derive the theoretical model is provided in Table 8.

Table 8 - Listing of variables and constants

Parameters (Bar-Cohen, 1983)	Descriptions
$c = 1.005 \times 10$ J/kg$^\circ$K	Specific heat of air
ε	Emissivity of a material
$g = 9.8$ m/s^2	Acceleration due to gravity
$k = k_f = 0.026 \ \frac{W}{m}{}^\circ C$	Thermal conductivity of air
$k_h = 204 \ \frac{W}{m}{}^\circ C$	Thermal conductivity of aluminum (heater)
$L = L_C$ (or L_{CK} or L_{CS})	Characteristics length of SAW substrate. Mean of width and length of a plate
$L_h = 0.1 \times 10^{-6}$ m	Thickness of thin-film heater
L_S or L_L or t_S	Thickness of the substrate
$Pr = 0.708$	Pandtl number of air
$\mu = 1.98 \times 10^{-5}$ kg/m s	Viscosity of air
$\rho = 1.1774$ kg/m^3	Density of air
$\upsilon = \eta = 15.68 \times 10^6$ m^2 /s	Kinematics viscosity of air
$\alpha = 0.221 \times 10^4$ m^2 /s	Thermal diffusivity of air
$\beta = 0.00338{}^\circ$ K^{-1}	Coefficient of thermal expansion of air
$\sigma = 5.67 \times 10^8$ W/m^2 K^4	Steffan-Boltzmann's constant
x, y	Cartesian coordinates (x measured from channel inlet).

Thermal Resistances

1. Conduction Components, R_{COND}: Substrate (Crystal) + Contacts

2. Convection Components, R_{CONV}: Horizontal (top and bottom) + Vertical (sides)

3. Radiation Components, R_{RAD}: Horizontal + Vertical

4. R_{LS} is lid to substrate holder resistance; it is assumed negligible for large metallic area

The derivation of each of the component of thermal resistances listed above under free and forced convection steady states is carried out as follows.

Conduction Losses

Mickic (Bar-Cohen, 1983) has proposed a method for the determination of the temperature at discrete heat sources on the face of a conducting medium. As noted in Figure 3, the heat will diverge from the concentrated area under the heat source. This, for a heat source of constant magnitude, gives rise to what is called a constriction effect; as a result, the temperature just under the discrete heat source T_j is given by:

$$T_j = T_o + \Delta T_c \qquad (49.)$$

where T_o is the temperature that would be obtained if all of the heat were spread over the entire area and ΔT_C is the constriction effect as shown in Figure 4.
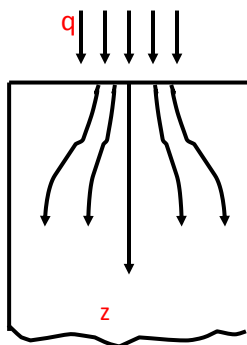
Figure 20 – Discrete heat source on the face of a conducting medium.
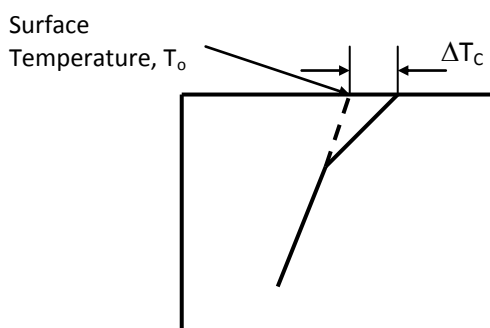
Figure 19 – The constriction effect allows the calculation of the temperature directly under the heat source by adding ΔT_C to the average surface temperature obtained by spreading the heat over the entire surface.
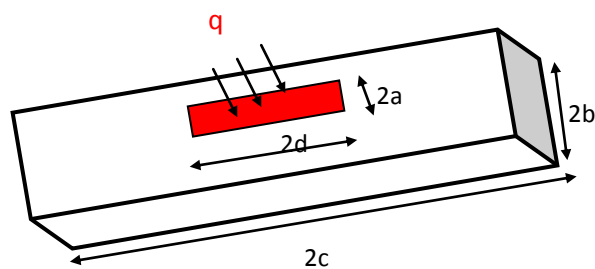
Figure 18 – Short strip heat source on finite conducting medium, Mickic (Bar-Cohen, 1983).

Conduction Thermal Resistances (Bar-Cohen, 1983)**:**

Substrate thermal resistance:

$$R_S = \frac{L_S}{k_S A_S} \tag{50.}$$

Contact resistance:

$$R_{CNCT} = \frac{L_{SINK}}{2k_{Al}A_{CNCT}}$$ (51.)

Heater thermal resistance:

$$R_h = \frac{L_h}{k_{Al}A_h}$$ (52.)

Constriction thermal resistance, Mickic (Bar-Cohen, 1983):

$$R_{CH} = \frac{\Delta T_{CH}}{Q_{COND}}$$ (53.)

where,

$$\Delta T_{CH} = \Delta T_{C1} + \Delta T_{C2} + \Delta T_{C3}$$ (54.)

$$\Delta T_{C1} = \frac{Q_{COND}b}{2\pi^2 k_L ac} \sum_{m=1}^{\infty} \frac{\sin\left(\frac{m\pi a}{b}\right)}{m^2}$$ (55.)

$$\Delta T_{C2} = \frac{Q_{COND}c}{2\pi^2 k_L db} \sum_{m=1}^{\infty} \frac{\sin\left(\frac{m\pi a}{b}\right)}{m^2}$$ (56.)

$$\Delta T_{C3} = \frac{Q_{COND}2}{2\pi^2 k_L ad} \sum_{m=1}^{\infty} \sum_{n=1}^{\infty} \frac{\sin\left(\frac{n\pi d}{c}\right)\sin\left(\frac{m\pi a}{b}\right)}{mn\left[\left(\frac{m\pi}{b}\right)^2 + \left(\frac{n\pi}{c}\right)^2\right]^{1/2}}$$ (57.)

The constriction resistance R_{CH} is caused by thin film heater on the substrate (crystal).

Free Convection Losses

In natural or free convection, temperature and density gradients are produced by heat transfer due to the temperature difference between a stagnant fluid and the surface of a body. Fluid motion is the result of buoyancy forces arising from temperature and the density variations within the fluid. In natural convection, the velocity is zero at the heated body, but increases rapidly in a thin boundary layer adjacent to the body. If ρ_∞ is the density of the cold undisturbed fluid and ρ is the density of the warmer fluid, the buoyancy force per unit volume in earth's gravitational field is $(\rho_\infty - \rho)g$ where g is the

acceleration of gravity. The density differences are related in terms of the coefficient of

volume expansion of the fluid by β by the following definition (Kreith & Black, 1980):

$$\beta = \frac{1}{V}\left[\frac{\partial V}{\partial T}\right]_P = \frac{1}{V_\infty}\frac{V-V_\infty}{T-T_\infty} = \frac{1}{\rho_\infty}\frac{\rho_\infty-\rho}{T_\infty-T} \tag{58.}$$

where V is the volume. For an ideal gas, $\beta = 1/T$. Therefore, the buoyancy force for an

object at temperature T_S will be $\rho g \beta (T_S - T_\infty)$. The three parameters ($\rho$, g, and β) in

Equation (58) are used to relate data for heat transfer in natural convection:

Nusselt Number is defined as the ratio of heat transferred from surface to heat

conducted away by fluid (Kreith & Black, 1980):

$$Nu_S = \frac{hL_{CK}}{k_S} \tag{59.}$$

where h is the convection coefficient, L_{CK}, is the characteristic length of the

plate/substrate, and k is the thermal conductivity of air.

$$\text{Prandtl Number} = Pr = \frac{\mu\, C_p}{k} = \frac{\text{momentum diffusivity}}{\text{thermal diffusivity}} \tag{60.}$$

$$\text{Grashof Number} = Gr = \frac{(\text{buoyancy forces})\times(\text{inertia forces})}{(\text{viscous forces})^2}$$

$$\text{Grashof Number} = Gr = \frac{g\beta\rho^2 L_{CK}^3 \Delta T}{\mu^2} = \frac{g\beta L_{CK}^3 \Delta T}{\upsilon^2} \tag{61.}$$

where, $\upsilon = \frac{\mu}{\rho}$, μ is dynamic viscosity, υ is kinematic viscosity, ρ is density

Table 9 - Free Convection Parameters (Bar-Cohen, 1983)**.**

Parameter	Formula	Interpretation
Prandtl Number:	$Pr = \dfrac{\upsilon}{\alpha} = \dfrac{\mu\, C_p}{k}$	Ratio of fluid velocity boundary layer thickness to the fluid temperature boundary layer thickness.
Nusselt Number:	$Nu_S = \dfrac{hL_{CK}}{k_S}$	Ratio of heat transferred from surface to heat conducted away by fluid.

Grashof Number:	$Gr = \dfrac{g\beta\rho^2 L_{CK}^3 \Delta T}{\mu^2}$	Ratio of fluid buoyancy stress to viscous stress, which approximates the ratio of the buoyancy to viscous force acting on a fluid

All the parameters used in the above equations are defined in Table 8. The average Nusselt number is related to the Grashof and Prandtl numbers by the following equation (Kreith & Black, 1980):

$$Nu = C(Gr \times Pr)^n \tag{62.}$$

The Grashof number is to natural convection what the Reynolds number is to forced convection. In addition, the magnitude of the Grashof number serves to indicate what region the flow is in (laminar, transitional, or turbulent). For a flat plate, the critical Grashof number for transition ranges between 10^8 and 10^9 (Bar-Cohen, 1983). A Grashof number with a value higher than 10^9 would initialize a turbulent flow in natural convection; on the other hand, a value of less than 10^8 would signify laminar flow.

Free Convection in Enclosed Spaces

Heat will flow across the air gap by conduction and/or convection in parallel with radiation.

<u>Case 1</u>:

A fluid is confined between two large horizontal plates spaced a distance s apart. If the lower plate has a lower surface temperature than the upper plate, the process is one of pure conduction across the fluid layer (Bar-Cohen, 1983). If the end-effects are neglected and if the driving temperature difference is taken to be the difference in the plate temperatures, the Nusselt number is unity (Bar-Cohen, 1983):

$$\text{Nu}_S = \frac{hs}{k} = 1.0 \tag{63.}$$

Case 2:

For air confined between horizontal plates with the lower plate hotter than the upper plate, Jackob (Jakob, 1949) recommends the following correlations for the average Nusselt number, where the characteristic dimension is plate spacing s. The Grashof number based on the gap dimension dictates the actual mechanism and for horizontal air gaps[2] (Bar-Cohen, 1983):

$$\text{Nu}_s = 0.195(\text{Gr}_s)^{1/4} \qquad \text{for } 10^4 < Gr_s < 3.7 < 10^5 \tag{64.}$$

$$\text{Nu}_s = 0.068(\text{Gr}_s)^{1/4} \qquad \text{for } 10^4 < Gr_s < 3.7 < 10^7 \tag{65.}$$

where the Grashof number is defined as (Bar-Cohen, 1983):

$$\text{Grashof Number} = \text{Gr} = \frac{(\text{buoyancy forces}) \times (\text{inertia forces})}{(\text{viscous forces})^2}$$

$$\text{Grashof Number} = \text{Gr} = \frac{g\beta\rho^2 L_{CK}^3 \Delta T}{\mu^2} = \frac{g\beta L_{CK}^3 \Delta T}{\upsilon^2} \tag{66.}$$

where, $\upsilon = \frac{\mu}{\rho}$, μ is dynamic viscosity, υ is kinematic viscosity, ρ is density.

The properties are evaluated at the average of the two plate temperatures, and the driving-temperature difference is the difference between the surface temperatures of the plates. When s, the spacing of the horizontal gap, is small ($\text{Gr}_S < 1700$), the heat flow is primarily by conduction and the Nu_S number is equal to unity:

$$\text{Nu}_S = \frac{hs}{k} = 1.0 \tag{67.}$$

---

[2] A Grashof number with a value higher than 10^9 would initialize a turbulent flow in natural convection; on the other hand, a value of less than 10^8 would signify laminar flow.

where, $h = \frac{k}{s}$; thus, to establish the conductance across the gap, the following criteria

must be met:

1. Below $Gr_S = 1,700$, use the pure conduction mode employing the relation:

$$q = \frac{k}{s} \times A \times \Delta T \tag{68.}$$

2. For $1,700 < Gr_S < 10,000$, use Figure 6 to establish Nu: $\tag{69.}$

3. For $Gr = 10,000$, use:

$$h = \frac{k}{s} Nu_S \tag{70.}$$

where Nu_S can be computed using *Equations (67).*
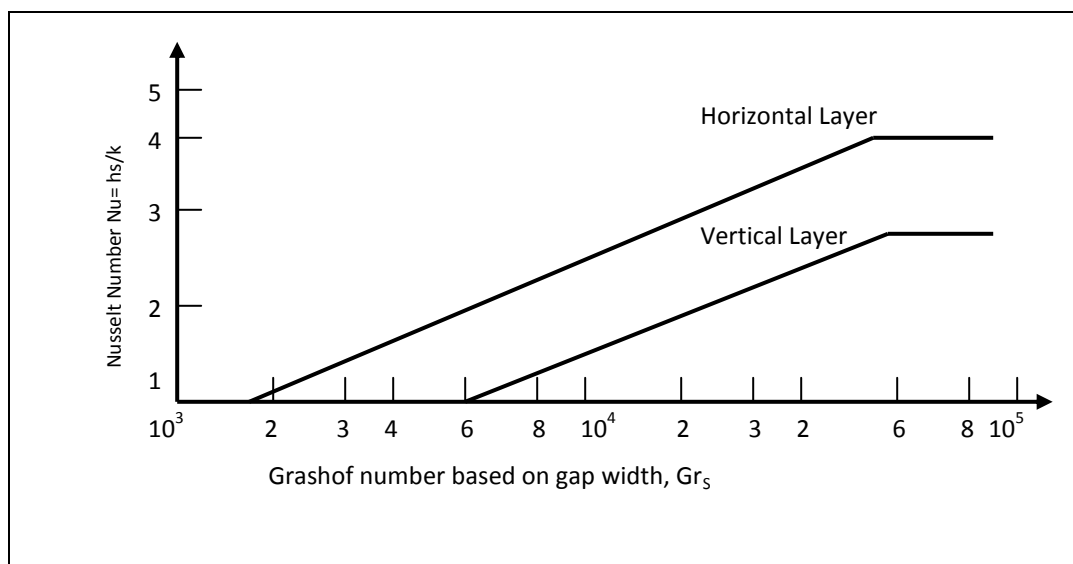
Figure 21. Heat transfer through enclosed plane air layers (Jakob, 1949).

Vertical Spaces

For vertical air spaces between two plates spaced a distance s apart of height L in

the vertical direction, Jackob (Jakob, 1949) recommends the following relations:

$$Nu_S = \frac{hs}{k} = 1.0 \qquad\qquad \text{for } Gr_s < 2000 \tag{71.}$$

$$\mathrm{Nu_S} \;=\; 0.18 \times \mathrm{Gr}_S^{\frac{1}{4}} \times \left(\frac{L}{S}\right)^{\frac{1}{9}} \qquad\qquad \text{for } 2 \times 10^4 < Gr_s < 2 \times 10^5 \qquad (72.)$$

$$\text{and } \mathrm{Nu_S} \;=\; 0.065 \times \mathrm{Gr}_S^{\frac{1}{3}} \times \left(\frac{L}{S}\right)^{\frac{1}{9}} \qquad \text{for } 2 \times 10^5 < Gr_s < 10^7 \qquad (73.)$$

For *Equations (71) - (73)* to hold it is required that $\frac{L}{S} > 3$. For values of $\frac{L}{S} < 3$, the surface coefficient for a vertical surface of freely convecting in a large fluid applies. Miyamoto et al. (1985) has reported free convection heat transfer from vertical and horizontal short plates in the range of Grashof numbers smaller than 105. The average Nusselt number of vertical short plates of height "l" was approximated by the following relation (Miyamoto et al., 1985):

$$\mathrm{Nul} = 0.448 + 0.46 \mathrm{Grl}^{1/4} \qquad\qquad (74.)$$

for Pr = 0.72 and $15 \leq Gr_l \leq 27{,}000$; where the Grashof number is given by:

$$\text{Grashof Number} = \mathrm{Gr} = \frac{g\beta\rho^2 l^3 \Delta T}{\mu^2} \qquad\qquad (75.)$$

The electro-thermal analog circuit in which the air gap heat transfer and radiation from the substrate to the lid of the substrate are taken into account is shown in Figure 17. The radiation across the air gap can be calculated as-(Kreith & Black, 1980):

$$Q_{RAD} = \sigma \times F_A \times F_\varepsilon \times A_S [(T_{AVG})^4 - (T_\infty)^4] \qquad\qquad (76.)$$

Here, one may assume that the SAW substrate is in full view of the top aluminum lid so that $F_A = 1.0$ and for parallel planes: $\qquad F_\varepsilon = \dfrac{1}{\left[\frac{1}{\varepsilon_1} + \frac{1}{(\varepsilon_2 - 1)}\right]} \qquad\qquad (77.)$

For the SAW substrate, consider that its surface mostly has aluminum overlays because of the inter-digital transducers (IDTS) and heating element. Taking emissivity value of 0.04 for Al, $F_A = 1$, $T_\infty = 273 + 25 = 298°K$, and with $\sigma = 5.67 \times 10^{-8}$ W/m^{2}K^4,

Equation (76) yields

$$Q_{RAD} = 5.67 \times 1 \times F_{\varepsilon} \times A_S \left[\left(\frac{T_{AVG}}{100} \right)^4 - (2.98)^4 \right] \tag{78.}$$

The radiation losses are calculated using *Equation (78)*[3].

Forced Flow

The flow response of thermal flow sensors is generally proportional to the square root of the velocity of the fluid (gas), $v_f^{1/2}$ (Jakob, 1949; Kays, 1986). The constant of proportionality is determined by the flow conditions (laminar, turbulent, and/or mixed), the geometry of the flow sensors, and the operating conditions (temperature, etc.).

The problem of heat transfers from a heat source in a wall and isothermal heat sources embedded in a large substrate have been studied (Ramachandrin e. a., 1985). Solutions were obtained by applying conjugated processes. The studies were carried out for various values of $\frac{k_S}{k_f}$ where k_S and k_f are the thermal conductivities of substrate and fluid, respectively. The results are significant when $\frac{k_S}{k_f} \gg 1$. For $\frac{k_S}{k_f} \cong 100$, more than 90% of the heat is transferred to the substrate which, under steady-state, is lost by convection. For substrate materials under consideration, the value of $\frac{k_S}{k_f} \cong 160$; it can be assumed that almost all of the heat is transferred to the substrate. Under steady-state radiation losses are assumed to be negligible and then the heat will be carried away by convection. To analyze forced flow results, following assumptions are made:

1. Sensor is operating at a constant heat flux (it was assumed that the heat flux was constant)

---

[3] The radiation loss occurs from both top and bottom surfaces of the SAW substrate

2. Temperature-dependent properties of the gas were included

3. Entrance effects were ignored

4. Laminar flow was assumed at flow rate

5. Forced convections losses from the side walls of the SAW were ignored

Mixed Convection Effects

Density gradients occur in any heat transfer process, and field natural convection currents arise in the presence of a force. If the forced convection effects are large, influence of free convection may be negligible. Similarly, when the natural convection forces are strong, the forced convection effects may be negligible. If both effects are of the same magnitude, then the heat transfer consists of both the natural convection and forced convection (Ramachandrin, 1983):

$$Nu^3{}_{COMBINED} = Nu^3{}_{FORCED} + Nu^3{}_{NATURAL} \tag{79.}$$

The ratio $\frac{Gr}{Re^2}$ gives a quantitative indication of the influence of buoyancy on the forced convection (Ramachandrin, 1983); this may be better understood by considering the ratio of buoyancy to inertial forces $\frac{F_b}{F_i}$. The buoyancy force is roughly given by:

$$F_b \cong g\Delta\rho L^3 \tag{80.}$$

where $\Delta\rho$ is the density differential in a cube of side L. The inertial force on a surface of side L in a flowing stream of normal velocity U is (Ramachandrin, 1983):

$$F_i = \rho U^2 L^2 \tag{81.}$$

thus,

$$\frac{F_b}{F_i} \cong \frac{g\Delta\rho L^3}{\rho U^2 L^2} \tag{82.}$$

which can be rearranged to give:

$$\frac{F_b}{F_i} \cong \frac{g\left(\frac{\Delta\rho}{\rho}\right)\left(\frac{L^3}{\eta}\right)^2}{\left(U\frac{L}{\eta}\right)^2} = \frac{Gr}{Re^2} \tag{83.}$$

When the Grashof number, Gr, is equal to or greater than the square of the

Reynolds number, Re, natural effects cannot be ignored compared to forced convection.

Lloyd and Sparrow (1979) performed a study on a constant temperature vertical plate and

concluded that the influence of natural convection is less than 5% of the forced-

convection prediction if $\frac{Gr}{Re^2} < 0.1$ for Pr = 1. Mori (Mori, 1961) analytically found that

the natural convection effects were less than 10% for a horizontal plate in laminar forced

convection of air if $\frac{Gr}{Re^2} < 0.083$. The effect of forced convection on free convection is

less than 10% for the local heat-transfer coefficient in laminar flow over a vertical plate if

$\frac{Gr}{Re^2} > 4$ for 0.73 < Pr <10 (Chen, 1979).

Chen et al. (1977) reported analytical studies on the effects of buoyancy on

laminar forced convective flow over a horizontal flat plate. The buoyancy effects were

significant for $\frac{Gr}{Re^{5/2}} > 0.05$. For $\frac{Gr}{Re^{5/2}} = 0.5$, the increase in the Nusselt number due to

buoyancy is about 27%.

Ramachandrin et al. (1983) reported the effect of buoyancy on forced convection

heat transfer for a wide range of Prandtl numbers. They found that fluids with lower

Prandtl numbers are more sensitive to the buoyancy parameter while fluids with higher

Prandtl numbers are more sensitive to forced convection parameters.

Entrance Effects

When a conduit is short, entrance effects are important. As a fluid enters a duct with uniform velocity, the fluid immediately adjacent to the tube wall is brought to rest. A short distance from the entrance, a laminar boundary layer is formed along the tube wall provided that the turbulence in the entering fluid is not high. The thickness of this boundary layer increases until it fills the entire duct. From this point on, the velocity profile across the duct remains essentially unchanged. If the entrance is square-edged, the initial development of the hydrodynamic and thermal boundary layers along the walls of the tube is quite similar to that along a flat plate.

The entrance flow is a special case of nearly parallel flow subject to a pressure gradient (Kays, 1986). From a uniform velocity of the inlet, boundary layers develop along the walls until they merge at the centerline to form a fully developed (parabolic) velocity distribution. The reduction of velocity in the boundary layers causes an acceleration of the core flow because of the conservation of mass. The effect of the uniform velocity at the entrance is to yield a mean Nusselt number that is always higher than if the velocity were parabolic at the entrance (Kays, 1986).

When $Pr = 1$, as in the case of air, the temperature and velocity profiles develop at about the same rate. For a short conduit, the length over which the flow develops is called the thermal entry length, $x_{e,t}$ and is given by (Burmeister, 1983):

$$x_{e,t} = 0.05 Re_D Pr_D$$

(84.)

for rectangular conduit of cross-section area A, and hydraulic diameter D is defined

as:

$$D = \text{Hydraulic diameter} = \frac{4A}{P} \tag{85.}$$

where P is the wetted perimeter. For the flow cell, the hydraulic diameter D is given by:

$$D = \frac{(w_C + L_C)}{2\,(w_C + L_C)} \tag{86.}$$

where w_C is the width and L_C is the height of flow cell. Similarly, the Reynolds

number for non-circular conduit of hydraulic diameter D is (Burmeister, 1983):

$$Re_D = \frac{(\rho u_{avg} D)}{\mu} \tag{87.}$$

For u_{avg} of 24 cm/s and 10 cm/s, using *Equations (84) - (86)*, $x_{e,t}$ = 4.3 cm and 1.8 cm,

respectively. Therefore, to avoid entrance effects the gas flow sensor should be placed at

a distance greater then $x_{e,t}$.

Temperature Dependent Properties

The thermal conductivity k and viscosity of the fluid may be temperature

dependent. The change in the value of k can cause the heat transfer coefficient, h, to

differ appreciably from a constant property value (Burmeister, 1983). The temperature-

dependent viscosity affects the velocity profile even in the case of a fully-developed flow.

A temperature-dependent density also gives rise to a longer-lasting radial velocity

component that lengthens the entrance region.

For a gas, specific heat and Prandtl number vary only slightly with temperature, but viscosity and thermal conductivity vary roughly with 0.8 power of absolute temperature and density varies inversely with absolute temperature.

Two ways of addressing temperature correction of constant-property results are the *reference-temperature* and the *property-ratio* schemes. In the reference-temperature scheme, a characteristic temperature is selected at which all properties are evaluated. The characteristic temperature can be the mixing-cup temperature which is suitably averaged between inlet and exit temperature, or a combination of these. In the property-ratio scheme, all properties are evaluated at the characteristic temperature described previously, and all effects of property variation transverse to the flow are then expressed as ratios of properties evaluated at the characteristic and surface temperatures (Burmeister, 1983).

For gases, all property variations can be represented by the absolute temperature; thus, the correction for temperature-dependent property is (Burmeister, 1983):

$$\frac{Nu}{Nu(T_M)} = \left[\frac{T_w}{T_M}\right]^n \tag{88.}$$

$$\frac{f}{f(T_M)} = \left[\frac{T_w}{T_M}\right]^m \tag{89.}$$

where $Nu(T_M)$ and $f(T_M)$ are the Nusselt number and the frictional factor at the mixing-cup temperature which is roughly the average temperature of its inlet and outlet values, respectively. T_w is the wall temperature. For a laminar boundary layer on a flat plate, n=-0.08, m=-0.08 when gas is heated and n=-0.045, m=-0.045 when gas being cooled.

Constant Heat Flux

In many cases the heat flux distribution is constant and the objective is to find the distribution of the plate-surface temperature. Kays (1986) derived an expression for the temperature of a plate with any arbitrary flux variation.[4]

$$T_w(x) - T_{amb} = \frac{0.632}{k} Pr^{-\frac{1}{2}} Re^{-\frac{1}{2}} \int_0^x \left[1 - \left(\frac{\xi}{x}\right)^{\frac{3}{4}}\right]^{-\frac{2}{3}} q(\xi)d\xi \qquad (90.)$$

When heat rate per unit area is constant, q" = constant, the integral is converted to the form of the beta function, and convection conductance and a Nusselt number can be defined. The result is (Kays, 1986):

$$Nu_x = \frac{hx}{k} = 0.453 \, Pr^{\frac{1}{3}} \, Re^{\frac{1}{2}} \qquad (91.)$$

Therefore, the average forced convection coefficient can be evaluated using the following *Equation (92)* (Kays, 1986):

$$h_{avg} = \frac{1}{L_{CK}} \int_0^{L_{CK}} \left[k \times \frac{Nu_x}{x}\right] dx \qquad (92.)$$

The average Nusselt number is:

$$Nu_x = 0.906 \, Pr^{\frac{1}{3}} \, Re^{\frac{1}{2}} \qquad (93.)$$

The correction for temperature dependent properties in our experiments is:

$$\frac{Nu}{Nu(T_M)} = \left[\frac{T_{AVG}}{T_M}\right]^{-0.08} \qquad (94.)$$

In the range of $35 < T_{AVG} \leq 70 \,^oC$, and if T_M, the average temperature of the air, taken as the average between the air and SAW package temperature, *Nu* is given by:

$$Nu = 0.96 Nu(T_M) \qquad (95.)$$

---

[4] $(T_{amb} = T_\infty)$

Therefore,

$$Nu = 1.04 \times 0.906 Pr^{1/3} Re_L^{1/2} \tag{96.}$$

corresponding average convection coefficient at T_M is (Kays, 1986):

$$h_{TM} = 0.943 \frac{k}{L_{CK}} Pr^{1/3} Re_L^{1/2} \tag{97.}$$

Temperature Distribution

The SAW substrate materials are anisotropic and to calculate average temperature, one must first derive temperature distribution across many nodes within the substrate. A simple heat flow model to derive the temperature and the average temperature of the SAW substrate for given input power levels and boundary conditions is presented here. Figure 22 identifies the parameters and coordinates used for a heat-flow model of the SAW substrate. The model uses one-dimensional heat-flux equations to describe the steady-state heat transfer within the SAW substrate. If we designate the heat-transfer rate in an elemental length along the substrate dx to the flowing gas (upward direction) by Q_{Up}, the equation can be expressed as express as (Tai, 1985):

$$Q_{Up} = H_{Top} w \left[T(x) - T_\infty \right] dx \tag{98.}$$

$T(x)$ is the temperature along the substrate and h_{Top} is the convective coefficient of the substrate. The heat flux downward toward the floor Q_{Bot} is given by (Tai, 1985):

$$Q_{Bot} = \frac{k_{air}}{S} \left[T(x) - T_\infty \right] dx \tag{99.}$$

where T_S is the substrate surface temperature, S is the spacing from the substrate to the

bottom of the flow cell, and k_{air} is the thermal conductivity of the air in the gap.
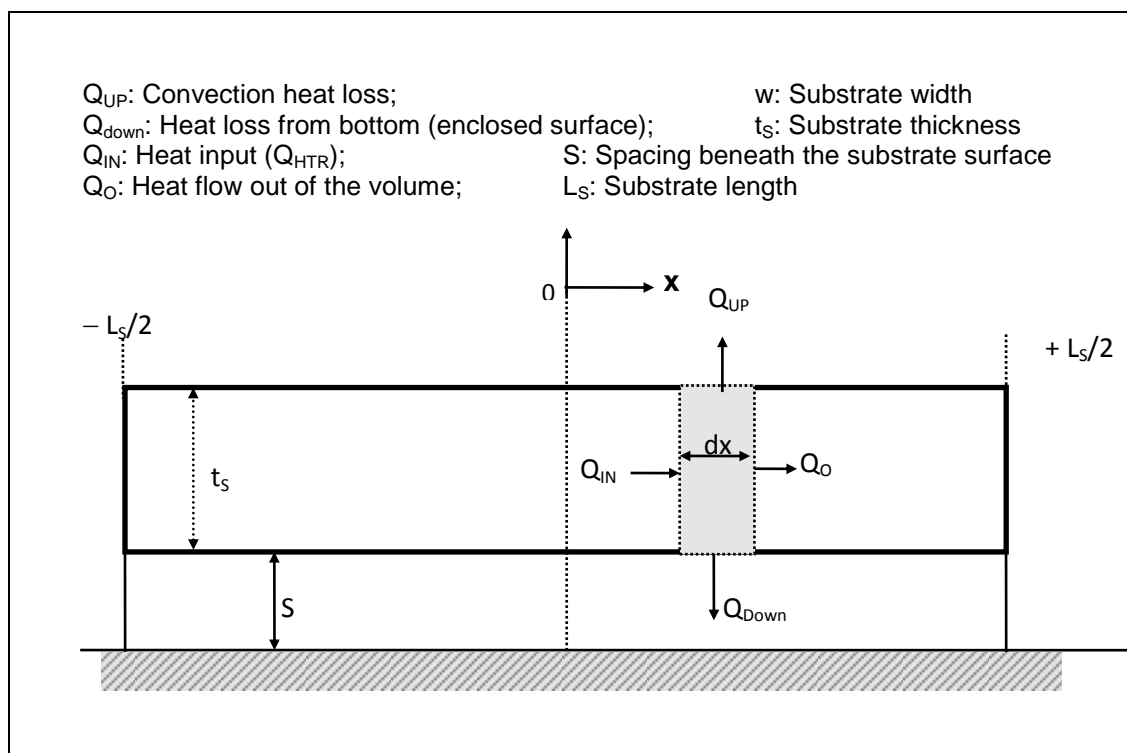
Figure 22 – Sketch of the SAW substrate cross-section showing the coordinates used for the heat-flow analysis.

The flow of heat into an elemental volume of length dx at location x along the substrate is

Q_{IN} is given as:

$$Q_{IN} = -k_s wt_s \frac{dT}{dx}\Big|_x \qquad (100.)$$

Similarly, the heat flow out of the volume Q_O is:

$$Q_{OUT} = -k_s wt_s \frac{dT}{dx}\Big|_{(x+dx)} \qquad (101.)$$

where t_S is the thickness of the substrate. If the heater input power Q_{HTR} is delivered over length l of the heater, the power input $Q(x)$ to the volume element dx is given by:

$$Q(x) = Q_{HTR}\frac{dx}{l} \tag{102.}$$

At steady state the power input (via heater element) plus the heat flow into the volume element equals the heat conveyed away from it:

$$Q(x) + Q_{IN} = Q_{Up} + Q_{Bot} + Q_{Out} \tag{103.}$$

Using *Equations (98-99)* in *Equation (100)*, subject to the boundary condition that the temperature at the mechanical supports $\left(x = \pm\frac{L_S}{2}\right)$ equals T_S (the substrate temperature), an equation to describe the temperature along the substrate is thus given by Tai et al. (1985):

$$T(x) = T_S + \left[\frac{Q_{HTR} - \{H_{Up} \times wL_S\} \times (T_S - T_a)}{wL_S\left\{H_{up} + \frac{k_{air}}{S}\right\}}\right] \times \left[1 - \left(\frac{\cosh Cx}{\cosh\frac{CL_S}{2}}\right)\right] \text{ where}$$

$$C = \left[\frac{\left(H_{Up} + \frac{k_{air}}{S}\right)}{k_S t_S}\right]^{\frac{1}{2}} \tag{104.}$$

Average Temperature

As expected, the maximum temperature is at the middle of the span, decreasing with hyperbolic cosine dependence toward either end. The equation for the average temperature is obtained by integrating *Equation (104)* as follows (Tai, 1985):

$$T_{avg} = \frac{1}{l}\int_{-1/2}^{1/2} T(x)\, dx \tag{105.}$$

$$T_{avg}(u_{avg}) =$$

$$T_S + \left[\frac{Q_{HTR} - \{h_{up}(u_{avg}) \times L_S^2\} \times (T_S - T_a)}{L_S^2 \{h_{up}(u_{avg}) + \frac{k_{air}}{S}\}} \right] \times$$

$$\left[1 - \left(\frac{2}{C(u_{avg}) \times L_S} \right) \times \tanh\left(C(u_{avg}) \times \frac{L_S}{2} \right) \right] \qquad (106.)$$

The terms in *Equation (106)* that depend on flow past the substrate are H, C (through H),

and T_S. The dependence of H on flow rate (for convective and forced cooling by flow

parallel to a surface) was discussed in the earlier section. From this dependence, using

Equation (106), T_{AVG} is calculated. Correspondingly, the output frequency change Δf as

a function of temperature for the SAW oscillator can be calculated.

Time Response

Assume that the crystal is suspended in the air, and also the sensor thickness t_S is

small compared to its length, L, the variation of temperature/thickness can be neglected,

and hence the sensor temperature T_S may be assumed to be a function of only ξ and time

t.

The transient (momentary) heat balance in the sensor can be written as (Jian-Bio,

2007):

$$\rho c_S t_S \frac{\partial T_S}{\partial t} = k_S \frac{t_S}{L^2} \frac{\partial^2 T_S}{\partial \xi^2} - q_f + q_h \qquad (107.)$$

$\xi = \frac{x}{L}$, where L lies between $\xi=0$ and $\xi=1$; q_h is the heat generation and q_f is the

convective heat loss. *Equation (107)* contains the time-transient effect, which is caused

by the redistribution of heat in the sensor due to conductive heat flows. Using the method

of separation of variables, the time-dependent function can be expressed as a Fourier

series which results in a solution for the response time given as (Giarratano, 1984):

$$\tau = \frac{c_s \rho_s \, L^2}{k_s \pi^2} \qquad\qquad (108.)$$

CHAPTER 4: THEORETICAL MODEL DERIVATION

In this chapter, a model is developed to characterize the behavior of the thermal SAW flow sensor: The methodology is based on developing a mathematical model for the heat flow for an enclosed flat plate with an embedded internal heat source. Energy balance equation, under steady state conditions, will include heat loss due to conduction, convection, and radiation. The theory of SAW oscillator and its dependence on temperature will be applied to predict behavior of the SAW flow sensor under wide range of variables including sensor's dimensions, substrate materials, vary input power (i.e., SAW substrate temperature) and flow conditions.

Model highlights and assumptions include:

1. The SAW sensor has an integrated heating source. The flat plate sensor (SAW substrate) is heated by a thin-film heater fabricated at the center.

2. The thermal properties stay uniform within the operating range of the SAW sensor.

3. To avoid thermal conduction losses, the SAW sensor has a high thermal isolation with surrounding.

4. Thermal analysis are rendered to:

   - Quantify input (power) sources

   - Quantify output (heating dissipation) sources with and without flow conditions

   - Determine temperature distribution for thermal characterizations

   - Derive time response

5. The model can be applied to a wide-range of SAW device and flow set-up geometrical dimensions.

6. The model will allow sensor characterization based on differing SAW substrate materials. Using theoretical analysis, a design of an optimal SAW flow sensor and its characteristics in terms of the frequency shift of the SAW oscillator versus gas velocity will be developed.

7. The model will result in analyses that will allow the development, characterization, and the further optimization of the sensor.

The theoretical models presented in Chapter 4 are applied to SAW-based gas flow sensing. Model (s) that validates and describes SAW-based flow sensor has not be reported. This is first such study that reports a detailed model to predict SAW-based gas flow sensor behavior for a wide range of variables and boundary conditions.

Data (Model) Limitations

The data and/or model developed are limited to predicting the behavior of SAW-based gas flow sensor under laminar flow conditions. The model doesn't address behavior of the SAW-based gas flow sensor under turbulent flow conditions. A proposed setup to measure flow rate using SAW is illustrated in Figure 16.
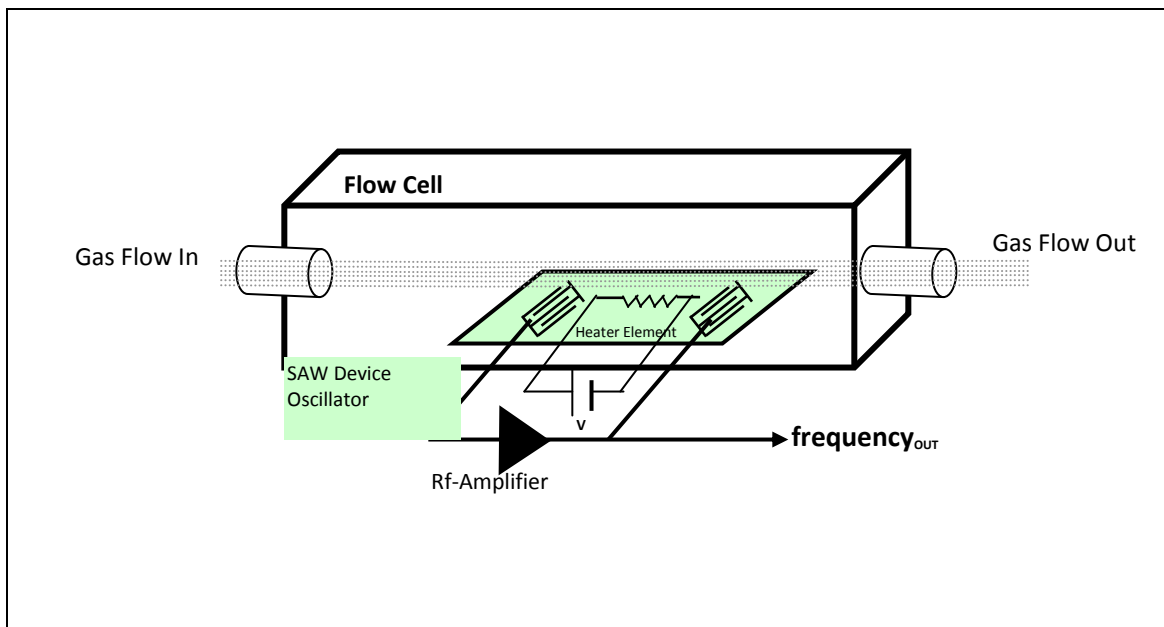
Figure 23 – Schematic representation of a proposed SAW flow sensor: SAW device with an integrated heater element situated in a flow cell.

Summary – Model Highlights

Derivation of the SAW-based flow sensor model for a wide range of variable and boundary conditions were derived in earlier sections of this chapter. A summary of the model based on above mathematical treatment of the problem is captured here. In the next chapter, this model is applied and the behavior of the SAW-based gas flow sensor for a wide range of variable and boundary conditions are presented.

SAW Temperature Dependence and Characteristics

Temperature dependent characteristics of the SAW substrate are summarized here.

$$\text{T (Stress Tensor)} = \text{C (Stiffness Tensor)} \times \text{S (Strain Tensor)} \qquad (109.)$$

- The stiffness tensor C is temperature dependent (Mathews, 1977):

$$\text{v (SAW velocity)} = \left(\frac{C}{\rho}\right)^{\frac{1}{3}} \quad \text{where } \rho \text{ is mass density} \qquad (110.)$$

- Temperature-dependent dimensional changes (Ebata, 1982):

$$\text{Delay time } \tau_d = \frac{l}{v} \qquad \text{l: center-to-center distance} \qquad (111.)$$

$$l = l_o[1 + \alpha(T - T_o)] \text{ and } v = v_o[1 + \delta(T - T_o)] \qquad (112.)$$

where: α = temperature expansion coefficient

$$\alpha = \frac{1}{l_o}\frac{dl}{dT} \qquad (113.)$$

δ = temperature dependence of v

$$\delta = \frac{1}{v_o}\frac{dv}{dT} \qquad (114.)$$

$$\frac{1}{\tau_d}\frac{d\tau_d}{dT} = \frac{1}{l_o}\frac{dl}{dT} - \frac{1}{v_o}\frac{dv}{dT} = \alpha - \delta \qquad (115.)$$

Similarly,

$$\frac{1}{f_o}\frac{df}{dT} = \delta - \alpha = \text{TCD} \qquad (116.)$$

and

$$\frac{\Delta\tau_d}{\tau_d} = -\frac{\Delta f}{f_o} = \Delta T \times \text{TCD} \qquad (117.)$$

The frequency-temperature relationship:

$$\frac{\Delta f(T)}{f} = \frac{f(T) - f(T_o)}{f(T_o)} = a_1(T - T_o) + \frac{1}{2}b_1(T - T_o)^2 + \cdots$$

$a_1 \gg b_1$ results in high temperature sensitivity and good linearity.

$$\frac{\Delta \tau_d}{\tau_d} = -\frac{\Delta f}{f_o} = \Delta T \times TCD = a_1 \Delta T \tag{118.}$$

The temperature sensitivity of the SAW oscillator depends on:

- The temperature coefficient of delay (TCD) and

- The synchronous frequency f_o

Thermal Conduction Resistances:

Substrate thermal resistance(R_L or R_S):

$$R_S = \frac{L_S}{k_S A_S} \tag{119.}$$

Contact resistance:

$$R_{CNCT} = \frac{L_{SINK}}{2k_{Al} A_{CNCT}} \tag{120.}$$

Heater thermal resistance:

$$R_h = \frac{L_h}{k_{Al} A_h} \tag{121.}$$

Constriction thermal resistance:

$$R_{CH} = \frac{\Delta T_{CH}}{Q_{COND}} \tag{122.}$$

$$\Delta T_{CH} = \Delta T_{C1} + \Delta T_{C2} + \Delta T_{C3} \tag{123.}$$

where,

$$\Delta T_{C1} = \frac{Q_{COND} b}{2\pi^2 k_L ac} \sum_{m=1}^{\infty} \frac{\sin\left(\frac{m\pi a}{b}\right)}{m^2} \tag{124.}$$

$$\Delta T_{C2} = \frac{Q_{COND} c}{2\pi^2 k_L db} \sum_{m=1}^{\infty} \frac{\sin\left(\frac{m\pi a}{b}\right)}{m^2} \tag{125.}$$

$$\Delta T_{C3} = \frac{Q_{COND2}}{2\pi^2 k_L ad} \sum_{m=1}^{\infty} \sum_{n=1}^{\infty} \frac{\sin\left(\frac{n\pi d}{c}\right)\sin\left(\frac{m\pi a}{b}\right)}{mn\left[\left(\frac{m\pi}{b}\right)^2 + \left(\frac{n\pi}{c}\right)^2\right]^{1/2}} \tag{126.}$$

Total thermal conduction resistance:

$$R_{COND} = (R_S + R_{CH} + R_{CNCT}) \tag{127.}$$

Radiation Loss Analysis:

$$Q_{RAD} = \sigma \times F_A \times F_\varepsilon \times A_S[(T_{AVG})^4 - (T_\infty)^4] \tag{128.}$$

$$F_\varepsilon = \frac{1}{\left[\frac{1}{\varepsilon_1} + \frac{1}{(\varepsilon_2 - 1)}\right]} \tag{129.}$$

$$Q_{RAD} = 5.67 \times 1 \times F_\varepsilon \times A_S\left[\left(\frac{T_{AVG}}{100}\right)^4 - (2.98)^4\right] \tag{130.}$$

The heat dissipation from radiation is ignored due to small contributions.

Free Convection Analysis – Enclosed Surfaces:

$$\text{Nusselt Number} = Nu = \frac{hL_{CK}}{k} \tag{131.}$$

$$\text{Prandtl Number} = Pr = \frac{\mu\, C_p}{k} = \frac{\text{momentum diffusivity}}{\text{thermal diffusivity}} \tag{132.}$$

$$\text{Grashof Number} = Gr = \frac{g\beta\rho^2 L_{CK}^3 \Delta T}{\mu^2} \tag{133.}$$

a) Top Surface Convection Loss Analysis

$$Nu_S = 0.195(Gr_S)^{1/4} \tag{134.}$$

$$\text{Grashof Number} = Gr = \frac{g\beta\rho^2 L_{CK}^3 \Delta T}{\mu^2} = \frac{g\beta L_{CK}^3 \Delta T}{\upsilon^2} \tag{135.}$$

Prandtl Number $= \nu/a$; where, $\nu = \frac{\mu}{\rho}$, μ is dynamic viscosity (m^2/s) , υ kinematic

viscosity, ρ is density

b) Top Surface Convection Coefficient

$$h_{TOP} = \frac{k_{air}}{L_{CK} \times Nu_S} \tag{136.}$$

Top surface thermal resistance:

$$R_{TOP} = \frac{1}{h_{TOP} \times A_S} \, ^{\circ}C/W \tag{137.}$$

c) **Bottom Surface Convection Loss Analysis**

$$Nu_S = \frac{h_{BOT}S}{k_{air}} = 1.0$$

Convection Coefficient:

$$h_{BOT} = \frac{k_{air}}{s} \tag{138.}$$

Bottom surface thermal resistance:

$$R_{BOT} = \frac{1}{h_{BOT} \times A_S} \, ^{\circ}C/W \tag{139.}$$

d) **Vertical Surface**

$$Nu_V = 0.448 + 0.46 Gr_V^{1/4} \tag{140.}$$

$$\text{Grashof Number} = Gr_V^{1/4} = \frac{g\beta l^3 \Delta T}{\upsilon^2} \text{ (l is height of vertical wall)} \tag{141.}$$

Vertical or side wall convection coefficient:

$$h_V = \frac{k_{air}}{I \times Nu_V} \tag{142.}$$

$$R_{VER} = \frac{1}{4 \times h_V \times A_V} - \text{Vertical surface thermal resistance} \tag{143.}$$

The factor 4 is used to account four sides.

e) **Total Convection Resistance – All surfaces**

$$R_{CONV} = [R_{TOP} \| R_{Bot} \| R_{VER}] \, ^{\circ}C/W \tag{144.}$$

f) **Total Thermal Resistance – Conduction + Convection**

$$\Sigma R_{TH} = R_{Tot} = [R_{COND} + R_{CONV}] \ ^\circ C/W \tag{145.}$$

$$R_{Tot}(A_S, t_S, A_V) = R_{CH} + R_L \ (A_S, t_S) + R_{CONV}(A_S, A_V) \tag{146.}$$

g) Total Thermal Power Loss

$$P = Q_{HTR} = Q_{Tot} = \frac{(T_{AVG} - T_\infty)}{\Sigma R_{TH}} \tag{147.}$$

$$Q_{Tot}(A_S, t_S, A_V) = \frac{\Delta T}{R_{Tot} \ (A_S, t_S, A_V)} \tag{148.}$$

h) Conduction Loss Calculation

Since conduction and convection losses occur in parallel, conduction heat loss can only be calculated after the total heat loss is calculated. The following relationship is used to calculate conduction losses:

$$Q_{COND}(A_S, t_S) = Q_{CONV} \ (A_S, A_V) - Q_{Tot}(A_S, t_S, A_V) \tag{149.}$$

Forced Flow Analysis

Temperature-dependent properties of air are taken into consideration (laminar flow over top surface). Reynolds number for flat plate with laminar flow conditions is given as (Kraus & Bohen, 1983),

$$Re_L(u_{avg}) = \frac{(\rho_{air} u_{avg} L_{CK})}{\mu_{air}} \tag{150.}$$

Forced convection coefficient:

$$h_{TM}(u_{avg}) = 0.943 \ \frac{k_{air}}{L_{CK}} \ Pr^{\frac{1}{3}} \ Re_L^{\frac{1}{2}}(u_{avg}) \tag{151.}$$

$$R_{FRD}(u_{avg}, A_S) =$$

$$\frac{1}{h_{TM}(u_{avg}) \times A_S} \, ^{\circ}C/W - Forced\ thermal\ resistance\ (top\ surface)$$

$$(152.)$$

$$Q_{FRCD}(u_{avg}, A_S, T_{avg}) =$$

$$h_{TM}(u_{avg}) \times A_S \times \Delta T(T_{avg}) - Top\ surface\ forced\ convection\ thermal\ loss$$

$$(153.)$$

$$R_{Tot}(A_S, t_S, A_V) =$$

$$R_{CH} + R_L (A_S, t_S) + R_{CONV}(A_S, A_V) - Total\ thermal\ resistance$$

$$(154.)$$

$$Q_{FTot}(A_S, t_S, u_{avg}, T_{avg}) =$$

$$\frac{\Delta T(T_{avg})}{R_{NET} (A_S, t_S, u_{avg})} - Total\ thermal\ loss\ from\ all\ surfaces\ of\ the\ sensor$$

$$(155.)$$

$$\delta T(A_S, t_S, u_{avg}, Q_{HTR}) =$$

$$\Delta T(T_{avg}) - T(A_S, t_S, u_{avg}, Q_{HTR}) -$$

$$Net\ Temperature\ change\ under\ forced\ flow\ for\ various\ operating\ conditions$$

$$(156.)$$

$$\delta f_{NET}\left(A_S, t_S, u_{avg}, Q_{HTR}\right)$$

$$= \delta T\left(A_S, t_S, u_{avg}, Q_{HTR}\right) \times TCD \times f_o$$

$- Net\ frequency\ change\ calculated\ from\ net\ temperature\ change\ under$

$forced\ flow\ for\ various\ operating\ conditions$

(157.)

Total Thermal Resistance – Under Forced Convection – $\sum R_{FTH}$:

$$\sum R_{FTH} = [R_{COND}\| R_{Bot} \| R_{FRD}] = R_{Tot}(A_S, t_S, A_V)\ ^\circ C\!/_W$$

(158.)

Total Power Loss– Under Free Convection:

$$P = Q_{HTR} = Q_{Tot} = \frac{(T_{AVG} - T_\infty)}{\sum R_{TH}} = Q_{FTot}\left(A_S, t_S, u_{avg}, T_{avg}\right) \quad (159.)$$

Time-response

$$\tau = \frac{c_S \rho_S\ L^2}{k_S \pi^2} \quad (160.)$$

Temperature Distribution

$$T_{avg}\left(u_{avg}\right) =$$

$$T_S + \left[\frac{Q_{HTR} - \{h_{up}(u_{avg}) \times L_S^2\} \times (T_S - T_a)}{L_S^2 \{h_{up}(u_{avg}) + \frac{k_{air}}{S}\}}\right] \times \left[1 - \left(\frac{2}{C(u_{avg}) \times L_S}\right) \times \tanh\left(C(u_{avg}) \times \frac{L_S}{2}\right)\right]$$

(161.)

where for free convection, use $h_{UP} = h_{TOP}$ and under forced convection, $h_{UP} = h_{TM}$.

Theoretical Results and Analysis

Theoretical analyses to determine the characteristics of a SAW flow sensor have

been derived earlier. Now these analyses to predict the response of the SAW-based flow

sensor for several SAW substrate materials, geometrical options and power requirements will be applied. From these analyses, a design of an optimal SAW sensor is proposed. This chapter describes:

1. The analyses of the characteristics and behavior of several SAW substrate materials as a means of determining their suitability for flow sensor applications. This includes:

   - Response (frequency-temperature) with or without flow conditions for different heater power levels, several substrate materials, and geometries

   - Temperature distribution and calculation of mean sensor's temperature

   - Time response

   - Experimental observations and analysis

2. An optimal sensor design

In this section, the theoretical model developed in Chapter 3 to predict the steady-state behavior of the SAW substrate for given input power levels to the heater element is applied.

Following this, the energy balance equation for the SAW-based flow sensor is applied:

$$P = Q_{COND} + Q_{CONV} + Q_{RAD} \qquad (162.)$$

The rate of energy supplied is equal to the rate of energy carried away from the SAW substrate by conduction, convection, and radiation.

In Chapter 3, the application of the energy balance equation yielded a model for a SAW-based flow sensor. The highlights of the model are captured in *Equations (119) –*

(161). Based on the model that was developed in Chapter 3, the results and data for a practical SAW-based flow setup with appropriate geometries and operating conditions is provided.

Characterization and Analysis

The theoretical characteristics and the analyses of SAW-based flow sensors for several substrate materials are presented here in this section.

SAW Substrates Properties

A summary of properties and characteristics of potential SAW substrate materials for SAW flow sensor applications is provided in Table 10. The analysis is presented in terms of SAW velocity, temperature coefficient of delay, coupling coefficient, and insertion loss. This information is necessary to characterize SAW-based flow sensors for each substrate material, compare and contrast the results, and finally be able to design an optimal SAW oscillator in terms of temperature characteristics, coupling coefficient and/or insertion loss for the amplifier.

Table 10 – Summary of the SAW substrate materials characteristics and SAW device analysis for potential flow sensor applications.

Substrate	Properties				
	Velocity (m/s)	Coupling Parameter [5] ($\Delta v/v_\infty$)	TCD (a_1) (ppm/°C)	Insertion loss (dB)	Comments/Analysis
$LiNbO_3$ (Y-Z) (Inaba et al., 1982) $LiNbO_3$ (128°)	3480	0.0241	-88.4 -72	Low: 12-15 at (142.5 MHz)	• An optimal SAW oscillator design for flow sensing application would require moderate or high *TCD*, higher coupling parameter, lower insertion loss. • $LiNbO_3$ has high *TCD*, good coupling parameter and low insertion loss. SAW devices are reported only bulk $LiNbO_3$ substrate. • Another important criteria is mass of the sensor. Thin film technology allows miniaturization. Among various SAW substrate, SAW devices on thin **ZnO**, **GaAs** and **AlN** films have been reported. • Quartz, $Bi_{12}GeO_{20}$ and GaAs have lower coupling parameter and higher insertion loss. Specific cuts (e.g., LST of Quartz) and GaAs have moderate *TCD*. $Bi_{12}GeO_{20}$ has high *TCD*. • Higher insertion loss would require a higher gain RF-amplifier(s), which is not desirable.
Quartz (LST) (Ebata, 1982)	3158	0.00058	28	Higer $\cong$ 40	
ZnO (Kim et al., 1995; Kadota et al., 1985)) (Thickness dependent)	2800-2900	$\cong$ 0.166 - 0.157	+35	Low: 2.9 - 3.7 at λ_o=3.6 μm (700 Mhz range)	
$LiTaO_3$ (y-z) (Crystal Technology Notes)	3230	0.0033	35	Moderate to high	
GaAs (Cambon et al., 1981)	2822	0.00008	+50	Very High	
$Bi_{12}GeO_{20}$ (Inaba et al., 1982; Matthews, 1977)	1681	0.0068	130	Moderate	
Al N (Pearce, 1981)	$\cong$6100	0.007	-	28 at 122 MHz	

---

[5] The coupling parameter expresses the fractional change in the phase velocity of a surface wave produced by a change in the electrical boundary condition from free to short circuit. Similarly, an effective electromechanical coupling factor for surface waves is defined as: $K^2 = -2\Delta v/v$. The coupling factor depends on the substrate material and propagation geometry. SAW device characteristics such as insertion loss, transducer efficiency, and band-width can often be expressed as an explicit function of the value of coupling factor.

Currently, Quartz and Lithium Niobate (LiNbO$_3$) are the most widely used materials for SAW applications. Based upon the above analysis, Zinc Oxide (ZnO), because of its attractive proprieties (coupling coefficients, thermal conductivity, and temperature coefficient of delay), was also selected. Therefore, in this research SAW-based characterization for the following substrate materials is presented:

1. Lithium Niobate

2. Zinc Oxide

3. Quartz

Thermal properties of various SAW substrate materials are provided in Table 11.

Table 11 – Thermal properties of SAW substrate materials.

Properties of the substrate materials (Lide, 1993-1994).								
Temp	Density (ρ) (kg/m^3)x10^3			Specific heat capacity(c) (J/kg ^{o}K) x 10^3			Thermal conductivity (k$_s$) (W/m ^{o}K)		
	Quartz	LiNbO$_3$	ZnO	Quartz	LiNbO$_3$	ZnO	Quartz	LiNbO$_3$	ZnO
Room	2.2	4.64	5.66	0.753	0.645	0.64	1.38	4.2	17

Methods and Tools

The theoretical models developed in Chapter 3 and 4 are general and are applicable to a wide range of variables including geometrical dimensions and substrate materials. Data that was obtained as a result of applying the theoretical models developed in Chapter 3 and 4 and the following analyses are presented here. The ***MATHCAD***, a software application package for mathematical calculation, was used to execute the models*.*

Substrate Material Characterization

A summary of the theoretical modelling analysis for following SAW substrates are presented here:

- Lithium Niobate (LiNbO$_3$)

- Zinc Oxide (ZnO)

- Quartz.

Relationships of many variables necessary for sensor characterization are plotted.[6]

Figure 24 – Calculated values of thermal conduction resistance (LiNbO$_3$) as a function of substrate area and various thickness values.
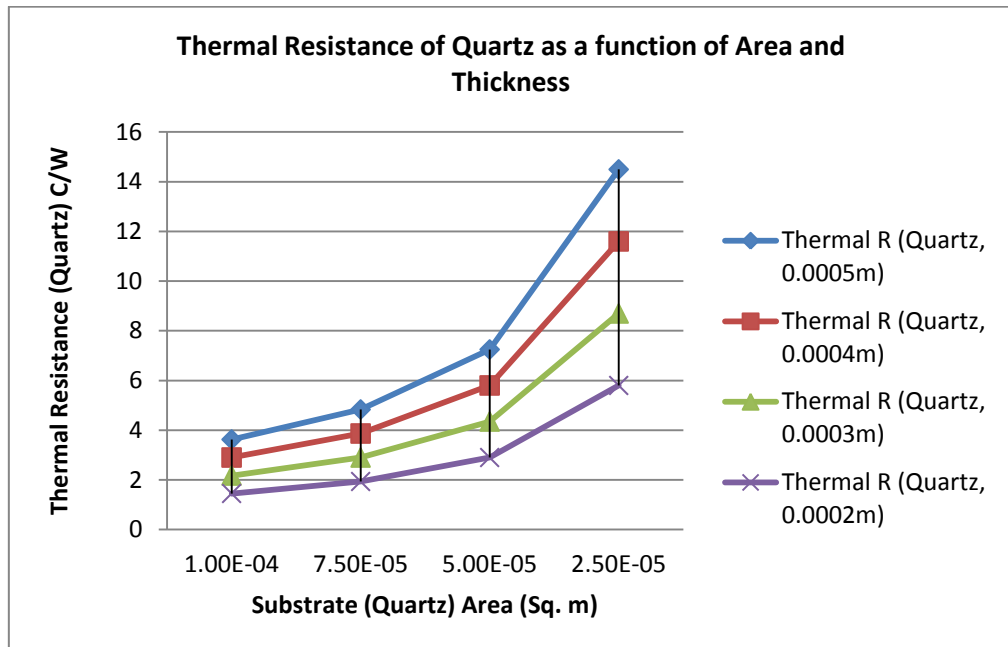
Figure 25 – Calculated values of thermal conduction resistance (Quartz) as a function of substrate area and thickness various thickness values.

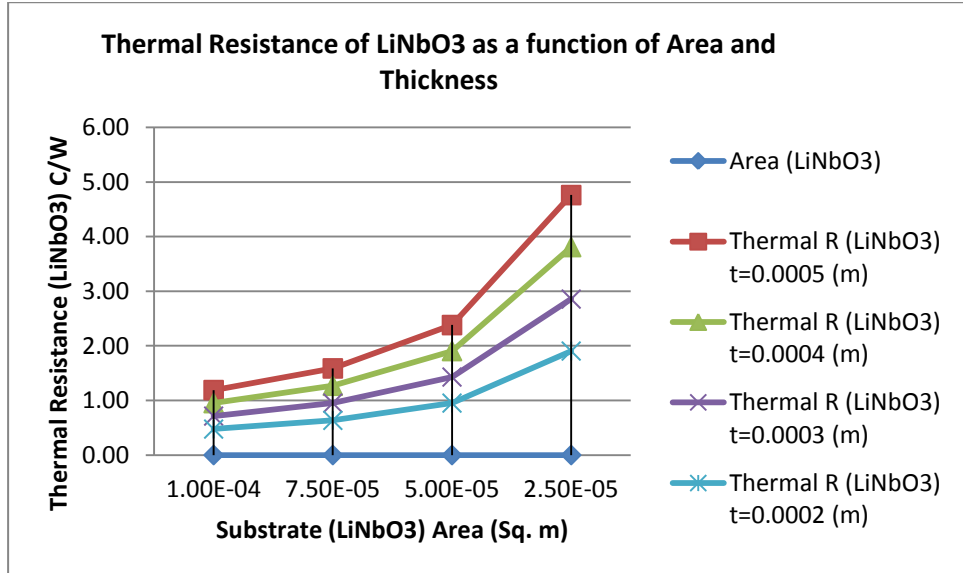[6] Unless specified, the value of $\Delta T = 50^{\circ}C$ used in following plots.
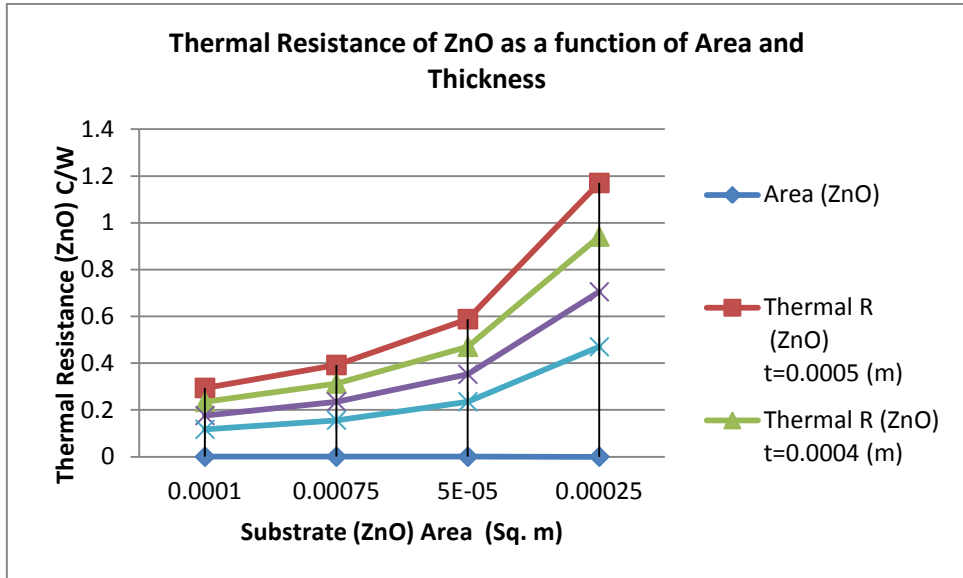
Figure 26 – Calculated values of thermal conduction resistance (ZnO) as a function of substrate area various thickness values.

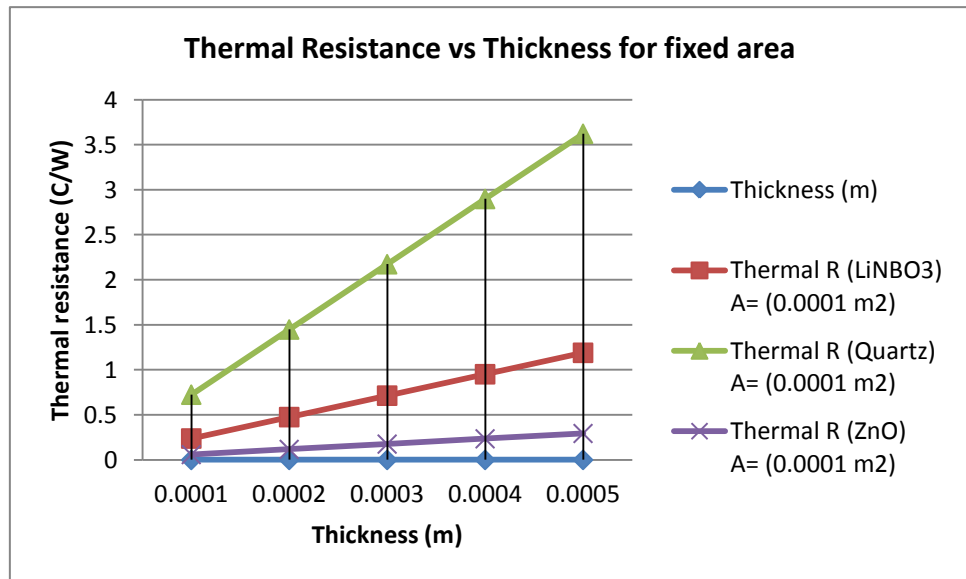**Figure 27 – Calculated values of thermal conduction resistance as a function of thickness (substrates: LiNbO₃, ZnO and Quartz).**
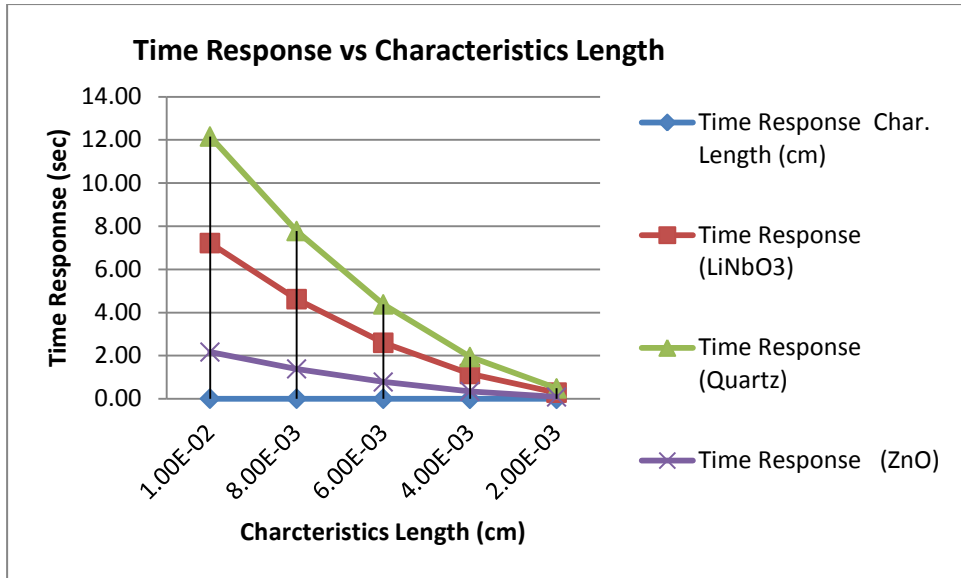
Figure 28 − Calculated values of Time Response as a function of substrate's characteristics length.
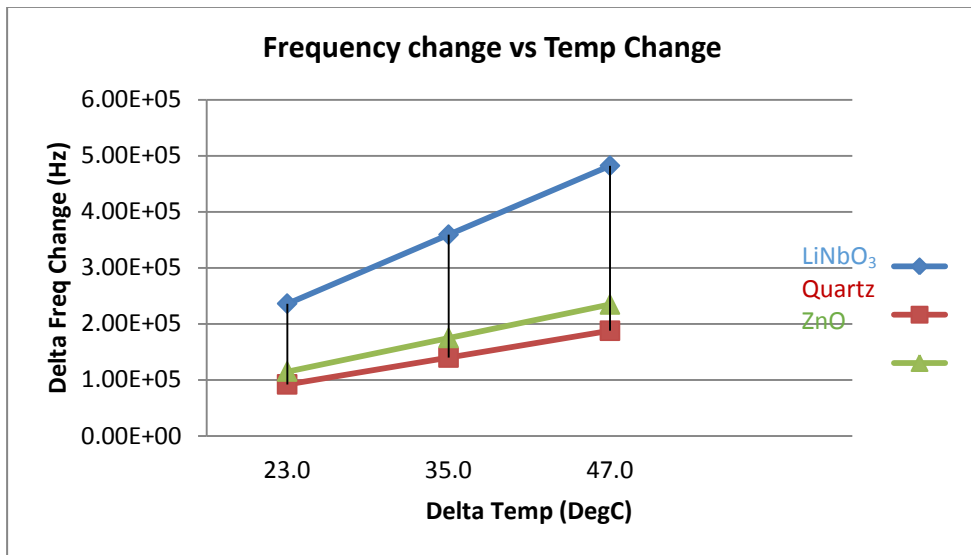

Figure 29 – Calculated values of Frequency versus temperature characteristics (LiNbO$_3$, ZnO and Quartz).
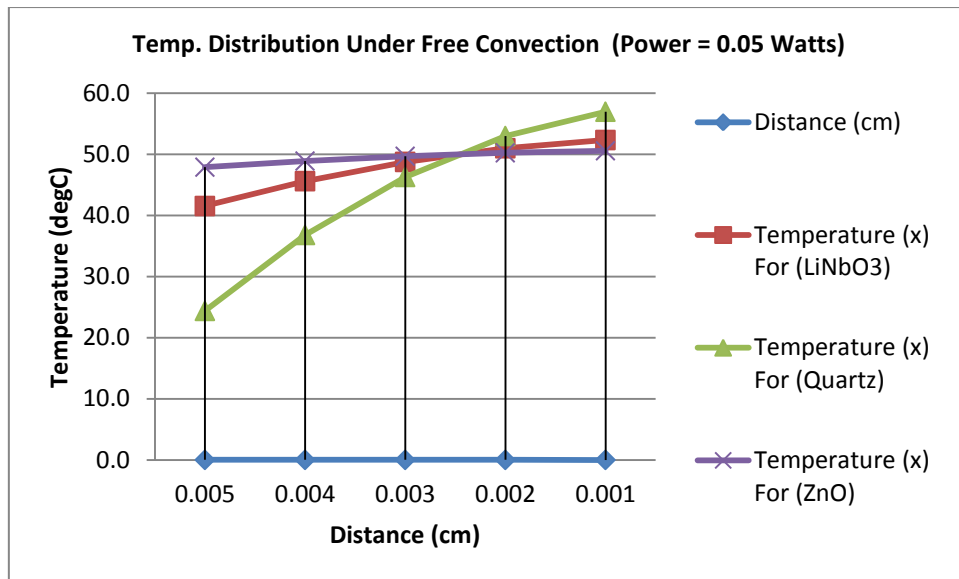
Figure 30 – Calculated values of Temperature distribution as a function a function of substrate's characteristics length

Analyses

A summary of the analyses based on the data presented in earlier sections

covering the relationships between the features of LiNbO$_3$, Quartz, and ZnO is

provided in the following table:

Table 12 – Summary of LiNbO$_3$, Quartz and ZnO results and/or characteristics (Free convection condition).

Total Power (Convection plus conduction) Loss (Q$_{TOT}$) and Time Response for several substrate materials and dimensions.[7] (Substrate thickness t$_S$=0.05 mm, and ΔT=50 ^{o}C)									
	Quartz			**LiNbO$_3$**			**ZnO**		
Area, A$_S$ (m^2) x10^{-5}	Q$_{TOT}$ (W)	Q$_{COND}$ (W)	Time Resp. (sec)	Q$_{TOT}$ (W)	Q$_{COND}$ (W)	Time Resp. (sec)	Q$_{TOT}$ (W)	Q$_{COND}$ (W)	Time Resp. (sec)
10	0.0596	0.0016	**12.17**	0.0584	0.00139	**7.22**	0.0597	0.0013	**2.17**
7.5	0.0451	0.0009	**7.79**	0.0444	0.00082	**4.62**	0.0452	0.00077	**1.39**
5.0	0.0306	0.0005	**4.38**	0.0303	0.00039	**2.59**	0.0306	0.00036	**0.78**
2.5	0.0161	0.00017	**1.97**	0.0160	0.00012	**1.15**	0.0161	0.0001	**0.08**

These findings can be interpreted as follows:

- Changes in the substrate conduction thermal resistance (R$_L$) versus thickness

  for a fixed value of the substrate area shows that the *thermal resistance*

---

[7] Heat loss fairly the same across all substrates, implying that the dominant mechanism of heat loss is convection under forced flow conditions. As expected conduction losses are higher in Quartz.

increases linearly as thickness increases. Changes in the substrate thermal resistance (R_L) versus area of the substrate for fixed value of the substrate thickness shows that the *thermal resistance* decreases as the area increases. Quartz has the highest conduction thermal resistance among the substrates. That means that the conduction losses in the Quartz substrate are among the highest of the three materials discussed in this research. For an optimal sensor, the area should be minimized to reduce conduction losses. This will enable a lower operating power for the sensor. In additional, lowering the value of the conduction losses will result to a better time response for the sensor. Therefore, a material with higher thermal conductivity should be more promising for this application.

- Radiation losses are directly proportional to the substrate area; the larger they are, the higher are the radiation losses. For an optimal sensor, the area should be minimized to reduce radiation losses[8].

- Changes in the substrate thermal convection resistance (R_{CONV}) decreases as the area of the substrate increases and it is independent of substrate thermal properties (e.g., thermal conductivity).

- Changes in the substrate total thermal resistance (R_{Tot}) versus area, for a fixed value of the substrate thickness, are plotted. The total thermal $(R_{tot} = R_{conv} + R_{cond})$ resistance decreases as area of the substrate increases. This indicates that convection is the major source of heat dissipation (within the scope of this research).

- Total power losses as a function of the substrate area are plotted. The higher the area is, the higher the power losses are. For an optimal sensor, the area

---

[8] The radiation losses are however, minimal and can be ignored from the analysis.

should be minimized to reduce power losses. This enables the sensor to operate at a lower power.

- Changes in the total thermal resistance under forced convection as a function of forced convection coefficient (corresponding to air velocity) for a given fixed value of the substrate area is plotted. The R_{FRD} decreases as velocity or convection coefficient increases. For fixed area and input power, the sensor flow detection range can be determined.

- Changes in the total thermal resistance under forced convection as a function of forced air velocity for a fixed value of the substrate area are plotted. The R_{FRD} decreases as velocity or convection coefficient increases. For fixed area and input power, the sensor flow detection range can be determined.

- Total thermal losses under forced convection as a function of forced air velocity for a fixed value of the substrate area are plotted. The total thermal losses increase as velocity or convection coefficient increases. For fixed area and input power, the sensor flow operating range can be determined.

- Note that the thermal heat losses are pre-dominantly due to convection losses for the geometries considered in this analysis.

- The time response depends on the ratio ($c\rho/k$). To optimize time response:
  - reduce the ($c\rho/k$) ratio
  - reduce crystal dimensions

- Among the three materials, ZnO offers the best time response values.

- τ (ZnO) is 3.5 and 6 time better than respectively $LiNbO_3$ quartz. Employing thin film of ZnO, further miniaturatization is possible that can substantially improve time response.

Optimal Design

From the analysis the following features of the SAW flow sensor are inferred:

1. The sensitivity, Δf, varies as $(u_{AVG})^{1/2}$, where u_{AVG} is the average fluid velocity.

2. The sensitivity of the sensor, Δf, is directly proportional to the input power, or the temperature of the sensor. $LiNbO_3$ offers the **best** output frequency sensitivity among three materials; ZnO is the second best.

3. Assume $A_S = (L_C)^2$, then the sensitivity is proportional to $L_C^{3/2}$, where L_C is the characteristics length of the sensor.

4. To improve the response time, the mass of the sensor should be reduced and a substrate material of higher thermal conductivity should be used. ZnO has the desired properties in accordance to these.

5. Note that the thermal heat losses are pre-dominantly due to convection losses and conduction for the geometries considered in these analyses. ZnO has minimal conduction losses compared to $LiNbO_3$ and Quartz.

6. ZnO-based SAW sensor offers the best response compared to $LiNbO_3$, and Quartz-based sensors as they require low input power due to their low conduction losses

7. The time response depends on the ratio $(c\rho L^2/k)$. To optimize time response:

    - The $(c\rho L^2/k)$ ratio must be minimal. This means that reducing crystal dimensions and selecting a substrate material with higher k and lower values of c, and ρ are vital to a good design

    - ZnO oxide offers the optimal value of $c\rho L^2/k$

8. Among the three materials, ZnO offers the fastest time response values and is found to be 3.5 and 6 times better than $LiNbO_3$ and Quartz, respectively.

9. Aluminum suffers from oxidation, an inert material such as gold or platinum should be used to fabricate thin-film heater.

10. The coupling coefficient and thus the insertion loss of ZnO-based SAW devices are lower. This results in requiring a low gain rf-amplifier for SAW oscillator design. Note that using low-gain/low power amplifier results in higher stability of SAW oscillator.

The application of the design criteria above results to a SAW flow sensor on thin film ZnO. High thermal isolation is achieved by etching SiO_2 layer beneath the ZnO layer. The design is similar to a microchannel Silicon flow sensor structure. Fabrication is consistent with well-established silicon IC production processes. The structure is described as follows:

1. Start with a Silicon substrate

2. Grow SiO_2 layer – a couple of μm in thickness

3. Grow ZnO layer – 2 to 3 μm in thickness

4. Etch SiO_2 layer beneath ZnO for thermal isolation

5. Grow a metallization layer on top of ZnO for SAW device and heater fabrication.

(a) ZnO layer over SiO_2/Si

(b) SAW device on ZnO layer over etched SiO_2

(c) Design/dimension of SAWR/heater device on ZnO layer
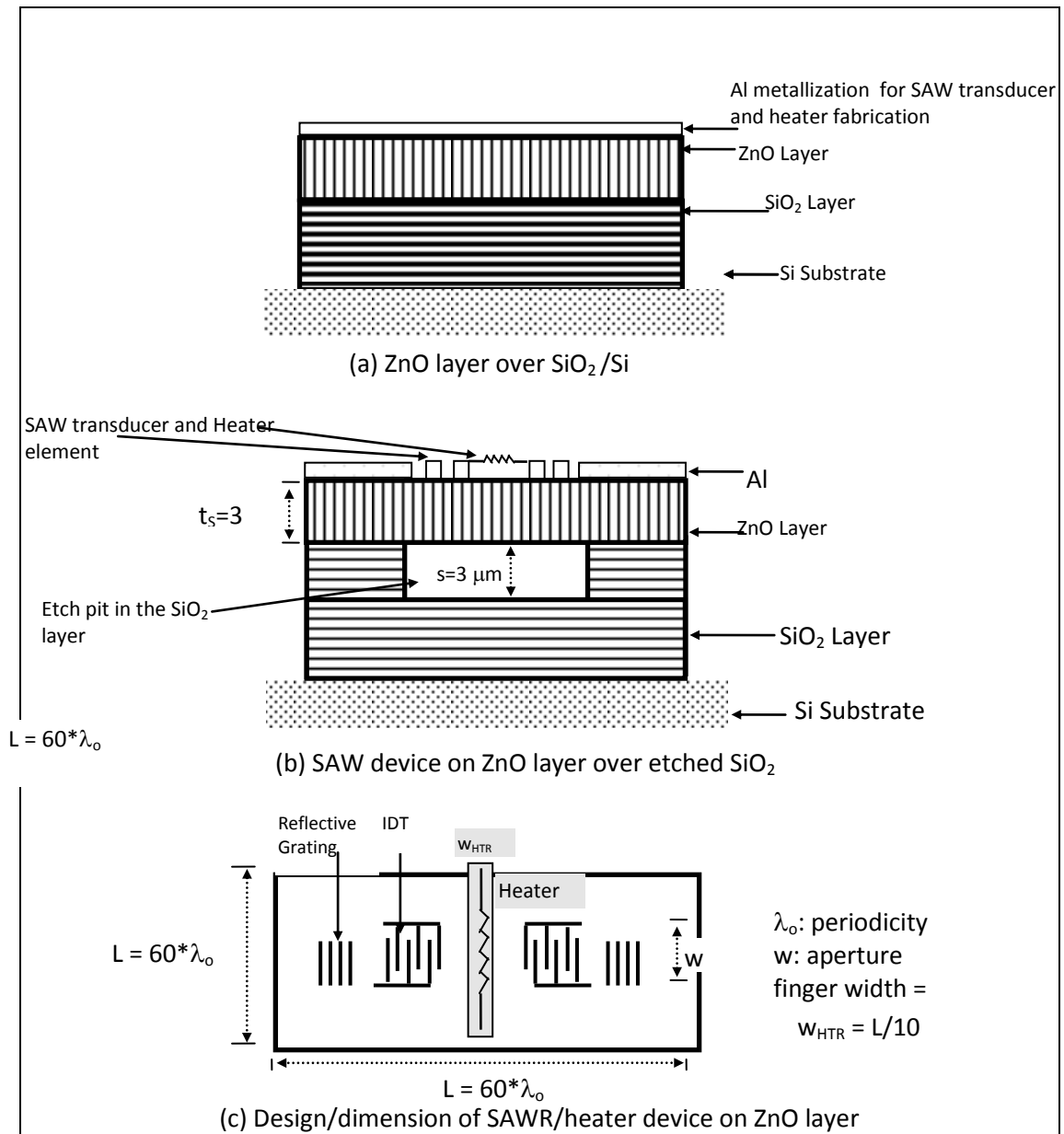
Figure 31 – Schematic of ZnO-based SAW flow sensor with optimal design, dimensions and structure.

SAW Device Design

Assume 20 finger pairs per transducer. One transducer is about $20 \times \lambda_o$ in length (aperture); where λ_o is refers to the periodicity or spacing between two consecutive transducer fingers. The total length of SAW device is assumed to be about $3 \times 20 \times \lambda_o$. The length and width of the SAW device is assumed to be the same.

The heater element consists of fine lines of metallic thin film, e.g., aluminum or gold similar to that used for SAW transducers fabrication to avoid processing steps.

The length of the heater element is same as the ZnO film length used to fabricate the

SAW device, i.e., L (= 0.00022 m). The effective width of the heater element is L/20.

A summary of the SAW device and heater parameters is provided in Table 13.

Table 13 – Thin film ZnO SAW device characteristics.

Thin film ZnO SAW device and Heater characteristics							
Parameters of SAW Transducer						Heater	
SAW Velocity, v (m/s)	Finger spacing (λ_o) (m)	Center Freq, $f_o = v/\lambda_o$ (MHz)	Length or Width $\cong$ $20^{\times}\lambda_o$ (m)	Aperture, $w = 20^{\times}\lambda_o$ (m)	(Area) A_S L^2 (m^2)	Length (m)	Width (m)
2800	$3.73{\times}10^{-6}$	750	0.00022	0.00019	5.0×10^{-8}	0.00022	L/20

Sensor Characteristics

Characteristics of ZnO based optimal SAW flow sensor are summarized here.

Time Response:

Time response is calculated using *Equation 119*; where L_C is the characteristic

length of the ZnO-based SAW device. Physical properties, such as specific heat

capacity of ZnO (C_{ZnO}), thermal conductivity of ZnO (k_{ZnO}), and density is provided

in Table 8. The resulting time constant is 0.00109 seconds or 1.1 msec.

CHAPTER 5

Experimental Results

The results on SAW-based gas flow measurements presented here are

preliminary and require further improvements to the overall design in order to develop

a practical sensor. There are severe limitations in the design of the flow cell used in

these experiments. Because of limited resources, a custom flow cell with narrow

channels and optimal length of entrance and exit channels (consistent with Equations

84-86) for gas flow was not available. In addition, there were intrusions, such as

electronic connections (radio frequency connectors) and SAW package mounting

elements, that could affect the gas flow profile.

The theoretical treatment of the proposed problem suggests deficiencies in the

structure of the SAW device used in these experiments. An optimal design resulting

from a theoretical model will significantly improve flow sensor characteristics.

Figure 32 is a block diagram showing the experimental setup. SAW delay

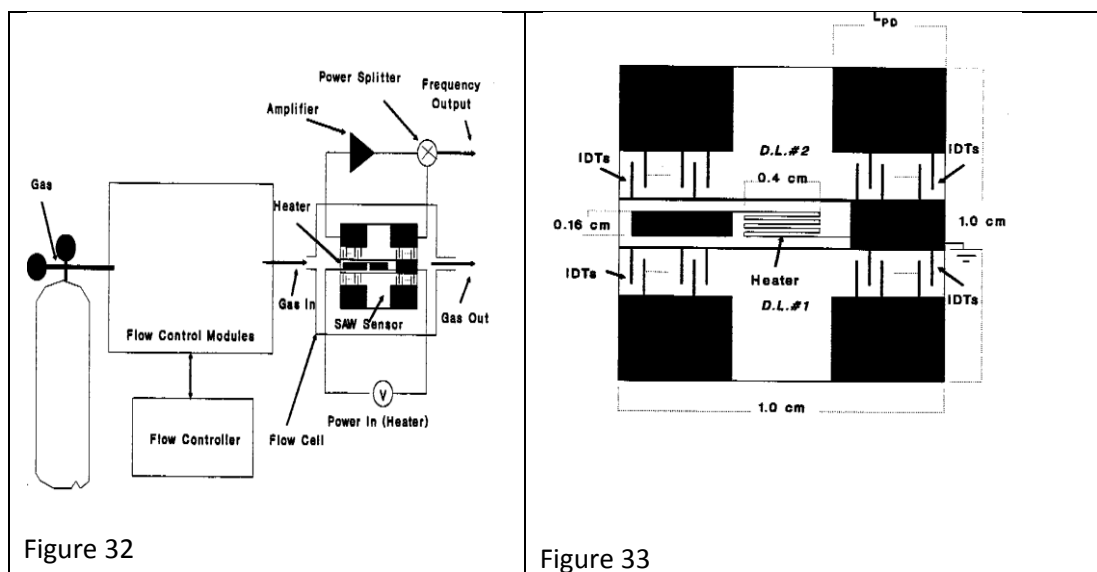lines were used in this research. The substrate materials were 128° y-rotated $LiNbO_3$.

Figure 32

Figure 33

Figure 32 Block diagram of the Flow setup used to conduct experiments.
Figure 33 Structure of SAW Device with built in heater element.

SAW Device

Lithium niobate was selected because of its excellent piezoelectric properties and high first order temperature coefficient of delay. SAW delay lines were custom-designed around a center frequency of 142.5 MHz on a 128° y-rotated $LiNbO_3$ substrate. A thin-film heater adjacent to the delay lines was also fabricated (see Figure 33). SAW devices used in these experiments, each consisting of a dual delay line and a centrally located thin-film heater, were obtained from SAWTEK (SAWTEK is now owened by Triquint Semiconductor Inc.).

The parameters of the SAW delay lines and the thin-film heater element are given in Table 14.

Table 14 – Parameters of the SAW-based flow sensor used in the experiments.

Parameters of Delay Line and Heater.	
Center frequency, f_o	= 142.5 MHz
Number of finger pairs of each transducer	= 50
Wavelength, λ_o	= 28 x 10^{-6} m
Aperture	= 2.24 x 10^{-3} m
Thin film heater metal	= Aluminum
Thickness of thin-film heater	= 0.1 x 10^{-6} m
Thin film heater line width	= 20 x 10^{-6} m
Number of lines	= 7
Spacing between the lines	= 200 x 10^{-6} m
Length of each line	= 4.0 x 10^{-3} m
Heater resistance at 22 ^{o}C	= 388 Ω

SAW Package

Throughout this dissertation, a SAW package has been defined as consisting of a SAW crystal (lithium niobate, 1 cm x 1 cm x 0.05 cm) mounted on a kovar holder. The kovar holder is used to mount SAW substrates and has 24 pins. Two identical delay lines and a centrally located thin-film heater were custom-fabricated on a lithium niobate substrate. The physical layout of the SAW delay lines and heater-element is illustrated in Figure 33. The crystal was glued to a kovar flat-pack substrate holder using RTV adhesive 10 to 15 mils thick (1 mil = 10^{-4}m). Figure 34 is

photograph of the SAW package, with details shown in Figure 20. The pins of the

SAW package were bent to align parallel to the surface of the kovar holder (see

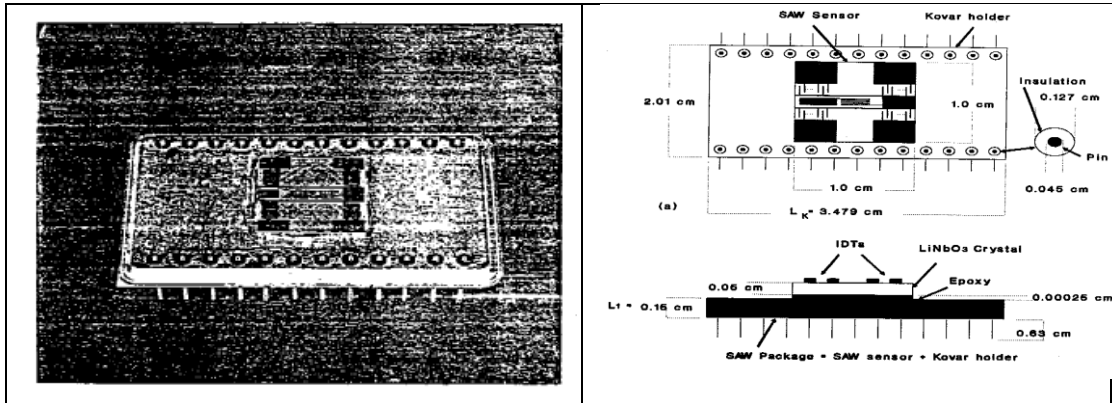Figure 34). A scaled side view of the SAW package is illustrated in Figure 35.

Figure 34 Photograph of the actual SAW package used to carry out experiments.
Figure 35 Cross-sectional and side views of SAW package with details and dimensions.

Saw Flow Cell

An airtight aluminum flow cell was designed, with outer dimensions of 7.2cm

x 4.8cm x 2.2cm. Figure 36 is a photograph of the flow cell. Figure 37 is a three-

dimensional view of the flow cell, including the SAW package within it. The flow cell

has a hollow region, designed to mount the SAW package. Cross-sectional views of

the flow cell are provided in Figure 37. The flow cell contains two ports: one port

interfaced with a Linde mass flowmeter Model FM 4580 and the other port used as
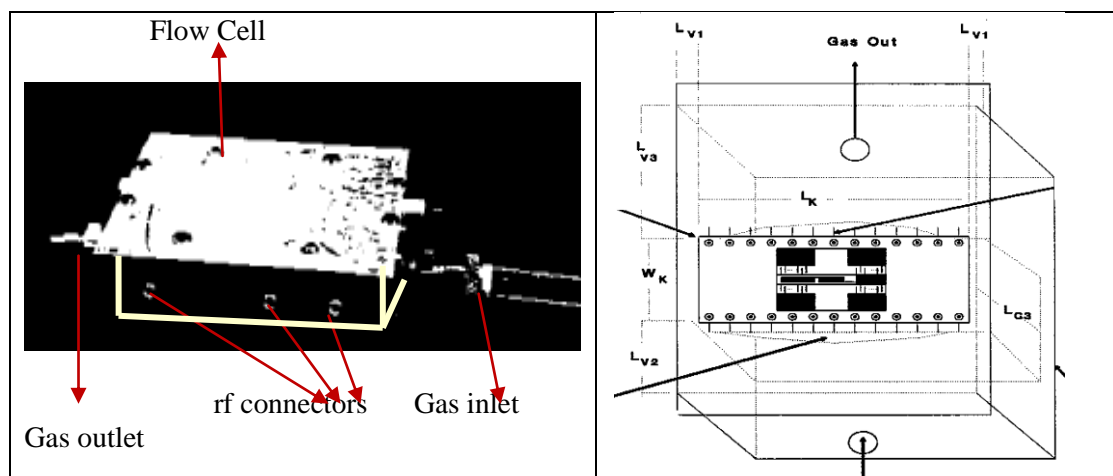
outlet.

Figure 36 – Photograph of the actual flow cell used to carry out experiments.
Figure 37 – Inner structure and SAW-package arrangements in the actual Flow cell.

The pins of the SAW package were bent as shown in Figure 37, and it was mounted above the hollow region in the flow cell; two pins were allowed to make contact with the base of the flow cell. The effective area in contact is defined as A_{CNCT}. A schematic representation is presented in Figure 38. When power is applied to the heater, this scheme offers a higher thermal resistance across the contact of the kovar substrate holder and the flow cell. Therefore, most of the input power is used to increase the temperature of the SAW substrate. Since the thermal resistance of contact is high, a very small amount of heat is transferred to the sink (flow cell). This is also important for response time considerations of the SAW flow sensor. Details of the SAW package arrangement in the cell and cross-sectional views including the SAW package are shown in Figure 38. Cross-sectional and side view of the flow cell, with dimensions, is provided in Figure 39.
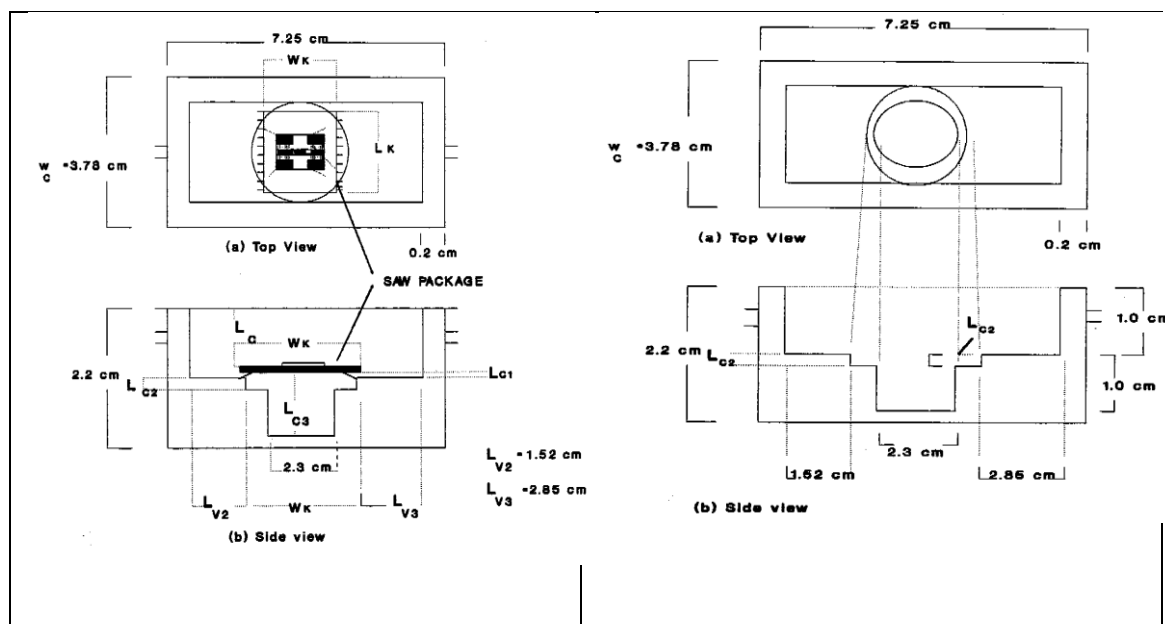

Figure 38 – Cross-sectional and side views of the SAW package arrangement in the flow cell.
Figure 39 – Cross-sectional and side views with dimensional information of the flow cell.

Experimental Results

A delay line oscillator was implemented by connecting the SAW delay line in a feedback loop of an Avantec model GPD 201 RF-amplifier. The measured SAW-

stabilized oscillator frequency at room temperature was 142.8637 MHz. The thin-film heater element was operated at constant current conditions.

The experiments were carried out after the oscillator had stabilized for at least 30 minutes. A setup to perform flow measurements using the SAW device is shown in Figure 33. The temperature of the SAW package was monitored by using a thermistor (part number YSI 44002A, Yellow Springs Instrument Co). The thermistor was glued on one edge of the SAW crystal by using silver conducting paint. Silver conducting paint has high values of thermal conductivity and obtains a low thermal resistance between the thermistor and the SAW package. Temperature versus input heater power characteristics of the SAW delay line oscillator are plotted in Figure 40. Fractional frequency ($\Delta f/f_o$) changes versus input power to the heater element under no flow conditions are plotted in Figure 41. Using the thermistor temperature of the SAW package is also monitored. The temperature sensitivity of a SAW oscillator depends on the temperature coefficient of delay (TCD) of the substrate and the synchronous frequency.

Nitrogen (N_2) gas (99.99% pure) was used to carry out the experiments. The temperature of the SAW substrate is elevated by applying power to the thin film heater at constant current conditions. Once the frequency of the SAW oscillator was stabilized, the valve of the flow system is opened to allow the flow of gas. The volumetric flow rate is read through a Linde flow meter that can be calibrated in terms of velocity. The frequency of the SAW oscillator changed in proportion to the flow rate of the gas. Measurements of frequency change and flow rate were taken at various substrate temperatures. Measurements of frequency change versus flow rate of air at various SAW substrate temperatures are plotted in Figure 42.

Each data point was registered after five minutes of run time. The data collected used a consistent timing interval. For example, the change in the frequency of the SAW oscillator was registered five minutes after the flow valve was opened (and/or the flow rate was changed).

Frequency changes, thus corresponding to temperature changes (calculated from) $\Delta T = \frac{\Delta f}{a_1 \times f_o}$ versus flow rate, are plotted in Figure 43. In the above equation, a_1 is the first order temperature coefficient of delay of the lithium niobate (-72 ppm/^{o}C). The SAW package, in the flow cell, sits above a hollow region and is supported through the pins of the SAW substrate holder (from both sides) as shown in Figure 38.

Under forced flow conditions, N_2 gas will enter and leave through the small openings, and forced convection from the bottom surface of the SAW package can also take place. All of the above experiments were carried out for the case when the openings between the pins of the SAW package were not covered. Under forced flow conditions, the gas enters the openings to and flows through the hollow region beneath the SAW package. Under these circumstances, forced convection from the bottom surface should be taken into account (which complicates the theoretical treatment). To simplify the problem, the small openings are covered so that gas cannot escape and forced convection effects from the bottom surface can be avoided. To stop gas from escaping, the openings between the pins on each of the SAW package were covered using transparent adhesive tape and the experiments were repeated. It is assumed that covering the openings by transparent adhesive tape does not influence the free convection effects from the bottom surface and that steady state analysis under free convection still holds.
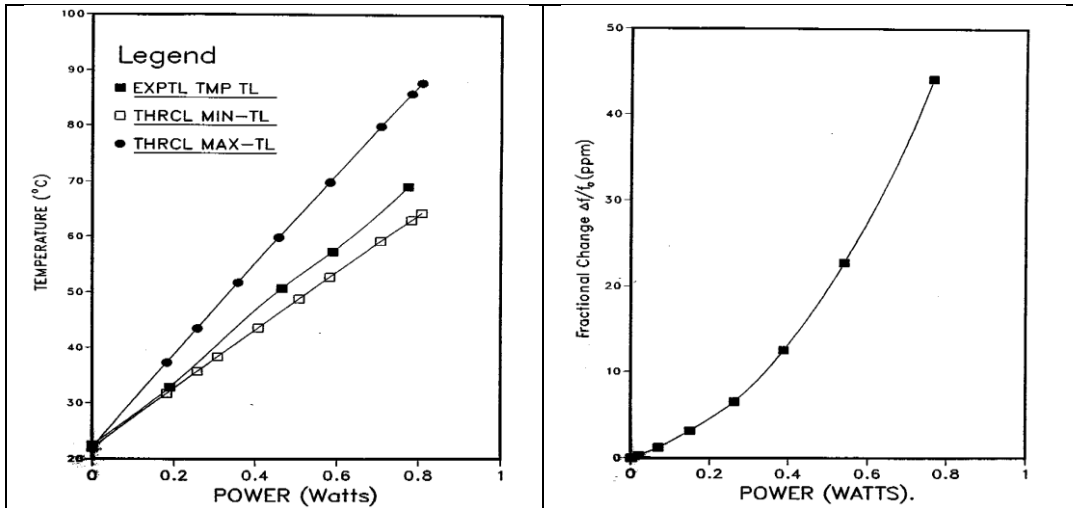
Figure 40 Frequency versus input power.
Figure 41 Fractional frequency ($\Delta f/f_o$) change versus input power.

The plots indicating temperature rise versus input power to heater are shown in Figure 40. The frequency (fractional frequency, $\Delta f/f_o$) versus input power (to the heater element) characteristics are plotted in Figure 41. These temperature characteristics were calculated using the frequency of the SAW oscillator, as well as by means of thermistors on the SAW package. The change in the frequency of the delay line oscillator with flow rate, for various input power to the heater, is plotted in Figure 42.
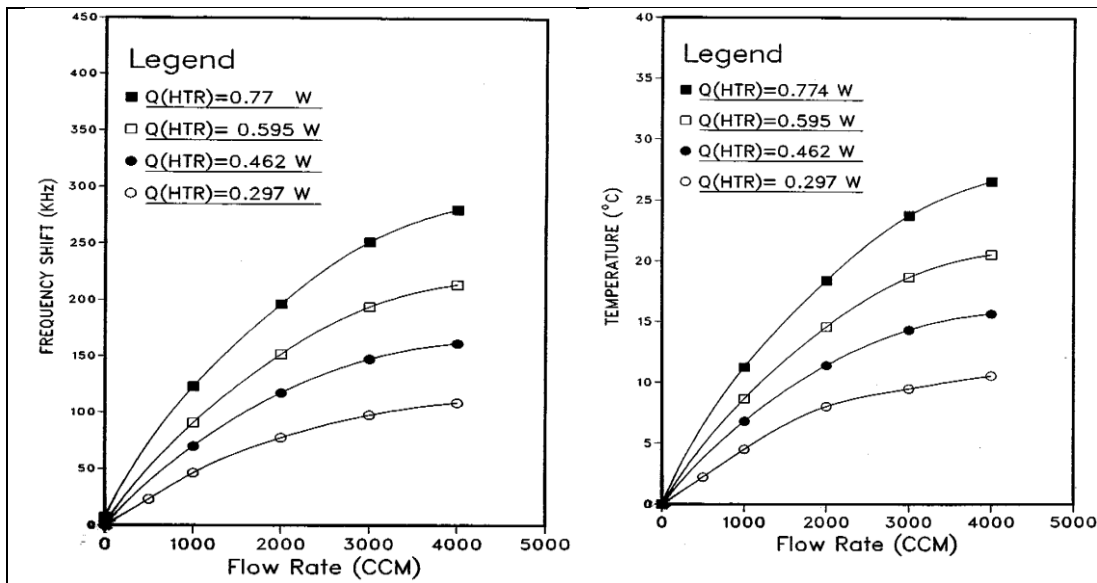

Figure 42 – Plots of Frequency versus flow rate for various heater input power levels.
Figure 43 – Plots of Temperature change (calculated from SAW frequency-temperature) versus flow rate for various heater input power levels.
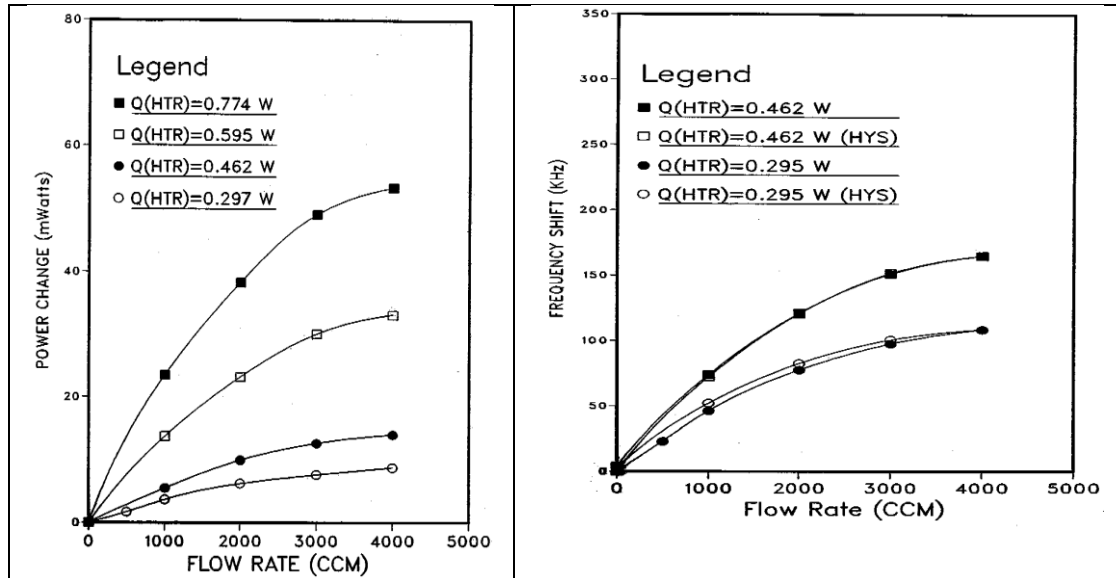
Figure 44 – Plots of change in heater power versus flow rate for various heater input power levels
Figure 45 – Hysteresis behavior of the SAW flow sensor.

Hysteresis behavior of frequency change with flow rate were also measured and plotted (see Figure 45). Direct changes in the temperature of the SAW crystal and kovar holder with flow rate were also monitored using thermistors. Both measurements yielded similar results. The changes in temperature (as measured by thermistor) with flow rate for various input power to heater are plotted in Figure 44.

Several SAW delay lines were used, all of which reproduced identical experimental results under the same operating conditions. The characteristics of a thin-film heater under applied power conditions were also investigated. When the input power was raised to about 1.25 watts, the thin-film heater burnt instantaneously. The thin-film heater was also operated continuously at a constant power of about 1.057 watts; it failed after one week. No further investigations were made into the heater element's resistance to damage since a limited number of SAW devices was available.

The principle of operation of a hot-film/wire anemometer is based on convective heat transfer from the heated sensor to the surrounding fluid to measure the velocity. The amount of heat transferred per unit time is calculated from an

electric signal that is related to the temperature of the sensor. This signal results from the unique relationship between the temperature and resistance of the sensor.

A basic circuit for constant operation, shown in Figure 11 (Chapter 2), consists of a voltage supply, variable resistor R_1, limiting resistor R_2, and sensor R. The output of the circuit is the voltage drop ΔV across the sensing element. If the supply voltage is constant, a change in resistance R will change the current by:

$$\Delta I = \frac{\Delta R}{(R_1 + R_2 + R)} \qquad (163.)$$

The current through the sensor can be determined by measuring the voltage drop across R_2 using Ohm's law.

Simultaneous use of the SAW flow sensor as a hot-film anemometer was also made. Since the thin-film heater is operated at constant current, the change in the voltage against the low rate of the air was monitored. This change in voltage is measured across the thin-film heater. As the flow rate increases, the heater cools. The temperature coefficient of resistance of aluminum, a_{Al}, is positive with a value of $0.011/^oK$ (Ashcroft, 1976). Since the input to the heater is applied at a constant current, a change in temperature of the heater will result in a change in voltage across it. Change in power to the heater with flow rate is computed by multiplying the difference in voltage by the operating current of the heater. Figure 44 is a plot of power change versus flow rate of the gas for various values of input power to heater. Commercial thermal flow sensors operate at constant power or constant current conditions.

Response time measurements to a step change in air velocity were also carried out. The frequency changes versus a step change of 4000 ccm flow rate of N_2 gas for various values of the input power to the thin-film heater were also measured. Generally, the frequency of the SAW oscillator takes four to six minutes to stabilize

to about 95% of the maximum value to a step change in the flow rate. The high value of response time is attributed to the complicated and bulky nature of the SAW-package arrangement.

Theoretical Verification

In this section the theoretical model developed in Chapter 4 is used to analyze the experimental results. The SAW substrate is heated by a thin-film heater fabricated at the center of a rectangular substrate of $LiNbO_3$; the substrate is glued to the base of the kovar substrate holder with a conducting epoxy (RTV), and the power leads are of very small cross-section; then the amount heat conducted away from these leads will be very small. Therefore, as a first approximation, these leads can be neglected. Furthermore, the kovar substrate is resting in an aluminum flow cell (sink) in a way to yield a high thermal resistance between the SAW package and the sink.

The aluminum flow cell was designed to have a hollow region of depth, L_{C3}, beneath the SAW package. The steady-state temperature of the SAW substrate can be determined by applying the model developed in Chapter 3. An electro-thermal analog circuit of the set-up is drawn in Figure 46. Heat transfer by conduction, free convection, and radiation takes place in parallel with respect to one another. Thermal resistance of each of the dissipating sources will be computed. The theoretical temperature rise at various nodes in the circuit of Figure 46 can be predicted once the values of the thermal resistances are known.

Quantities and parameters used in the following discussion are listed in Table 15.
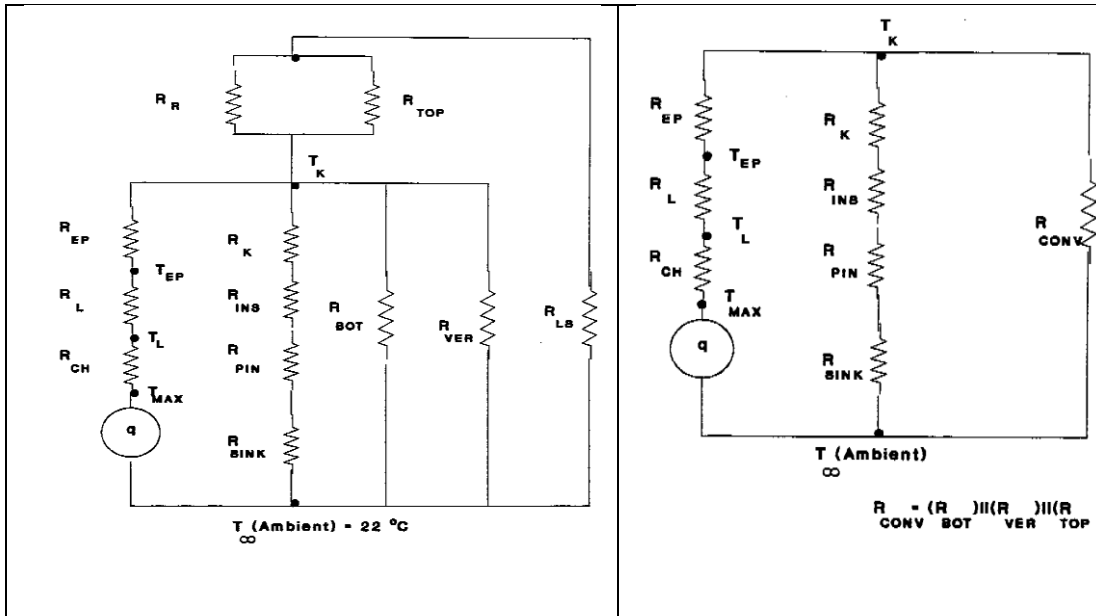
Figure 46 – Electrothermal analog circuit of the SAW Flow sensor setup.

Figure 47 – Electrothermal analog equivalent circuit of Figure 31.

Table 15 – Lists of Parameters

Lists of Parameters
A_h = effective area of heater element = 0.064×10^{-4} m^2;
A_L = area of the LiNbO$_3$ substrate = 1.0×10^{-4} m^2
A_{INS} = Area of the insulation = 0.0141   cm sup 2
A_K = area of the Kovar holder (flat pack) = 7.0×10^{-4} m^2
A_{K1} = area of kovar holder above space L_{C1} = 0.44×10^{-4} m^2
A_{K3} = area of kovar holder above space L_{C3} = 4.82×10^{-4} m^2
A_{V1} = area of the side wall of kovar holder = 0.38×10^{-4} m^2
A_{V2} = area of the side wall of kovar holder = 0.53×10^{-4} m^2
A_p = area of the pin = 0.00159 cm^2
c = specific heat of air = 1.005×10^3 J/kg ^{o}K
D_p = diameter of the kovar flat pack pin = 0.mj0457 cm
D_{INS} = diameter of insulation surrounding the pin = 0.00142 m
g = acceleration due to gravity = 9.8 m/ s^2 , and
k = k_f = thermal conductivity of air = 0.026   {W/m} ^{o}C
k_{BR} = thermal conductivity of brass = 111   W/m ^{o}C
k_{CU} = thermal conductivity of copper = 380   W/m ^{o}C
k_h = 204 W/m ^{o}C = thermal conductivity of heater (Al)
k_E = thermal conductivity of epoxy = 2.2   W/m ^{o}C [SAWTEK specs]
k_{INS} = thermal conductivity of insulation = 1.13   W/m ^{o}C (Corning 7052 glass) [Isotronics]
k_k = thermal conductivity of kovar (Thaw, 1987)$^{]}$= 14.12 W/m ^{o}C
k_{ST} = thermal conductivity of stainless steel = 14.4   W/m ^{o}C
k_L = thermal conductivity of LiNbO$_3$ = 4.2 W/m ^{o}C
k_S = thermal conductivity of substrate material
L_{B1} = spacing between SAW package and top lid of stainless - steel flow cell = 0.0575 m
L_{B2} = spacing between SAW package and pc-board = 0.025 m
L_C = channel height =s = 0.074 m
L_{C1} = spacing, defined in Figure 4.10 = 0.0005 m
L_{C2} = spacing as defined in Figure 4.10 = 0.0023 m
L_{C3} = spacing as defined in Figure 4.10 = 0.01 m
L_{CH} = characteristic length of the plate, for a rectangle it is the mean of the two sides.
L_{CK} = characteristic length of the kovar holder = 0.0275 m
L_{CS} = Characteristics length of SAW substrate = 0.01 m
L_E = thickness of epoxy (RTV) = 0.0254×10^{-2} m
L_{EFF} = effective length of pin in contact with sink = 0.028 m
L_h = thickness of thin-film heater = 0.1×10^{-6} m
L_K = length of kovar flat package = 0.348 m
L_L = thickness of LiNbO$_3$ substrate = 5.0×10^{-4} m
L_o = length of channel
L_1 = thickness of kovar holder = .0015m [Isotronics #CD-2040]
L_p = length of a pin of the kovar holder = 7.8×10^{-3} m
L_{PIN} = difference between length of pin, L_p, and the length in contact with the flow cell) = 0.0048 m
L_{SINK} = thickness of the base of aluminum cell = 0.011 m
L_{ST} = thickness of the wall of stainless steel cell = 0.035 m
L_{V1} = side wall spacing (see Figure 4.10) = 0.00165 m
L_{V2} = side wall spacing (see Figure 4.10) = 0.0152 m

Lists of Parameters
L_{V3} = side wall spacing (see Figure 4.10) = 0.0285 m
L_o = length of channel
N_p = number of pins of the kovar holder = 24
Pr = Prandtl number of air = 0.708
R_{BOT}, Q_{BOT}: Free Convection (thermal resistance, heat loss) from bottom surface
R_{TOP}, Q_{TOP}: Free Convection (thermal resistance, heat loss) from topsurface
R_{FRD}, Q_{FRD}: Forced Convection (thermal resistance, heat loss) from top surface
r_{INS} = radius of insulation = 0.00063 m [Isotronics #CD-2040]
r_{pin} = radius of pin = 0.00022 m [Isotronics #CD-2040]
r_{SP} = outer radius of the brass spacer = 0.0023 m
r_{SI} = inner radius of the brass spacer = 0.001 m
s = spacing
T_{AVG} = Average temperature of the SAW package
t_{CU} = thickness of 1 oz copper claddings = 3.56 x10^{-5} m
T_H = temperature under the heater element,
T_∞ = temperature of the ambient air = 22 ^oC
t_h = thickness of heater element = 0.10 x 10^{-8} m
t_{INS} = thickness of insulation = D_{INS} - D_P = 0.00096 m
u = fluid velocity
W_{EFF} = effective width of pin in contact with sink = 0.001 m
W_K = width of kovar flat pack = 0.0202 m
μ = viscosity of air = 1.98 x 10^{-5} kg/m s
ρ = density of air = 1.1774 kg/ m^3
η = kinematic viscosity of air = 15.68 x 10^{-6} m^2/s
α = thermal diffusivity of air = 0.221 x 10^{-4} m^2 /s
β = coefficient of thermal expansion of air = 0.00338 $^oK^{-1}$
ξ = streamwise coordinate with origin at leading edge of heat

Free Convection Discussion

The theoretical analysis for heat transfer under free convection in *enclosed spaces* described in Chapter 3 and 4 is applied. A fluid is confined between two horizontal plates spaced a distance s apart. Heat will flow across the air gap by conduction and/or convection in parallel with radiation.

When an input power Q_{HTR} is applied to thin-film heater embedded on the SAW device, heat flows via conduction from the top surface of lithium niobate crystal (SAW substrate) to the thin layer of epoxy, from which the heat then spreads out to the kovar substrate holder. The calculation of each component of thermal resistances and later heat dissipation from each source is calculated and presented here.

The kovar holder has twenty-four pins surrounded by insulation. All the pins are bent and are aligned parallel to the kovar holder surface (see Figure 23). Two pins make contact with the base of the flow cell (the sink), the conduction heat flow from the kovar holder to the sink takes place through these pins. The other thermal resistances shown in Figure 46 are calculated as follows:

The thermal resistance of insulation is determined by using the approach used to calculate the thermal resistance of a hollow cylinder (Holeman, 1986). The insulation of length L_1 (kovar holder thickness), radius r_{INS}, surrounds a pin of radius r_{pin}. Thermal resistance of the insulation is given by:

$$R_{INS} = \frac{\ln\left[\frac{r_{INS}}{r_{pin}}\right]}{(2\pi k_{INS} L_1)} \cong 85.86°\{C/W\} \tag{164.}$$

Thermal resistance of the pin:

$$R_{Pin} = \frac{\ln\left[\frac{2L_{Pin}}{r_{pin}}\right]}{(2\pi L_{pin})} \cong 3.44°\{C/W\} \tag{165.}$$

Since two pins make contact with the flow cell, the effective thermal resistance of the insulation and pin is given by:

$$R_{INS1} = \frac{R_{INS} + R_{Pin}}{2} = 44.65 \, °C/W \tag{166.}$$

The SAW package area of contact with the cell is given by:

$A_{CNCT} = L_{EFF} \times W_{EFF} = 0.028 \times 0.001 = 2.8 \times 10^{-5} m^2$

Thermal resistance of contact:

$$R_{CNCT} = \frac{L_{SINK}}{2k_{Al} A_{CNCT}} \cong 89.9°\{C/W\} \tag{167.}$$

Ideally, the contact resistance should be made high. It can be accomplished by minimizing the contact area and using contact material with low value of thermal

conductivity. Assuming extremely small area of contact and contact material(s) with low thermal conductivity, the thermal resistance of contact, R_{CNCT} can be assumed to be very high:

$$R_{CNCT} = \infty \tag{168.}$$

$$R_{EFF} = R_{INS1} + R_{CNCT} = 134.6°\{C/W\} \tag{169.}$$

or, for a worst case (assuming high value of R_{CNCT}), using Equation 168 in Equation 169,

$$R_{EFF} = \infty \tag{170.}$$

The surface of the SAW substrate has large area, $A_{PD,}$ covered with aluminium (also called aluminum padding) at each end of the transducer. The thermal resistance of aluminum padding is calculated as following:

$$R_{PD} = \frac{L_{PD}}{k_{Al} \times A_{PD}} = 24509.8 \, °C/W \tag{171.}$$

where L_{PD} is the length of a pad and $t_{Al,}$ is the thickness of metallization on the crystal. Therefore, the cross-sectional area of aluminum padding, A_{PD}, is,

$$A_{PD} = L_{PD} + t_{Al} = 4 \times 10^{-10} \tag{172.}$$

$$R_{TOP} = \frac{1}{h_{TOP} \times A_K} = 350.88 \, °C/W$$

$$Q_{TOP} = h_{Top}A_K \, [T_{TOP} - T_\infty] = h_{Top}A_K \, \Delta T$$

$$R_{BOT} = \frac{1}{h_3 \times A_{K3}} = 188.81 \, °C/W$$

$$Q_{BOT} = [2(h_1 A_K + h_2 A_{K2}) + h_3 A_{K3}]\Delta T_B$$

$$R_{VER} = \frac{1}{2 \times \ (h_V \times A_{V1} + h_V \times A_{V1})} \cong 224.5 \, °C/W$$

$$Q_{VER} = 2(h_v A_{v1} + h_v A_{v2})\delta T_v$$

$$\sum R_{TH} = (R_{CH} + R_L + R_{EP} + R_{NET})$$

$$Q_{FRE} = Q_{TOP} + Q_{BOT} + Q_{VER}$$

$$Q_{FRE} = [(h_{TOP} A_K) + 2(h_1 A_{K1} + h_2 A_{K2}) + h_3 A_{K3} + 2(h_V A_{V1} + h_V A_{V2})] \Delta T$$

$$R_{CONV} = [(R_{TOP}\|R_{BOT}\|R_{VER})] = (350.88\|188.81\|224.5) = 79.02°C/W$$

Let's define R_{NET} as:

$$R_{NET} = R_{EFF}\|R_{CONV}$$

$$R_{NET} = 134.6\|79.02 = 49.78°\{C/W\}$$

Therefore:

$$= 18.87 + 1.19 + 1.15 + 49.78 = 70.99 \ ^oC/W$$

$$\sum R_{TH} = (R_{CH} + R_L + R_{EP} + R_{NET})$$

$$= 18.87 + 1.19 + 1.15 + 49.78 = 70.99°C/W$$

The temperature of the lithium-niobate substrate T_{LF} is calculated as:

$$T_{LF} = T_{KF} + (R_L + R_E)Q_{HTR} = 36.26 \times Q_{HTR} \tag{173.}$$

and the temperature beneath the heater element (includes constriction resistance R_{CH})

$$T_{HF} = (R_L + R_{CH} + R_{EP} + R_{OUT}) \ x \ Q_{HTR}$$

$$T_{HF} = (R_L + R_{CH} + R_{EP} + R_{OUT}) \times Q_{HTR} \tag{174.}$$

Energy balance requires:

$$P = Q_{HTW} = Q_{Tot} = \frac{(T_{AVG} - T_\infty)}{\sum R_{TH}} \tag{175.}$$

Table 16 – Summary of calculated values of thermal resistances under free convection, $R_{Thermal}$ $^oC/W$

$R_{Thermal}$ $^oC/W$											
R_{CH}	R_L	R_{EP}	R_K	R_{INS}	R_{pin}	R_{cnct}	R_{BOT}	R_{TOP}	R_{VER}	R_{LS}	R_R
18.87	1.19	1.15	0.151	44.65	3.44	89.80	188.81	350.88	224.5	≈ 0	∞

Forced Convection Discussion

The flow response of thermal flow sensors is generally proportional to square root of the velocity of the fluid (gas), $v_f^{1/2}$. The constant of proportionality is determined by flow conditions (laminar, turbulent, and/or mixed), geometry of the flow sensors and operating conditions (temperature, etc.). To analyze forced flow experimental results, the following constraints and assumptions are applied:

1. Sensor is operating at a constant heat flux.

2. Temperature-dependent properties of the gas are included.

3. Entrance effects are ignored.

4. Laminar flow is assumed in calculations.

5. Forced convections losses from the side walls of the SAW substrate were
    ignored.

A steady-state solution of heat dissipation from the SAW substrate under natural convection has been derived earlier in Chapter 3.

The average velocity of air flowing over the SAW package can be found by using the continuity equation:

$$Flow\ rate\ (CCM) = A_1 u_1 = A_2 u_2 \qquad (176.)$$

where A_1, A_2 are the cross-sectional areas, and u_1 and u_2 are the corresponding air velocities through them. For example, the effective cross-sectional area of the flow cell is given by

$$A_2 = 0.0378 \times 0.0074 = 2.8 \times 10^{-4} m^2 \qquad (177.)$$

At a flow rate of 4000 CCM, the average velocity from Equation (176) is about 24 cm/s. The Reynolds number over a flat plate of characteristic length L_{CK} is given by:

$$Re_L(u_{avg}) = \frac{(\rho_{air} u_{avg} L_{CK})}{\mu_{air}} \qquad (178.)$$

For N_2 gas of velocity at 24 cm/s, Re_L lies between 431 and 367 at temperature of 24^oC and 45^oC; at 2 cm/s Re_L varies from 35.70 to 30.70 respectively. In the channels, where the entrance effects are not important, the flow is laminar when the Reynolds number is below 2100 (Bohn, 1986).

The operating flow range of our experiments is from 2 to 24 cm/s. For example, at 24 cm/s, the Reynolds number from *Equation (178)* is about 28 and 392,

respectively. The Grashof number, Gr_S from *Equation (135)* in the entire operating

temperature range varied from 3200 to 1700. Hence for u_{AVG} of greater than 4 cm/s,

$$\text{Re}^2 > Gr_s \qquad\qquad\qquad (179.)$$

whereas, for u_{AVG} of less than 4 cm/s,

$$\text{Re}^2 \cong Gr_s \qquad\qquad\qquad (180.)$$

Therefore, in these experiments heat transfer by forced convection is dominant

from the top surface of the SAW package for $u_{AVG} > 4$ cm/s (800 CCM). For flow rate

less than 4 cm/sec, heat loss occurs by mixed convections (free and forced). The

bottom surface of the SAW package is completely shielded. Therefore, the heat loss

from the bottom surface of SAW package takes place by free convection.

Forced convection losses from the vertical sides of the SAW package are

difficult to calculate because of the geometry of the setup. Two sides of the SAW

package are spaced by L_{V1} from the walls of the flow cell (see Figure 38). The

remaining two sides are separated by a distance L_{V2} and L_{V3} (see Figure 38). The heat

loss by free convection has been derived. Since the thickness L_1, of these sides is

small, the forced convection effects may be ignored. For simplicity, only free

convection losses from the sides of the SAW package will be considered.

At low velocities or flow rates (<1000 CCM), free convection effects from all

the surfaces of the SAW package may contribute. The contribution from free

convection has been obtained previously. Thus total heat loss is obtained by adding

components of heat losses as follows:

$$\text{For } u_{AVG} > 4 cm/s, Q_{TOT} = Q_{FRD} + Q_{BOT} + Q_{VER} \qquad\qquad (181.)$$

at low velocities $<=$ 4 cm/s, free convection from top surface plays role:

$$Q_{TOT} = Q_{FRD} + Q_{BOT} + Q_{VER} + Q_{TOP} \qquad\qquad (182.)$$

The electro-thermal analog circuit that includes the forced convection effect is similar to Figures 46-47, define R_{COM} as:

$$R_{COM} = R_{FRD}\|R_{BOT}\|R_{VER} = R_{FRD}\|102°C/W \qquad (183.)$$

where $R_{FRCD} = 1/(h_{TM} A_K)$, and its value ranges from 83.6 $°C/W$ to 274 $°C/W$ when u_{AVG} varies from 24 cm/s to 2 cm/s; R_{BOT} and R_{VER} have already been defined earlier. For example, when $R_{FRD} = 81.7 \,°C/W$; $R_{COM} = 45.36 \,° C/W$.

$$R_{OUT} = R_{EFF}\|R_{COM} \qquad (184.)$$

$$= 134.6 \| 45.36$$

$$= 33.92 \,°C/W$$

$$\sum R_{FTH} = R_L + R_{CH} + R_{EP} + R_{OUT} \qquad (185.)$$

$$= 55.13 \,° C/W$$

The temperature rise beneath the heater element, T_{HF}, is calculated as:

$$Q_{HTR} = \frac{(T_{AVG} - T_\infty)}{\sum R_{FTH}} \qquad (186.)$$

Therefore, under steady-state forced convection conditions, the temperature of the kovar holder, T_{KF} is given by:

$$T_{KF} - T_\infty = R_{OUT} \times Q_{HTR} \qquad (187.)$$

A mathematical model developed earlier yielded:

$$h_{TM}(u_{avg}) := 0.945 \frac{k_{air}}{L_C} \times Pr^{1/3} \times Re_L(u_{avg})^{1/2} \qquad (188.)$$

Forced convection thermal resistance, R_{FRD} is then given by:

$$R_{FRD}(u_{avg} A_S) = \frac{1}{(h_{TM}(u_{avg})) \times A_S} \qquad (189.)$$

The results and values used for the forced convection analysis, such a flow rate, u_{AVG}, Nusselt number, h_{TM}, T_{HTR}, forced convection loss, Q_{FRD}, Re_L, R_{FRD}, T_L, R_{COM}, and total power loss under steady state forced convection, Q_{TOT}, can be calculated.

Therefore, the forced convection losses from the surface of the SAW package can be calculated as follows:

$$Q_{FRD} = h_{TM}A_k(T_{AVG} - T_\infty) = h_{TM}A_k\Delta T_F \tag{190.}$$

where ΔT_F is the average SAW package temperature at steady-state forced flow conditions. The frequency changes versus temperature and, thus, input power (to the heater element) characteristics are linear; we can describe these characteristics by a relationship:

$$\Delta f = BQ_{HTR} \tag{191.}$$

Now, for the SAW oscillator:

$$\Delta f = a_1(T - T_\infty)f_o \tag{192.}$$

where a_1 is the first order coefficient of temperature delay. For 128° y-cut $LiNbO_3$, a_1 is -72 ppm. From *Equation (181)* and *(192)* value of B is derived as follows:

$$B = \frac{1}{Q_{HTR}a_{1(T_L-T_\infty)}} \tag{193.}$$

Equation (193) predicts the theoretical value of B if the relation between Q_{IN} (or Q_{HTR}) and ΔT is known. Experimentally, the value of B can be obtained from the f-Q characteristics of Figure 40. The slope of the characteristics is B and is equal to 551.56 kHz/W. The forced convection loss is given by *Equation (189)*. Under steady state conditions, the frequency shifts. Under forced convection, Δf_F can be expressed as:

$$\Delta f_F = B \times Q_{FRD} \tag{194.}$$

Substituting Equation (193) in (194)

$$\Delta f_F = Bh_{TM}A_k\Delta T_F \tag{195.}$$

From Equations (187-195), following relationship is derived:

$$\Delta f_F = Bk \left[\frac{0.943}{L_c}\right] A_s \Delta T_F Pr^{1/3} Re_L^{1/2} \qquad (196.)$$

The change in average temperature of the SAW package can be calculated

using the frequency shift, Δf_F, as follows:

$$\Delta T_F = a_1 \times f_0 \times \Delta f_F \qquad (197.)$$

where

$$\Delta f_F = a_1 \times f_0 \times \Delta T_F \qquad (198.)$$

where f_o is the synchronous frequency of the SAW oscillator at room temperature.

Theoretical calculations of ΔT_F, versus average velocity, u_{avg}, were calculated

and plotted against experimental results (see Figure 48 and 49).
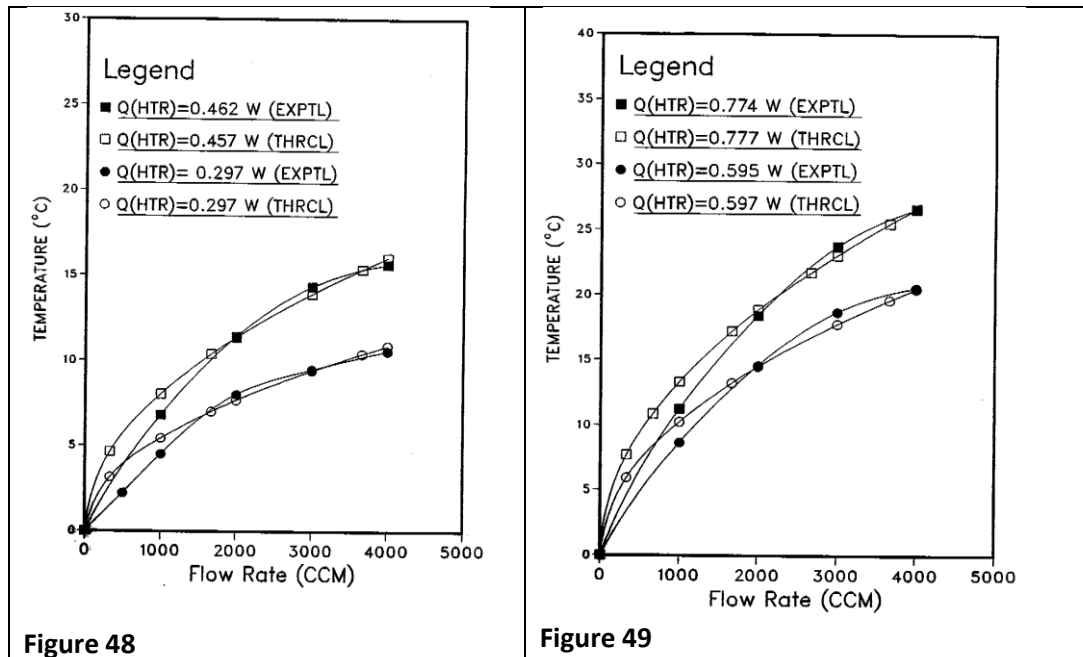
Figure 48

Figure 49

Figure 48 – Theoretical and experimental plots of Temperature (calculated from SAW frequency-temperature relationship) versus flow rate for various heater input power levels.

Figure 49 – Theoretical and experimental plots of Temperature (calculated from SAW frequency-temperature relationship) versus flow rate for various heater input power levels.

These theoretical analyses are compared with the experimental results in

Figure 48 and 49. The theoretical values of temperatures, at various nodes (see Figure

48-49), are obtained by utilizing the model. At flow rates greater than 1000 CCM, the

theoretical predicted analyses are within 20% of experimental observations. At flow rates below 1000 CCM, the discrepancy between experimental and theoretical values is higher (about 32 % inaccuracy).

The theoretical calculations were compared and plotted out against the experimental results. These calculations show 20 to 30% errors with the experimental measurements. At higher operating temperatures, some discrepancy between the experimental and theoretical results may be attributed to the following factors:

1. Inaccuracy in the local temperature rise under the thin film heater surface.

2. At low values of flow rate, the velocity profile may not be fully developed.

3. The film heater is of extremely low mass and may suffer from instabilities due to higher current densities.

4. The SAW package and flow cell design is very complex. Eliminating variables, such as SAW substrate holder and epoxy beneath, can simplify and, thus, make the response more predictable.

From analysis the following features of the SAW flow sensor are inferred:

1. The sensitivity, Δf, varies as $(u^{1/2}_{AVG})$, where u_{AVG} is the average fluid velocity.

2. The sensitivity of the sensor, Δf, is directly proportional to the input power, or the temperature of the sensor.

3. It is assumed that $A_{CK} = (L_{CK})^2$, than the sensitivity is proportional to $(L_{CK})^{3/2}$, where L_{CK} is the characteristic length of the sensor.

CHAPTER 6: SUMMARY, DISCUSSION, AND RECOMMENDATION

The research and theoretical model presented in this dissertation validate and describe a SAW-based gas flow sensor. The author (Ahmad, 1985) was first to report on SAW-based gas flow sensors. The output frequency signal yields accurate measurements, and interfaces easily with microprocessors (Ahmad, 1987). Since then there has be continued interest in this field of studies (Nomura, 2000; Wang, 2011).

Theories of heat transfer with electrical engineering disciplines were successfully applied in this research. This study reports a detailed model to predict SAW-based flow sensor behavior for a wide range of variables and boundary conditions.

1. This study validated gas flow rate measurements using SAW-based technology.

2. The behavior of SAW-based gas flow sensor is consistent with a thermal gas flow sensor. The change in frequency with gas flow, Δf, varies as $(u_{AVG})^{1/2}$, where u_{AVG} is the average fluid velocity.

3. A SAW device implemented on substrate material having large temperature coefficient will provide high sensitivity to small changes in temperature.

4. As a SAW-based gas flow sensor operates as a temperature sensor, it could have a wide operating range. In general SAW-based temperature sensors have a wide linear operating range. For $LiNbO_3$ a linear operating range from near 20 ^{o}C to 140 ^{o}C has been reported (Bao, Burkhard, & Varadan, 1987). Similarly, for quartz, the SAW-based temperature sensor enables temperature measurement for a large temperature range   -100 ^{o}C to 200 ^{o}C, with an accuracy of about 10^{-4} K (Hauden, Jaillet, & Coquerel, 1981).

5. The analyses carried out in this research are based on laminar gas flow. The upper limit of the SAW-based gas flow range is dependent on value of the Reynolds Number (Re_L) given in Equation (178). In the channels, where the entrance effects are not important, the flow is laminar when the Reynolds number is below 2100 (Bohn, 1986). For substrate characteristics length L_C of 0.01 m, the upper limit where the flow rate of gas (air) remains laminar is about 3.5 m/sec. This is almost 15 folds better than the Linde Flow meter used in the experimental setup of this research. Similarly, by reducing the characteristics length L_C to 0.005 m, the theoretical upper limit where gas (air) flow remain laminar would be 7 m/sec. More work is needed to design develop a practical SAW-based gas flow sensor.

6. The measurement resolution of the propagation delay time depends on the SAW frequency; using a higher frequency can improve both the resolution and the sensitivity.

7. Assuming $A_S = (L_C)^2$, then the sensitivity is proportional to $L_C^{3/2}$, where L_C is the characteristics length of the sensor.

8. ZnO-based SAW sensors are promising; theoretical modeling predicts a response time in a few millisecond ranges. This compares well with the best Silicon-based thermal micro sensor characteristics. Experimental verification will be needed. .

9. The SAW-based sensor operation requires low to moderate temperature (e.g., 50-90 ^{o}C) ranges. This is an important advantage over the commercially available thermal sensor that requires very high temperature for their operation 200-300 ^{o}C).

10. By using higher conductivity material (e.g., ZnO), the thermal heat losses to conduction can be minimized. The dominant losses due to convection result in better sensitivity and operating ranges. Experimental verification is needed.

11. Among the three materials, based on theoretical analysis, higher thermal conductivity ZnO substrate offers the best time response.

12. Based on theoretical modelling, τ (ZnO) is 3.5 and 6 times better than LiNbO$_3$ or quartz respectively. Employing a thin film of ZnO, further miniaturization is possible that can substantially improve time response. Further experimental work to determine frequency-temperature characteristics for SAW devices on thin ZnO is required.

Comparative Analysis

Here SAW-based flow sensors are compared and contrasted with existing *Thermal Flow Sensors.* These analyses are based on theoretical interpretation of SAW-based gas flow sensors and have not been verified experimentally.

Table 17 – Comparative analysis of SAW-based and conventional thermal sensors.

Comparative Analysis of Thermal Flow Sensors	
Si-based and other Microsensors Characteristics	**SAW Sensors' Characteristics**
• The microsensor is far less sensitive to external influences because the sensing element is buried in the flow stream.	• Sensitive to external influences.
• The microsensor has a fast response time of 0.5 to 5 milliseconds depending on the type of gas. This is tremendous improvement/the typical through-the-wall types which have response time of about 1 to 10 seconds.	• Higher response time – improvements possible by miniaturization. For example, using ZnO thin-film based SAW sensor will be able to support response time in a few milliseconds.
• The higher operating temperature of the microsensor results in contaminant for reactive gases, resulting in degradation of the sensor response with time.	• The SAW-based sensor will operate at much lower operating temperature (50-90 ^{o}C range). Therefore, the SAW-based sensor will avoid contaminant production in reactive gases environment.
• The inert surface material used in the microsensor increases reliability.	• Possible.
• The small size of the microsensor results in a number of system packaging advantages, such as reductions in a gas system size, closer placement to the process chamber, minimized dead volumes, faster atmosphere change dynamics, and greater freedom of design in equipment architecture.	• Currently not possible.
• The fluid temperature-sensing element is thermally isolated from the heating element.	• Currently not possible.
• Currently not possible.	• The robust thermal isolation structures make it possible for the sensor to be used in measuring liquid flow rate as well.
• The flat surface of the chip does not disturb flow.	• True.
• The sensors are fragile, and design is difficult because the characteristics of each sensor chips with thermal isolation structures depends on a number of structural parameters.	• Sensor not fragile. Design easy and sensor characteristics reproducible.
• The output is not digital.	• Frequency output – better precision in measurements and higher sensitivity.
• Wireless signal for remote and difficult geometries is not possible. Signal is analog.	• Wireless signal for remote and difficult geometries is possible.
• Compatible with advanced micro-fabrication techniques.	• True.
• Less susceptibility.	• EMI/RFI interference-susceptible
• Inexpensive – mass production possible.	• Relatively expensive –substrate material more expensive than Si.
• Aging problems.	• Same is true – frequency drifts with time.

Recommendations

The following recommendations are made to improve the performance of the SAW flow sensors and the arrangement of the experimental setup:

1. Devise a useful SAW-based flow sensor, physical design of a flow cell is critical. Work is needed to implement an actual SAW-based flow sensor and to characterize it for several gases.

2. Minimize the thermal contact area of the SAW sensor/substrate for gas flow measurements.

3. Reduce the mass of the SAW sensor/substrate by reducing the substrate area as well as its thickness. For optimal performance, use a substrate material of higher thermal conductivity.

4. Reduce the input power level to the heater element. This is is possible by reducing the mass of the substrate/sensor and using high conductivity substrate material.

5. Design the flow cell with longer entrance and exit channels consistent with theoretical analysis in Chapters 3 and 4.

6. Since at low flow rates, the velocity profile may not be fully developed, solve this problem by the design of narrow channels to enable fully developed laminar flow.

7. The performance versus cost effectiveness to realize a commercial SAW-based gas flow sensor is still unknown. However, the SAW-based flow sensing presents some compelling advantages over the conventional thermal sensing techniques.

Optimal Sensor Design

1. Among the many substrate materials listed in Table 6, ZnO offers the best optimal operating range and response. Compared with LiNbO$_3$, and quartz-based sensors, ZnO-based SAW gas flow sensor:

   - Requires low input power because it has low conduction losses.

   - The time response depends on the ratio ($c\rho L^2/k$). To optimize time response, the ($c\rho L^2/k$) ratio must be minimal. Reducing crystal dimensions, and selecting substrate material with higher *k* and lower values of *c*, and ρ are keys to a good design.

   - ZnO oxide offers most suitable value of $c\rho L^2/k$.

   - Based on theoretical analysis, time response, τ (ZnO), is 3.5 and 6 times better than LiNbO$_3$ and quartz respectively. Experimental verification is required.

2. Aluminum suffers from oxidation; an inert material such as gold or platinum should be used to fabricate thin-film heater.

3. The coupling coefficient of ZnO and, thus, the insertion losses of ZnO-based SAW devices are lower. This results in requiring a low gain rf-amplifier for SAW oscillator design. Note that using low-gain/low power amplifier results in higher stability of SAW oscillator.

Key Contributions

1. The author (Ahmad, 1985) first to report SAW-based flow sensor. The present work is an extension of the work done in 1985.

2. This research provides a generalized mathematical model that will enable characterization of SAW-based gas flow sensor for any substrate material, flow

geometries, and sensor structure and, thus, permit the design of an optimal SAW-gas based SAW sensor design.

3. Quantitative theoretical model of a SAW-based gas flow sensor are derived with following considerations:

    a. Thermal analysis dealing with a flat plate geometry with an internal heat source are carried out. The published knowledge was applied on flat plate geometries with an embedded heating source. A generalized electrothermal analog circuit was derived.

    b. The Model is applicable to any gaseous fluid.

    c. Model a thermal flow sensor independent of a given substrate and evaluate characteristics under following conditions:

        i.   Steady state *no flow* condition

        ii. Steady state *laminar forced flow* conditions

4. The study determines (models) time response for the sensor with wide range of parameters.

5. A SAW-based gas flow sensor experimental setup was designed and experiments were carried out to validate the model. The experimental measurements consisted of the following variables:

    a. Changes in the frequency of the SAW oscillator as a function of input power to thin-film heater element

    b.   Frequency versus temperature characteristics of SAW devices

    c. Changes in the frequency of SAW oscillator as a function of flow rate for various values of power to heater

6. Comparative analysis was performed with other thermal flow sensors.

Future Work

1. Validate theoretical model with experiments to a wide range of gaseous fluids.

2. SAW sensors show hysteresis and suffer from long-term aging which can cause significant drift in the synchronous frequency of the oscillator and can degrade accuracy. Study impact of long-term aging to the behavior of the SAW gas flow sensor.

3. A temperature compensation scheme is required to accommodate variation in ambient temperature fluctuation is required. This can be accomplished by using a reference sensor or incorporating a temperature sensor in the system.

4. The film heater is of extremely low mass and may suffer from instabilities due to higher current densities. More studies are needed to optimize thin film heater design.

5. Aluminum suffers from oxidation; an inert metal such as gold is recommended for fabricating the thin film heater element. The characteristics and performance of materials other than aluminium should be studied.

6. A protective scheme and/or coating must be studied to develop SAW-based gas flow sensor for corrosive gases. In addition, the impact of a protective coating scheme in the behavior SAW-based gas flow sensors must be studied.

7. SAW-based gas flow sensor packaging is critical to success of a commercial sensor. Further studies are required to realize a practical SAW-based gas flow sensor.

BIBLIOGRAPHY

Al-Salaymeh, A., & Ashhab, M. S. (2006). Modelling of a novel hot-wire thermal flow sensor with neural nets under different operating conditions, *Sensors and Actuators, 126*(1), 7-14.

Ahmad, N. (1985). Surface acoustic wave flow sensor. *Proceedings of the IEEE Ultrasonics Symposium* (pp. 482-485). New York: IEEE.

Ahmad, N. (1986). A dual SAW resonator oscillator anemometer. In *Proceedings of the Sensors Expo* (pp. 245-254).

Ahmad, N. (1987). A microprocessor-based SAW resonator temperature sensor. In *Proceedings of the Sensors Expo* (pp. 347-351).

Allan, W., Shoaf, J. H., & Halford, D. (1974). Statistics of time and frequency data analysis. In B. E. Blair (Ed.), *Time and frequency: Theory and fundamentals.* (pp. 151-204). Washington, D. C.: National Bureau of Standards.

Anisimkin, V. I., & Verona, E. (1998). New properties of SAW gas sensing. *IEEE Transactions on Ultrasonics, Ferroelectrics, and Frequency Control, 45,* 1347-1354.

Arpaci, S., & Larsen, P. S. (1984). *Convective Heat Transfer.* Englewood Cliffs, NJ: Prentice-Hall, Inc..

Ashcroft, W. (1976). *Solid State Physics.* New York: Holt, Rinehart and Winston.

Aubert, T., Elmazria, O., Assouar, B., Blampain, E., Hamdan, A., Genève, D., & Weber, S. (2012). Investigations on AlN/Sapphire piezoelectric bilayer structure for high-temperature SAW applications. *IEEE Transactions on Ultrasonics, Ferroelectrics, and Frequency Control, 59*(5), 999 - 1004.

Bao, X. Q., Burkhard, W., Varadan, V. V., and Varadan, V. K. (1987). SAW Temperature Sensor and remote reading system. Proceedings of the IEEE Ultrasonics Symposium, Denver, 10-12 October (pp. 583-585). New York: IEEE.

Bar-Cohen, D. K. (1983). *Thermal Analysis and Control of Electronic Equipment.* New York: McGraw-Hill Book Company.

Barendsz, W., (1985). A SAW-chemosensor for NO2 gas concentration measurement. In *Proceedings of the IEEE Ultrasonics Symposium* (pp. 586-590). New York: IEEE.

Bohn, F. K. (1986). Thermal Analysis and Control of Electronic Equipment. *Harper and Row Publishers, New York* .

Brace, J. G., & Sanfelippo, T. S. (1990). United States Patent 4,932,255. Washington D.C.: U. S. Patent and Trademark Office.

Bray, R. C., & Chu, Y. C. (1981). SAWR fabrication, *Hewlett-Packard Journal*, 11-12.

Brosh, D. D., & Zalmanovich, Z. (1985). Conjugated Heat Source at the Wall. *Journal of Heat Transfer*, Vol. 104, 90-95.

Bryant, A., Lee, D. L., & Vetelino, J. F. (1981). A surface acoustic wave gas detector. In *Proceedings of the IEEE Ultrasonics Symposium* (pp. 171-174). New York: IEEE.

Buff, W., Klett, S., Rusko, M., Ehrenpfordt, J., & Goroll, M. (1998). Passive remote sensing for temperature and pressure using SAW resonator devices. *IEEE Transactions on Ultrasonics, Ferroelectrics, and Frequency Control 45*(5), 1388-1392.

Burmeister, C. (1983). *Convective Heat Transfer*. New York: John Wiley and Sons.

Campbell, K. (1976). Observation on the short term stability of a SAW delay line oscillator. In *Proceedings of the IEEE Ultrasonics Symposium* (pp. 200-203). New York: IEEE.

Carslaw, S., & Jaeger, J. C. (1962). *Conduction of Heat in Solids*. New York: Oxford University Press.

Chen, E. M. (1979). Mixed Convection on Inclined Surfaces. *Journal of Heat Transfer, 101*, 422-426.

Chen, E. M. (1977). Mixed convection in boundary layer flow on a horizontal plate. *Journal of Heat Transfer*, 66-71.

Chen, E. M. (1979). Mixed convection on inclined surfaces. *Journal of Heat Transfer, 101*, 422-426.

Chen, E.M. Sparrow, R. S. & Mucoglu, A. (1977). Mixed convection in boundary layer flow on a horizontal plate. *Journal of Heat Transfer*, 66-71.

Chopra, L., & Kaur, I. (1983). *Thin film device applications*. New York: Plenum Press, New York.

Cross, S., & Scott, S. C. (1981). Surface-acoustic-wave resonators", *Hewlett-Packard Journal*, 9-14.

Dias, F. (1981). Physical sensors using SAW devices. *Hewlett-Packard Journal*, 18-20.

Drafts, B. (2001). Acoustic wave technology sensors. *IEEE Transactions on Microwave Theory and Techniques*, *49*(4), 795-802.

Ebata, S. M. (1982). A surface acoustic wave thermal sensor. *Proceedings of the 2nd Sensor Symposium*, 107-110.

Edmonds, P. (Ed.). (1981). *Ultrasonics (methods in experimental physics)* (Vol. 19). New York: Academic Press.

Giarratano, P. J. (1984). Transient boiling heat transfer from two different heat sources: small diameter wire and thin film flat surface on a quartz substrate. *International Journal of Heat Mass Transfer, 27*(8), 1311-1318.

Guang-Ping Shen, M. Q. Huang (2006). SPICE model with lumped circuits for a thermal flow sensor. *IEEE Sensors 2006*, 1444-1447.

Hamilton, J., & Howard, W. G. (1975). *Basic integrated circuit engineering.* New York: McGraw-Hill Inc.

Hauden, G. Jaillet, R., & Coquerel, R. (1981). Temperature sensor using SAW delay line. In *Proceedings of the IEEE Ultrasonics Symposium* (pp. 148-151). New York: IEEE.

Hietala, S. L., Hietala, V. M., & Brinker, C. J. (2001). Dual SAW sensor technique for determining mass and modulus changes. *IEEE Transactions on Ultrasonics, Ferroelectrics and Frequency Control*, *48*(1), 262-268.

Holman, P. (1986). *Heat transfer*. New York: McGraw-Hill Book Company.

Huang, S., Fu, X., Ruan, X., & Zou, J. (2009). A numerical investigation of conjugate forced heat transfer for a micro thermal flow sensor. Paper given at Proceedings of 2009 IEEE/ASME International Conference on Advanced Intelligent Mechatronics Suntec Convention and Exhibition Center Singapore, July 14-17, 2009 (pp. 1510 - 1514). New York:IEEE.

Inaba, Y. K., & Kasahara, Y. (1982). Radiation temperature sensor using surface acoustic wave. Proceedings of the 2nd Sensor Symposium, 127-131.

Inaba, Y. K., & Wasa, K. (1982). An electrostatic voltage sensor using surface acoustic waves. *Japanese Journal of Applied Physics, 20*(S3), 197.

Jakob, M. (1949). *Heat transfer.* New York: John Wiley and Sons.

Johnson, G., & Higashi, R. E. (1987). A highly sensitive silicon chip microtransducer for air flow and differential pressure sensing applications. *Sensors and Actuators*, 11(1), 63-72.

Joshi, S. G., (1991). United States Patent 5,003,822**.** Washington, D. C.: U. S. Patent and Trademark Office.

Joshi, S. G., & Brace, J. G. (1976). Measurements of Humidity Using Surface Acoustic Waves. In P*roceedings of the IEEE Ultrasonics Symposium* (pp. 600-603). New York: IEEE.

Jian-Bio, M. Q.-A. (July 2007). Flip-Chip Packaging for a Two-Dimensional Thermal Flow Sensor Using a Copper Pillar Bump Technology. *IEEE Sensors Journal*, 990-994.

Karlekar, V., & Desmond, R. M. (1982). *Heat transfer* (2nd ed.), West Publishing Company.

Kays, M. (1986). *Convective heat and mass transfer.* New York: McGraw-Hill Book Company.

Kraus, D., & Bar-Cohen, A. (1983). Thermal analysis and control of electronic equipment. New York: McGraw-Hill Book Company.

Kreith, F., & Black, W. Z. (1980). *Basic heat transfer*. New York: Harper and Row Publishers.

Kreith, F., & Bohn, M. S. (1986). *Principle of heat transfer*. New York: Harper & Row, Publishers.

Krijnen*, G., Floris, A., Dijkstra, M., Lammerink, T., & Wiegerink, R. (2007). Biomimetic micromechanical adaptive flow-sensor arrays. *Proceedings of SPIE*, 6592, 65920F.

Kays, M. (1986). *Convective Heat and Mass Transfer.* McGraw-Hill Book Company.

Leblois, T. G., & Tellier, C. R. (2000). Micromachined resonant temperature sensors: Theoretical and experimental results. *IEEE Transactions on Ultrasonics, Ferroelectrics, and Frequency Control, 47*(2), 333-340.

Lee, L. (1979). Design consideration for electronically compensated SAW delay line oscillators. In *Proceedings of the IEEE Ultrasonics Symposium* (pp. 844-854). New York: IEEE.

Lewis, M. F. (1974). Improvements to the SAW Oscillator. In *Proceedings of the IEEE Ultrasonics Symposium* (pp. 274-275.

Liu, J. Z. T., Rahman, A. (2006) United States Patent 7,140,261. Washington, D.C.: U. S. Patent and Trademark Office.

Liu, Z. T., Carlson, S. C., & Magee, S. J. (2008). U. S. Patent 7,373,838. Washington, D.C.: U. S. Patent and Trademark Office.

Lloyd M., & Sparrow, E. M. (1979). Combined forced and free convection flow on vertical surfaces. *Journal of Heat Transfer, 101*, 434-438.

Martin, J., Gunshor, R. L., & Pierret, R. F. (1980). Zinc-oxide-on silicon surface acoustic wave resonators. *Applied Physics Letters, 37*(8), 700-701.

Mathews, E. H. (1977). *Surface Wave Filters.* New York: John Wiley and Sons.

Matsumoto, N., Sudo, Y., Sinha, B. K., & Niwa, M. (1999). Long-term stability and performance characteristics of crystal quartz gauge at high pressures and temperatures. *IEEE Transactions on Ultrasonics, Ferroelectrics, and Frequency Control, 47*(2), 346-355.

McGill, R. A., Chung, R., Chrisey, D. B., Dorsey, P. C., Matthews, P., Piqué, A.,…Stepnowski, J. L. (1988). Performance optimization of surface acoustic wave chemical sensors. *IEEE Transactions on Ultrasonics, Ferroelectrics, and Frequency Control*, 45, 1370-1380.

Miyamoto, et al.,. (1985). Free Convection heat transfer from vertical and horizontal short plates. *International Journal of Heat Mass Transfer*, *29*(9), 1733-1745.

Miyasaka, et al (1985). "Temperature compensated ZnO/ SiO$_2$ /Si thin film resonator for VHF voltage controlled oscillator. In *Proceedings of the IEEE Ultrasonics Symposium* (pp. 234-239). New York: IEEE.

Mori, Y. (1961). Buoyancy effects in forced laminar convection flow over a horizontal flat plate. *Journal of Heat Transfer*, 83 (4), 479-482.

Mucoglu, A., & Chen, T. S. (1979). Mixed convection on inclined surfaces. *Journal of Heat Transfer*, *101*, 422-426.

Nomura, T., Saitoh, A., & Koyama, K. (2007). Mass flow sensor using dual SAW device. *Proceedings of Frequency Control Symposium, 2007 Joint with the 21st European Frequency and Time Forum. IEEE International* (pp. 25 – 30). New York:IEEE.

Oliner, A. A. (Ed.). (1978). *Topics in applied physics* (Book 24). New York: Springer.

Owens, J. M. (1986). SAW devices designed for military and commercial systems. *MSN and Communications Technology*, 16(7), 349-359.

Parker, T. E. (1979). 1/f noise in quartz delay line and resonator oscillators. In *Proceedings of the IEEE Ultrasonics Symposium* (pp. 878-881). New York: IEEE.

Parker, T. E. (1982). Precision surface acoustic wave oscillators. In *Proceedings of the IEEE Ultrasonics Symposium* (pp. 268-274). New York: IEEE.

Parker, T. E., & Callerame, J. (1981). "Sensitivity of SAW delay lines and resonators to vibration. In *Proceedings of the IEEE Ultrasonics Symposium.* (pp. 129-134). New York: IEEE.

Parker, T. E. (1983) Random and systematic contributions to long term frequency stability in SAW Oscillators", In *Proceedings of the IEEE Ultrasonics Symposium.* (pp. 257-262).

Pedi, P., Loan, J., & McManus, E. (1983). The role of SAW Oscillators in military radar system. In *IEEE-MTTS Digest* (pp. 311-313). New York: IEEE.

Penavaire, L. ; Seguignes, D. ; Lardat, C. ; Bonnier, J.J. ; Chevalier, J.Y. ; Beson, Y]. (1980). A 120 MHz SAW resonator stabilized oscillator with high spectral purity. In *Proceedings of the IEEE Ultrasonics Symposium* (pp. 256-259). New York: IEEE.

Petersen, K. & Brown, J. (1985). High-precision, high-performance mass-flow sensor with integrated laminar flow micro-channels. In *Proceedings of Transducers' 85 Symposium*. (pp. 354-357).

Pohl, **A.** (2000). A review of wireless SAW sensors. *IEEE Transactions on Ultrasonics, Ferroelectrics, and Frequency Control, 47*(2), 317-332.

Polla, L. (1983). Monolithic integrated zinc-oxide on silicon pyroelectric anemometer. *Technical Digest International Electronic Devices Meeting* (pp. 639-642). Washington, D.C.

Qin-Yi, T., & Jin-Biao, H. (1987). A noval CMOS flow sensor with constant chip temperature (CCT) operation. *Sensors and Actuators*, *12*(1), 9-21.

Ramachandrin, B. F., & Chen, T. S. (1983). Mixed convection over a horizontal plate. *Journal of Heat Transfer*, *105*, 420-423.

Ramadhyani, et al., (1985). Conjugate heat transfer from small isothermal heat sources embedded in a large substrate. *International Journal of Heat Mass Transfer*, 1945-1952.

Reeder, M. Cullen, D. E., & Gilden, G. (1975). SAW oscillator pressure sensors. In *Proceedings of the IEEE Ultrasonics Symposium* (pp. 264-268). New York: IEEE.

Risch, R. (1984). Precision pressure sensor using quartz SAW resonators. *Sensors and Actuators*, 6, 127-133.

Rm Rich. (Ed.). (1981). *Methods of experimental physics* (Volume 18-Part A). New York: Academic Press.

Rohsenow, W. M.., & Choi, H. Y. (1961). *Heat, mass and momentum transfer.* Englewood Cliffs, NJ: Prentice-Hall, Inc.

Seidman, A. H. (1983). *Integrated circuits applications hand-book.* New York, NY: John Wiley & Sons.

Shah, R. K., & London, A. L. (1978). *Laminar flow forced convection in ducts*. New York: Academic Press.

Shen, G., Qin, M., & Huang, Q. (2006). SPICE model with lumped circuits for a thermal flow sensor. *Proceedings of IEEE Sensors 2006* (pp. 1444-1447). New York: IEEE.

Shereve, W. R. (1981). Power dependence of aging in SAW Resonators. In *Proceedings of the IEEE Ultrasonics Symposium* (pp. 94-99). New York: IEEE.

Sparrow, L. (1979). Combined Forced and Free Convection Flow pn Vertical Surfaces. *Journal of Heat Transfer , 101*, 434-438.

Stokes, R. B. (1982). Propagation loss effects on SAW oscillators aging. In *Proceedings of the IEEE Ultrasonics Symposium* (pp. 275-278). New York: IEEE.

Stokes, R. B., & Delaney, M. J. (1983). Aging mechanisms in SAW oscillators. In *Proceedings of the IEEE Ultrasonic Symposium* (pp. 247-256). New York: IEEE.

Tabata, O. (1986). Fast-response silicon flow sensor with an on-chip fluid temperature sensing element. *IEEE Transactions on Electron Devices*, *33*(3), 361-365.

Tai, Y. C., Muller, R. S., & Howe, R. T. (1985). Polysilicon-bridges for anemometer applications. In *Proceedings of Transducers 85 Symposium* (pp. 354-357)..

Thaw, C., Minet, R., Zemany, J., & Zweben, C. (1987). Metal Matrix Composite Microwave Packaging Components. *SAMPE Journal*, *23*(6), 40-43.

Tooru Nomura, A. S. (2007). Mass flow sensor using dual SAW device. *Frequency Control Symposium* , 25-30.

van Honschoten, J. W., Svetovoy, V. B., Lammerink, T. S. J., Krijnen, G. J. M., & Elwenspoek, M. C. (2004). Determination of the sensitivity behavior of an acoustic, thermal flow sensor by electronic characterization. *Sensors and Actuators A: Physical*, *112*(1), 1-9.

Walls, F. L., & Wainwright, A. W. (1975). Measurement of short-term stability of quartz crystal resonators and the implications for crystal oscillator design and applications. *IEEE Transactions on Instrumentation and Measurement*, *24*(1), 15-20.

Wang, Y., Li, Z., Qin, L., Chyu, M. K., & Wan, Q. (2011). Surface *Acoustic Wave Flow Sensor*. *Proceedings of Joint Conference of the IEEE International Year* (pp. 1 – 4). New York:IEEE.

Wang, Y., Li, Z., Qin, L., Chyu, M. K., & Wang, Q. (2012). Theoretical and experimental studies of a surface acoustic wave flow sensor. *IEEE*

Transactions on Ultrasonics, Ferroelectrics, and Frequency Control, 59(3), 483-490.

Weidong, C., Dong, Y., & Feng, G. (2000). A multi-resolution wireless force sensing system based upon a passive SAW device. *IEEE Transactions on Ultrasonics, Ferroelectrics, and Frequency Control***,** *48*(5) 1438-1441.

Weirauch, R., Scwartz, J., & Bennet, R. C. (1979) SAW resonator frit-bondaed pressure transducer. In *Proceedings of the IEEE Ultrasonics Symposium* (pp. 874-877). New York: IEEE.

White, R. M. (1970). Surface elastic waves. In *Proceedings of the IEEE*, *58*(8), 1238-1276.

Wohltjen, H., & Dessy, R. (1979). SAW probe for chemical analysis I. In Analytical Chemistry, (pp. 1458-1464).

Wohltjen , Snow, A., & Ballantine, D. (1985). The selective detection of vapors using SAW devices. In *Proceedings of the 1985 International Symposium on Solid-State Sensors and Actuators* (pp. 66-77). New York: IEEE.

Vellekoop, M. J., & Visser, C. C. G. (1988). An integrated SAW voltage sensor. In *Proceedings of the IEEE Ultrasonics Symposium* (pp. 575-578). New York: IEEE.

Vetelino, F. (1983). Methods for temperature compensations in SAW devices. *Proceedings of the National Electronics Conference* Kyoto, JP (pp. 140-142). Chicago, IL: National Electronics Conference, Inc.

Zhdanova, V. P. (1968). Thermal properties of lithium niobate crystals". *Soviet Physics - Solid State, 10*(7), 1360-1362.

Zhdanova, V., Klyuev, V. V., Lemanov, I. A., Smirnov, I, & Tikhonov, V. V. (1968). Thermal properties of lithium niobbate crystals. *Soviet Physics—Solid State, 10*(6), 1360-1362.

Yizhong Wang1, Z. L.M. (2011). Surface Acoustic Wave Flow Sensor. In Proceedings of 2*011 Joint Conference of IEEE International* (pp. 1-4). New York:IEEE.

APPENDIX A: SAW SUBSTRATES CHARACTERISTICS - DRAFT MATHCAD PLOTS

Lithium Niobate Substrate

A summary of the theoretical modeling analysis for LiNbO$_3$ is presented here.

Relationships of many variables necessary for sensor characterization are plotted.

Fig.   Resistance vs thickness

$t_S := 5.0 \cdot 10^{-4}, 4.0 \cdot 10^{-4} .. 1.0 \cdot 10^{-4}$

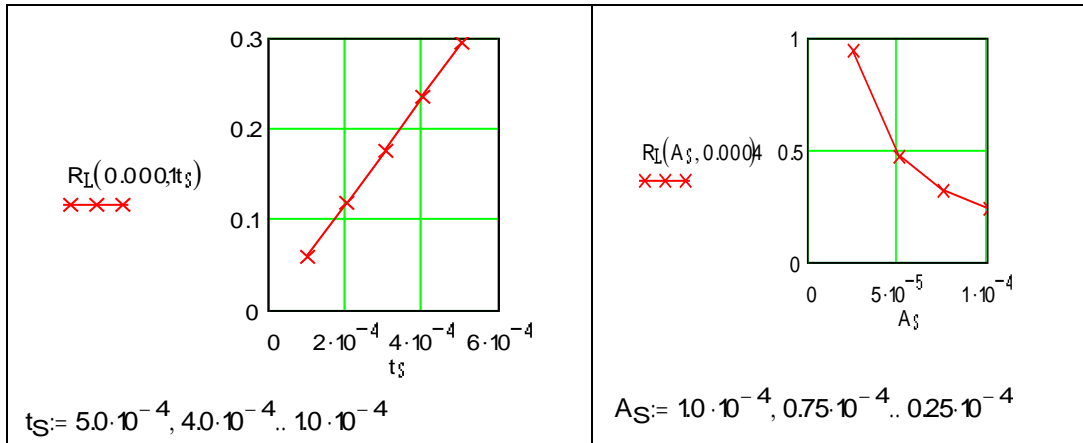Figure 23

Fig.   Substrate resistance vs area
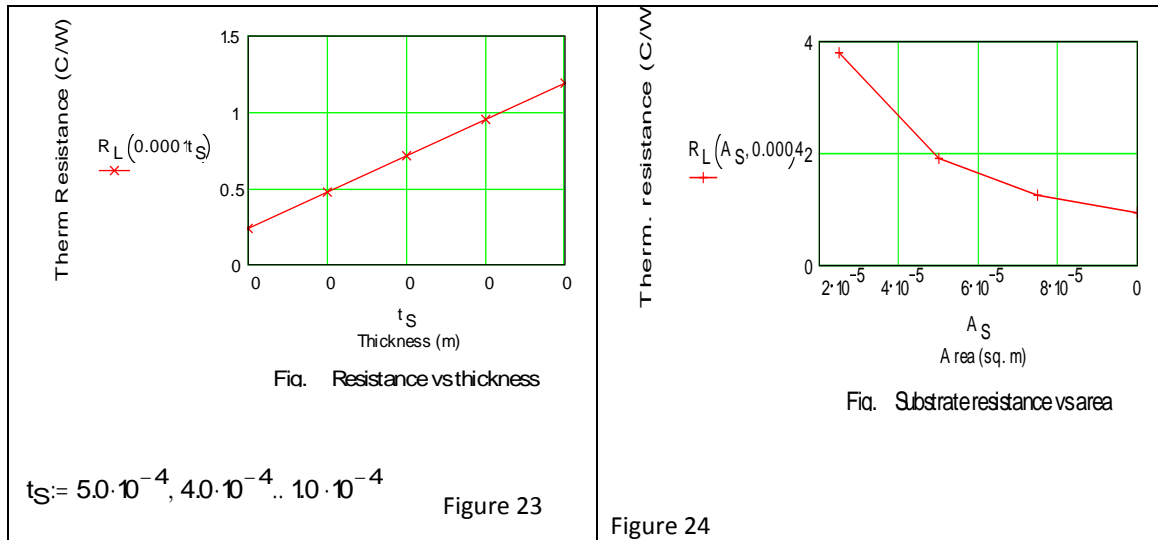
Figure 24

Figure 1 — Thermal conduction resistance as a function of thickness.
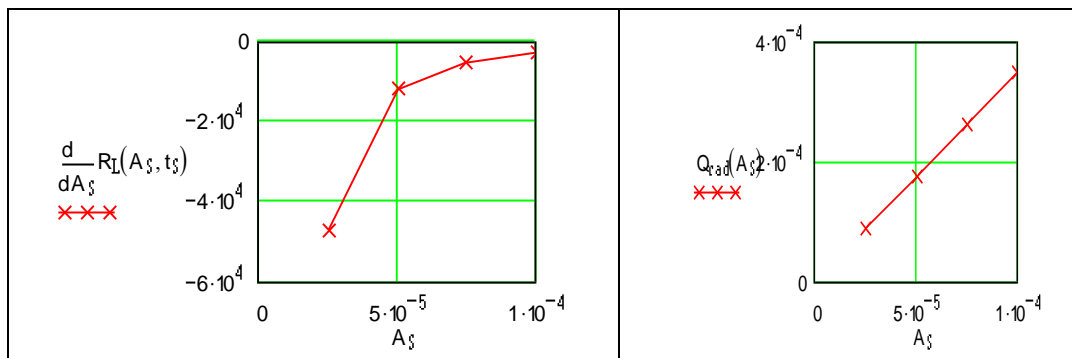Figure 2 — Thermal conduction resistance as a function of substrate area.

Fig.   Radiation loss vs area

Fig. Total conv. resistance vs area
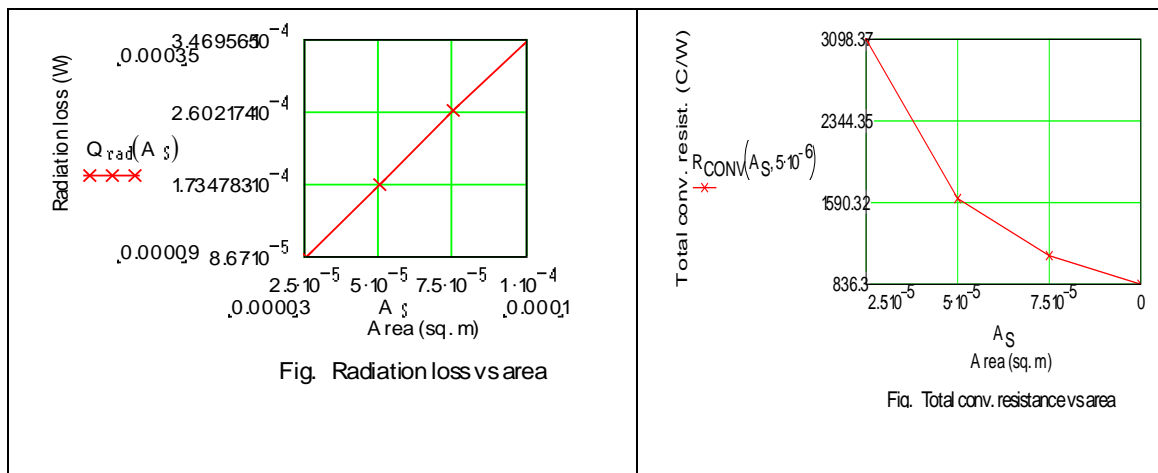
Figure 3 — Radiation losses versus substrate areas.
Figure 4 — Free convection thermal resistance as a function of substrate area.
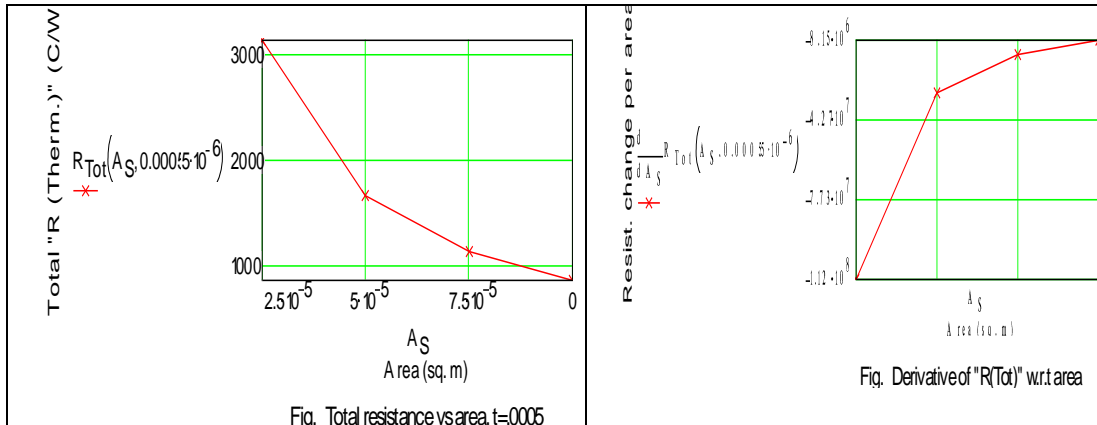
Figure 5 – Total thermal resistance (conduction and convection) under free convection as a function of area.

Figure 6 – Derivative of Total thermal resistance as a function of area.
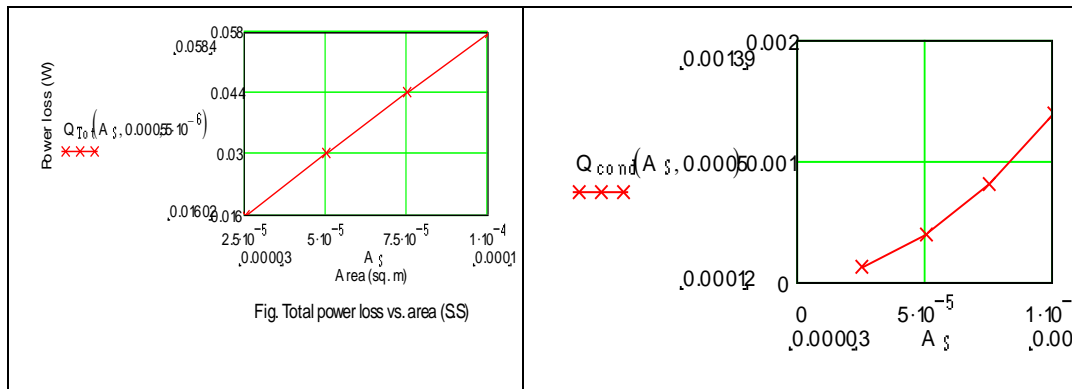
Figure 7 – Total heat loss (conduction and convection) under free convection, as a function of area.

Figure 8 – Conduction heat loss versus area (in presence of any convection).
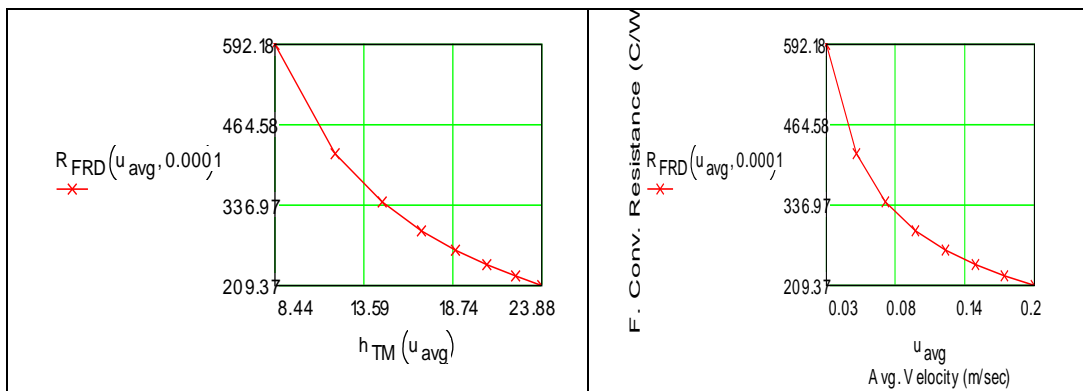
Figure 9 – Forced convection thermal resistance as a function of convection coefficient.

Figure 10 – Forced convection thermal resistance as a function of Avg velocity.
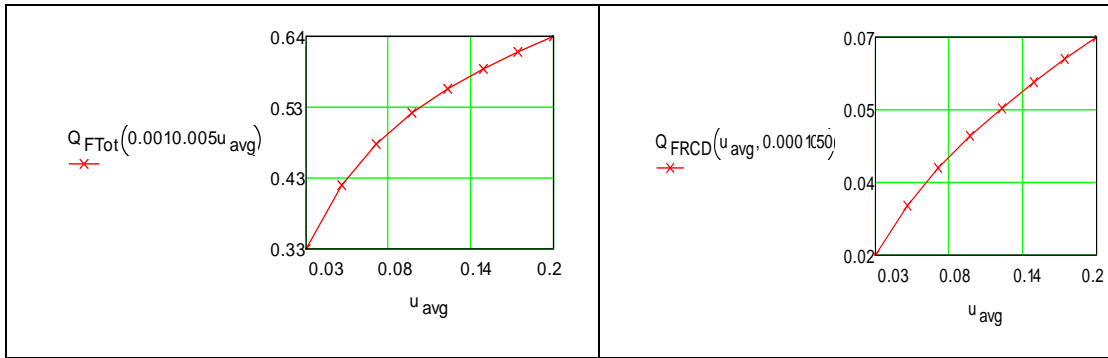
Figure 11 – Total thermal loss under Forced convection a function of average flow velocity.
Figure 12 – Forced convection thermal loss a function of average flow velocity.
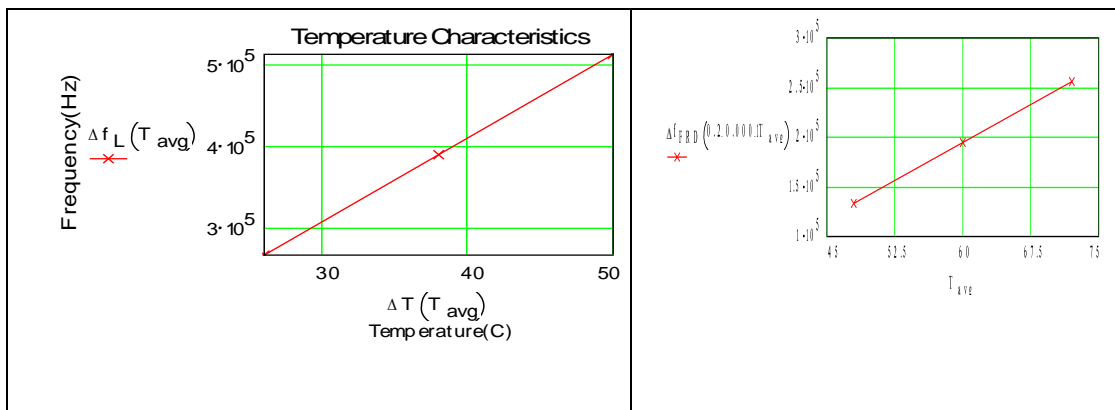
Figure 13 – Frequency versus temperature characteristics.
Figure 14 – Frequency change under forced convection as a function of average SAW substrate temperature.
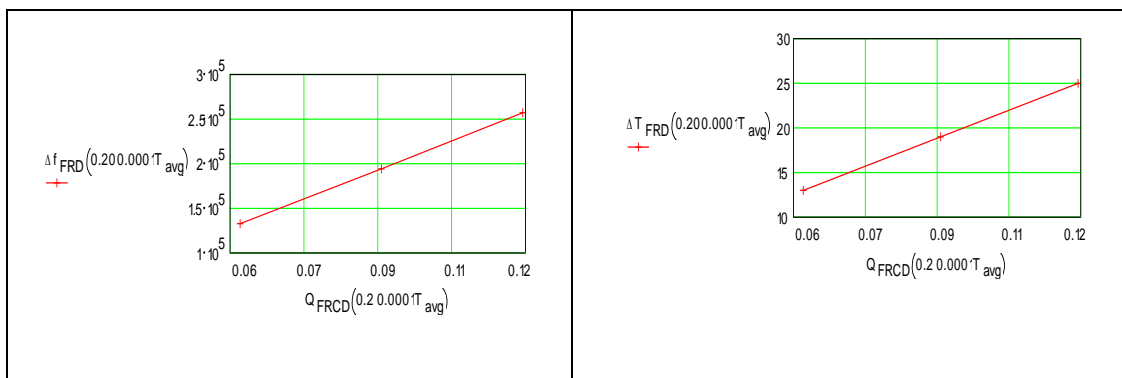
Figure 15 – Total thermal loss under Forced convection a function of average flow velocity.
Figure 16 – Change in temperature change versus forced convection thermal loss as a function of average flow velocity.
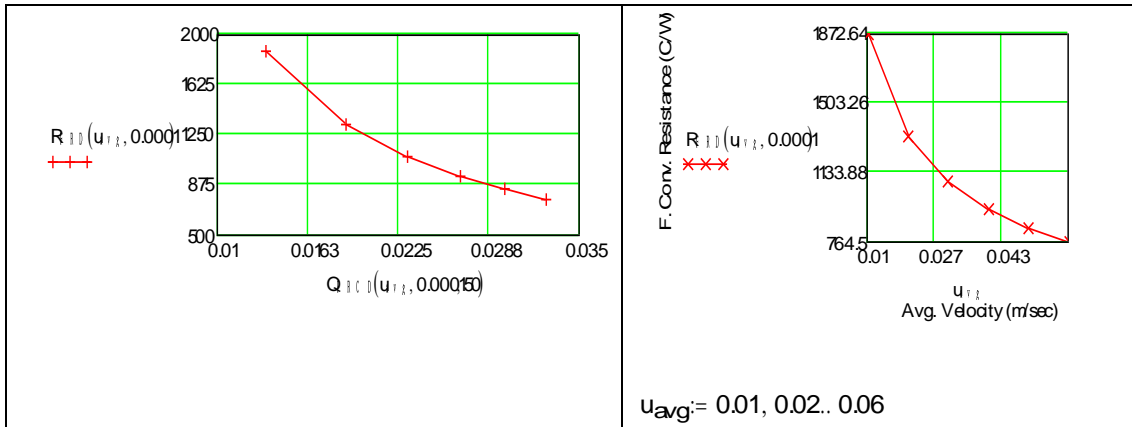
Figure 17 – Change in forced convection thermal resistance versus forced convection thermal loss as a function of average flow velocity.

Figure 18 – Change in forced convection thermal resistance as a function of average flow velocity.
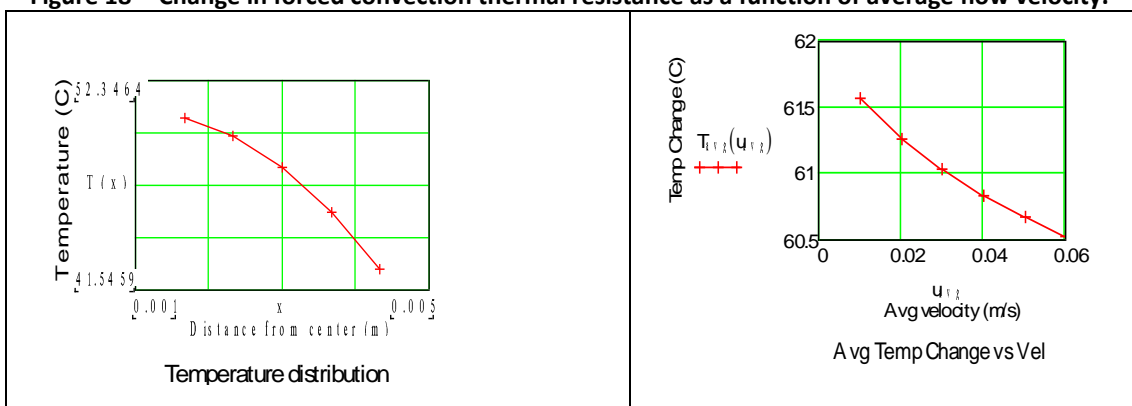
Figure 509 – Plot of temperature distribution as a function of characteristics length of the substrate.

Figure 510 – Average temperature of the sensor as a function of average flow velocity.
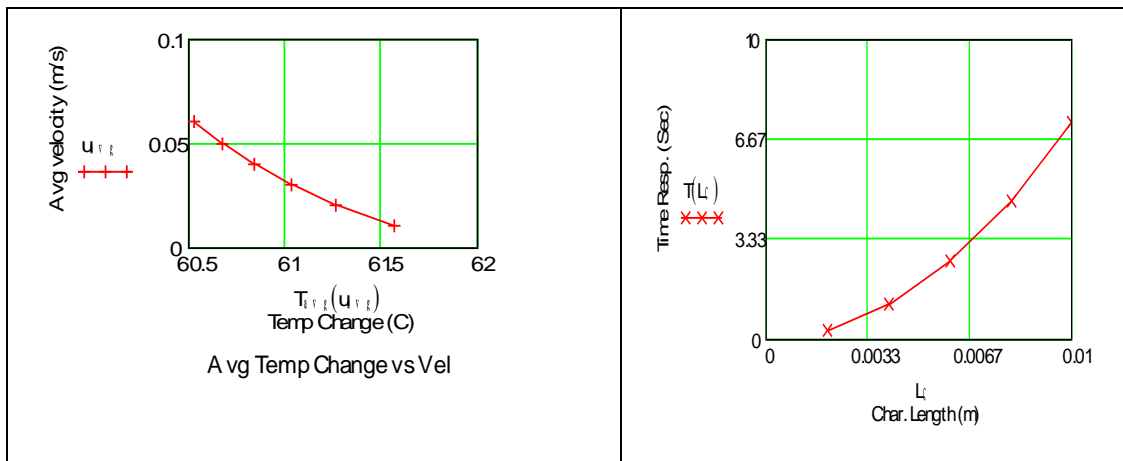
Figure 21 – Average temperature versus average velocity.
Figure 22 – Time Response Analysis as a function of substrate's characteristics length.
Zinc Oxide Substrate

Detailed results of theoretical analysis for ZnO-based proposed SAW are presented here.

$t_{S} := 5.0 \cdot 10^{-4}, 4.0 \cdot 10^{-4} .. 1.0 \cdot 10^{-4}$

$A_{S} := 1.0 \cdot 10^{-4}, 0.75 \cdot 10^{-4} .. 0.25 \cdot 10^{-4}$

Figure 23 – Thermal conduction resistance as a function of thickness.
Figure 24 – Thermal conduction resistance as a function of substrate area.

Figure 25 – Derivative of thermal conduction resistance as a function of area.
Figure 26 – Radiation loss as a function of substrate area.

$A_{S} := 1.0 \cdot 10^{-4}, 0.75 \cdot 10^{-4} .. 0.25 \cdot 10^{-4}$
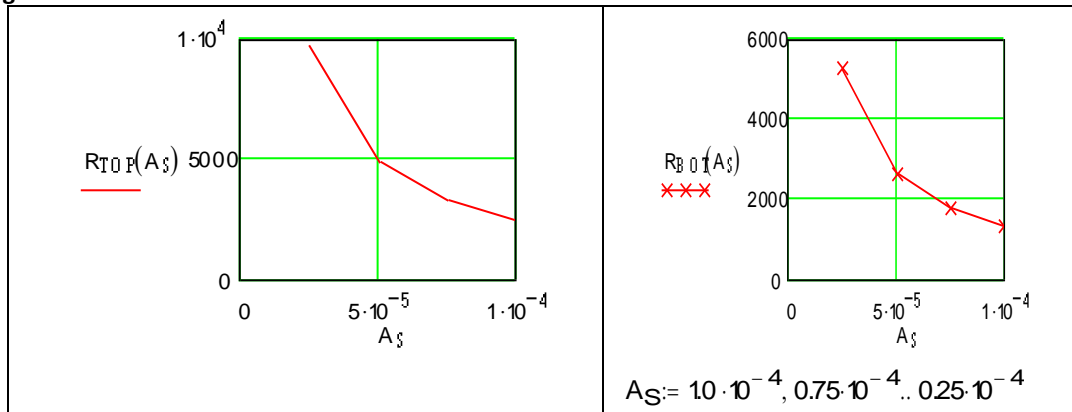
Figure 27 – Thermal convection resistance from top surface function of substrate area.
Figure 28 – Thermal convection resistance from bottom surface as a function of substrate area.
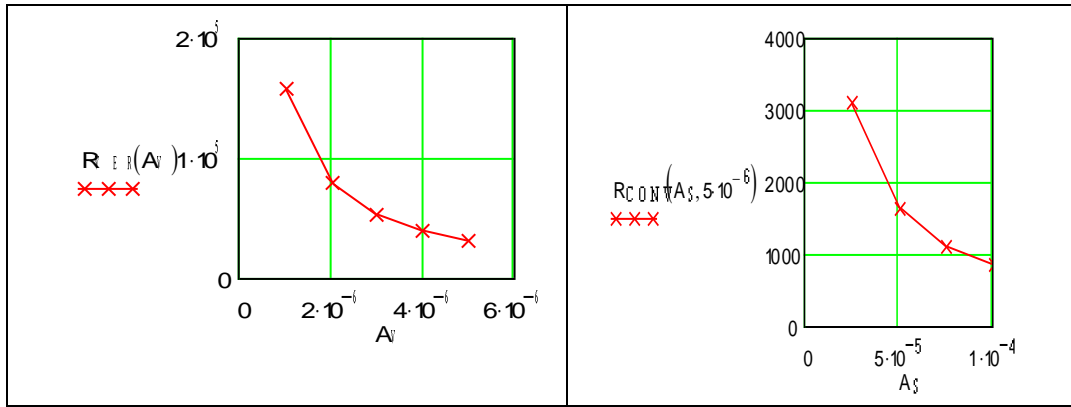
Figure 29 – Thermal resistance from vertical (side) walls as a function of wall area.
Figure 30 – Total Thermal resistance under free convection as a function of area (for fixed thickness of the substrate).
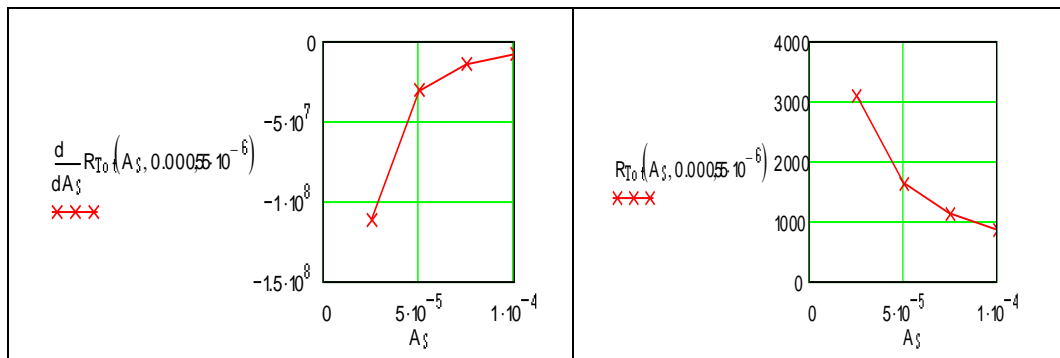
Figure 31 – Total Thermal (convection plus conduction) resistance fas a function of substrate area (for fixed thickness).
Figure 32 – Derivative of Total thermal resistance as a function of area (for fixed thickness).
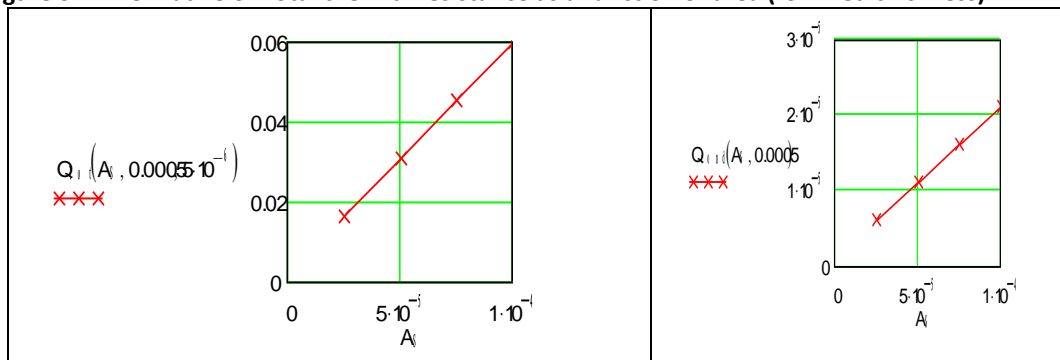
Figure 33 – Total (convection+conduction) thermal heat loss under free convection as a function of substrate area (for fixed thickness).
Figure 34 – Conduction) thermal heat loss under free convection as a function of substrate area (for fixed thickness).
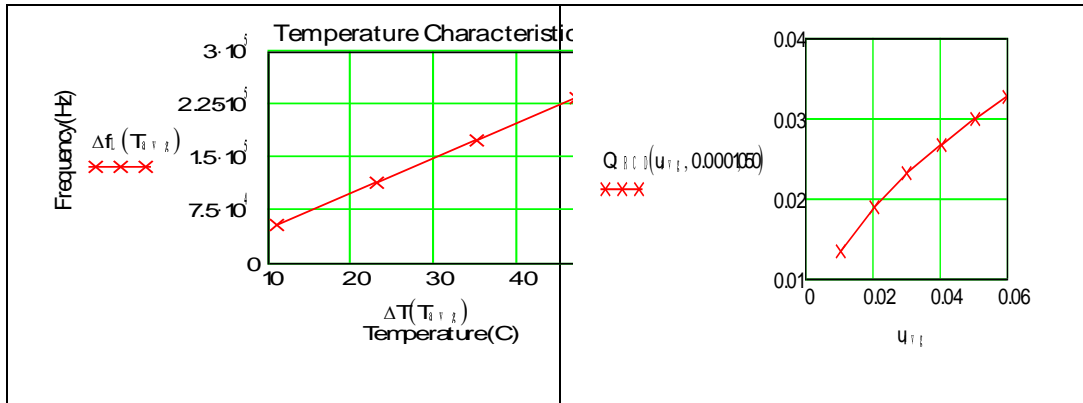
Figure 35 − **Frequency versus Temperature characteristics of ZnO-based SAW-flow sensor.**
Figure 36 − **Forced convection thermal loss a function of average flow velocity**.
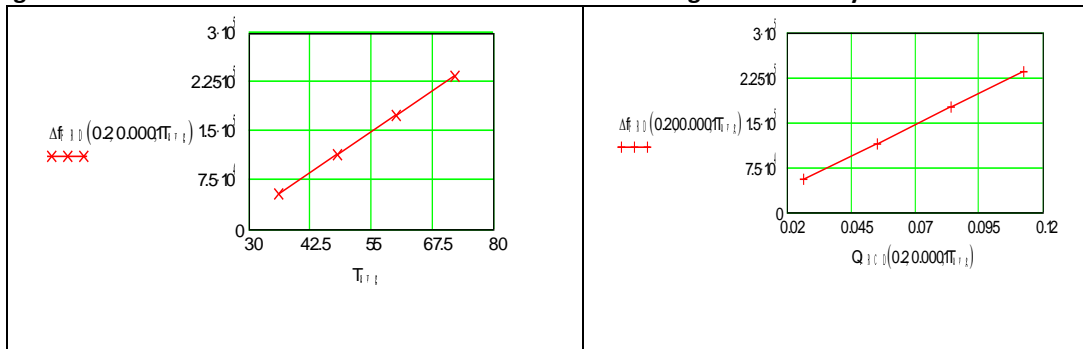
Figure 37 − **Frequency change under forced convection as a function of average SAW substrate temperature.**
Figure 38 − **Change in temperature change versus forced convection thermal loss as a function of average flow velocity**.
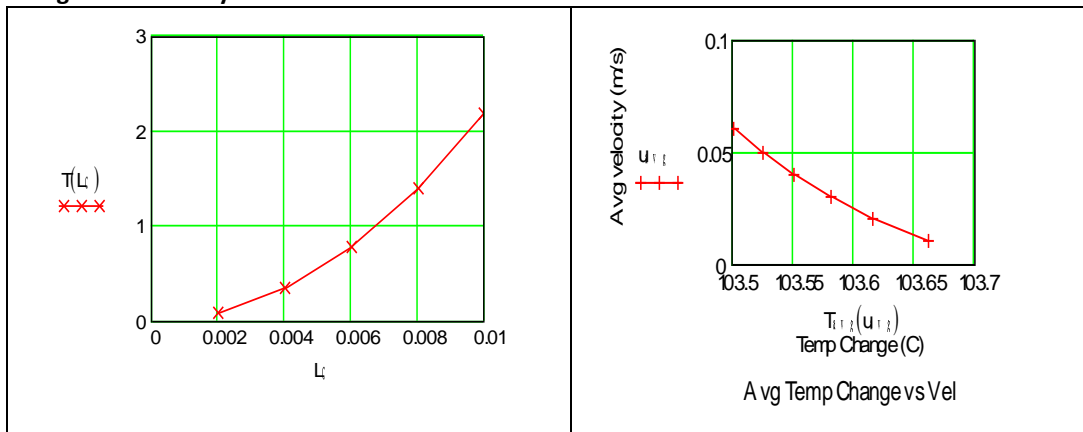
Figure 39 – Time Response Analysis as a function of substrate's characteristics length.
Figure 40 − **Average flow velocity as a function of temperature of the sensor (for fixed power input to heater).**
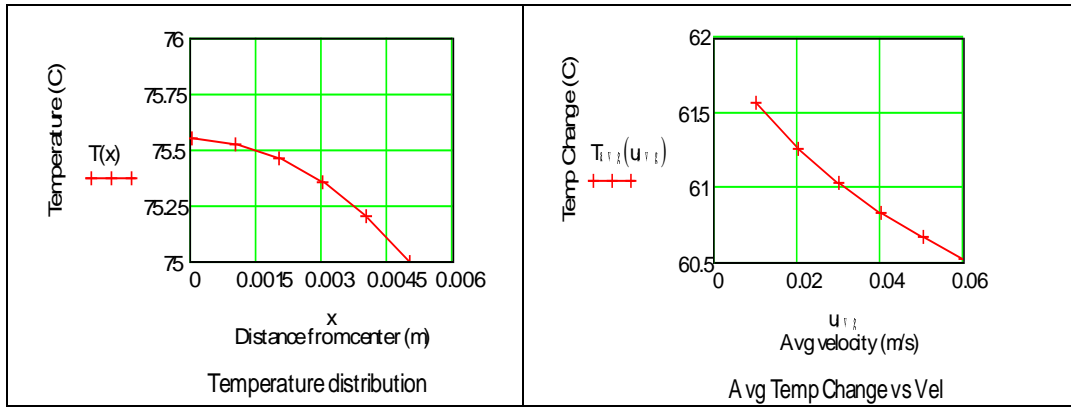
Figure 41 –   Plot of temperature distribution (under free convection, Q_{HTR}=0.058 W)).

Figure 42 – Average temperature (calculated from Figure 37) of the sensor as a function of average flow velocity (for fixed power input to heater).

Quartz Substrate Analysis

Detailed results of theoretical analysis for Quartz-based proposed SAW are presented here.
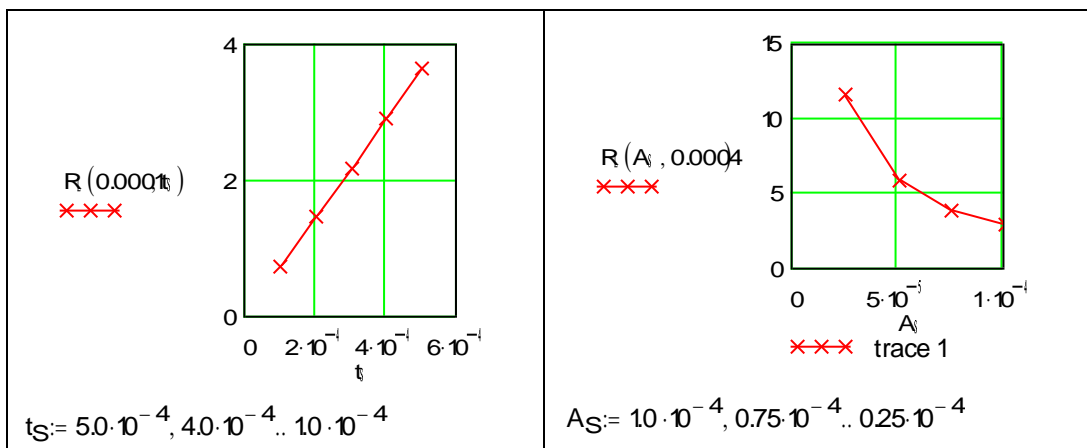
Figure 43 – Thermal conduction resistance as a function of thickness.
Figure 44 – Thermal conduction resistance as a function of substrate area.
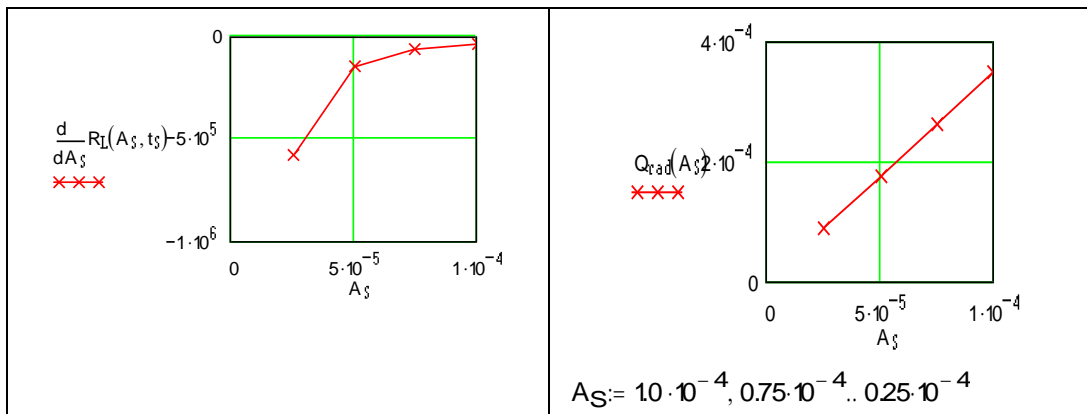
Figure 45 – Derivative of substrate thermal resistance as a function of area.
Figure 46 –   Radiation losses versus substrate areas.

$R_{TOP}(A_S)$ 5000

$R_{BOT}(A_S)$
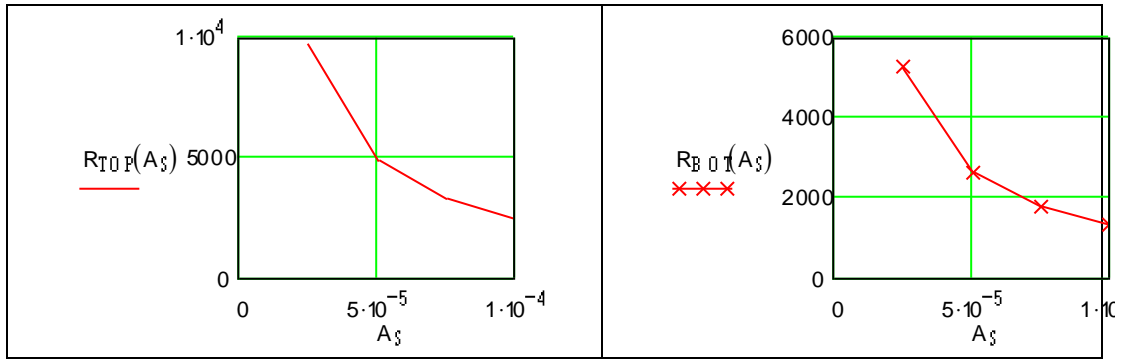
Figure 47 – Top surface thermal convection resistance as a function of surface area.
Figure 52 – Bottom surface thermal convection resistance as a function of surface area.

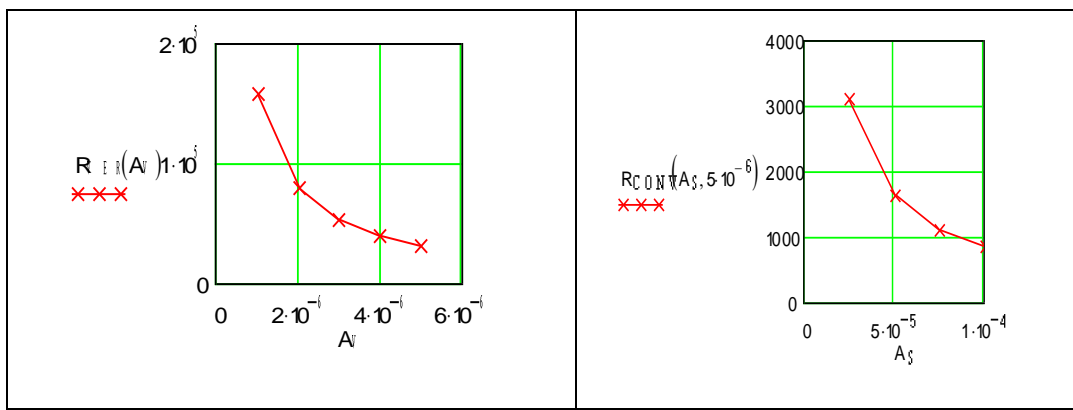$R_{VER}(A_V)$

$R_{CONV}(A_S, 5 \cdot 10^{-6})$

Figure 49 – Vertical surface thermal convection resistance as a function of surface area.
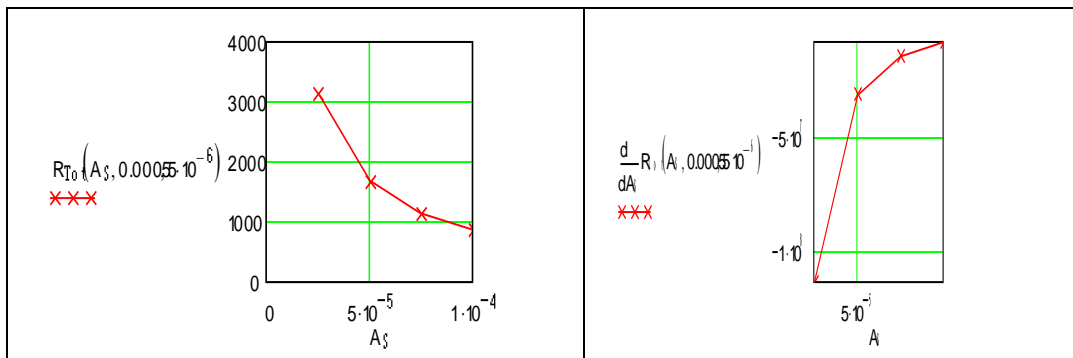**Figure 50 – Thermal free convection resistance as a function of surface area.**

$R_{Tot}(A_S, 0.0005, 5 \cdot 10^{-6})$

$\dfrac{d}{dA_V} R_V(A_V, 0.0005, 5 \cdot 10^{-6})$

Figure 51 – Total thermal resistance (conduction and convection) under free convection as a function of area.
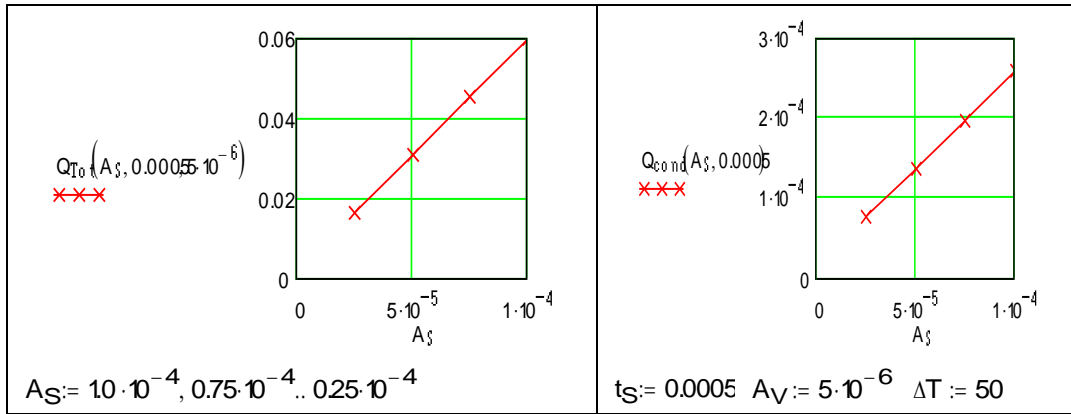**Figure 52 – Derivative of Total thermal resistance as a function of area.**

Figure 53 – Total thermal loss as a function of surface area of the substrate.

Figure 54 – Conduction thermal heat loss under free convection as a function of substrate area (for fixed thickness).
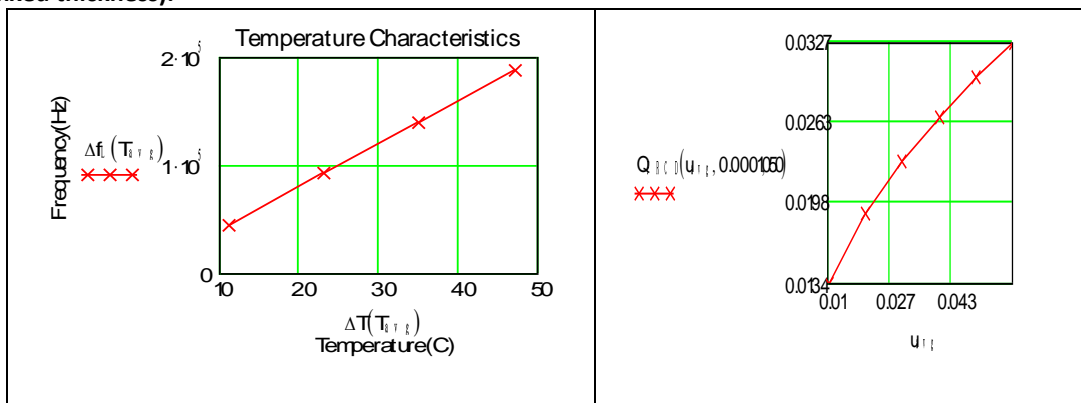

Figure 55 – Frequency versus Temperature characteristics of Quartz-based SAW-flow sensor.

Figure 56 − Forced convection thermal loss a function of average flow velocity.
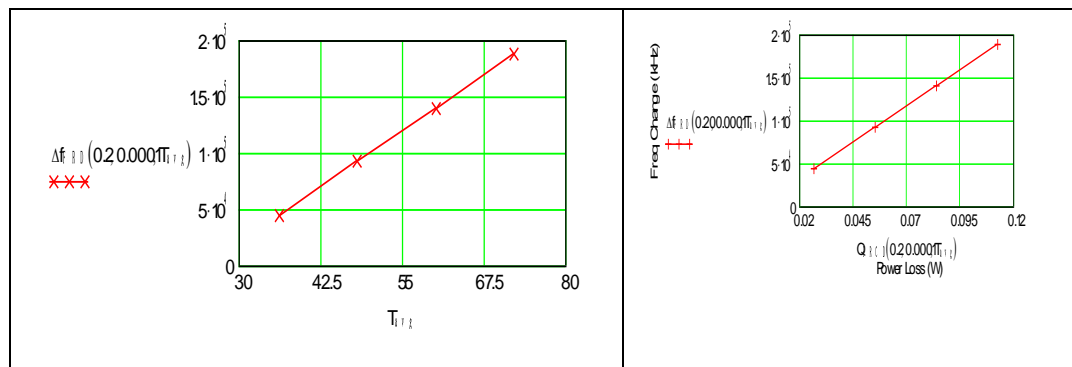

Figure 57 − Frequency change under forced convection as a function of average SAW substrate temperature.

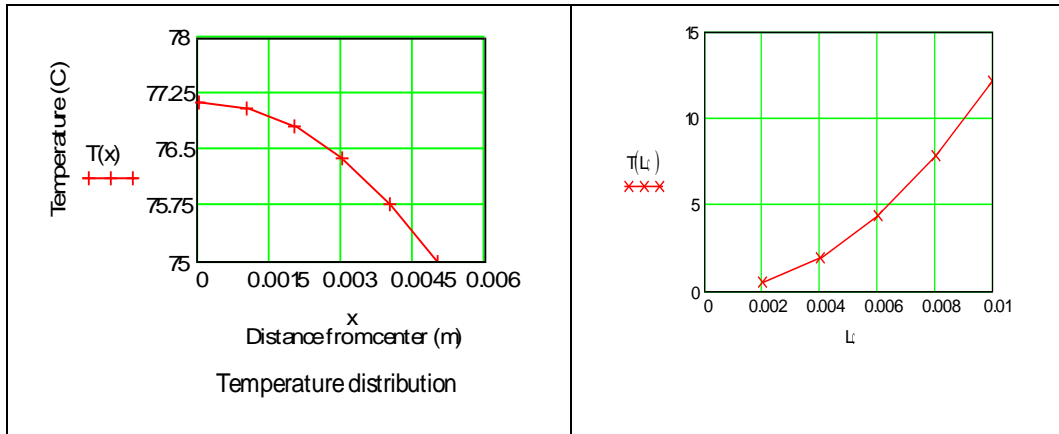**Figure 58 – Change in temperature change versus forced convection thermal loss as a function of average flow velocity**.

Figure 59 – Plot of temperature distribution (under free convection, Q$_{HTR}$=0.058 W)
Figure 60 – Time Response Analysis as a function of substrate's characteristics length